Modeling of Polymer Flow

Near Solid Walls

The research presented in this thesis was carried out within the chair of Applied Analysis and Mathematical Physics, Department of Applied Mathematics, in close collaboration with the Physics of Complex Fluids Chair, Department of Applied Physics, University of Twente, PO Box 217, 7500 AE Enschede, The Netherlands.

The research was supported by the Technology Foundation STW (TWI.5481), applied science division of NWO, and the technology programme of the Ministry of Economic Affairs of the Netherlands.

Publisher: Print Partner IPSKAMP,
Capitool 25 (Business & Science Park),
Postbus 333, 7500 AH Enschede.
www.ppi.nl

ISBN 9036521866

MODELING OF POLYMER FLOW NEAR SOLID WALLS

PROEFSCHRIFT

ter verkrijging van
de graad van doctor aan de Universiteit Twente,
op gezag van de rector magnificus,
prof. dr. W.H.M. Zijm,
volgens besluit van het College voor Promoties
in het openbaar te verdedigen
op donderdag 7 juli 2005 om 15.00 uur

door

Mikhail Alexandrovitch Tchesnokov
geboren op 9 maart 1976
te Uglich, Rusland

Dit proefschrift is goedgekeurd door de promotoren:

Prof. dr. J. Molenaar
en
Prof. dr. J.J.M. Slot

Abstract

Polymers are known to exhibit various flow instabilities during extrusion in which a molten polymer is forced to flow through a narrow die, in order to form a strand or acquire a desired shape of the final product. Recent developments in experimental techniques revealed that some of the instabilities are interfacial in nature, that is originate from the violation of the no-slip boundary condition at the polymer melt/die wall interface. The ability to control the extrusion instabilities thus lays through the understanding of the boundary conditions at the interface between a polymer melt and a solid wall.

The subject of the present work is the modeling of a polymer flow near a solid wall. Its ultimate goal is to develop a consistent mathematical formalism which is able to describe correctly the real mechanics of the melt, such as entanglements between different polymers and chain connectivity. The model should provide an adequate mathematical representation of all the major physical processes inherent to polymer chains in the melt, such as convection, retraction, reptation, and constraint release. Finally, it must be able to reproduce quantitatively available experimental data, provided that the necessary molecular parameters and processing conditions are known. A successful model for polymer melt flow will allow us to understand the mechanics of extrusion instabilities, and perhaps suggest a way to eliminate them.

To avoid using adjustable parameters, we start with the consideration of the single polymer dynamics in flow. The derived "microscopic" equations of motion are then used to find the corresponding constitutive equation for an ensemble of polymer chains. We show that the behavior of the ensemble can successfully be described in terms of the so-called bond vector correlator. All macroscopic quantities of practical interest which represent the state of the ensemble, e.g. local stress, can be readily expressed in terms of this correlator.

In a die, the polymer melt comes into contact with the die wall. Due to attractive polymer-wall interaction, some of the polymers become attached to the wall. So there are two "sorts" of molecules in the melt: adsorbed (i.e., attached to the wall) and bulk (i.e., unattached). As a result, two bond vector correlators must be introduced. We show that these correlators satisfy nonlinear integro-partial differential equations which account for all the major processes for polymers in the melt. Due to entanglements between bulk and adsorbed

molecules, these equations are coupled and must be solved simultaneously.

The Brownian motion of an adsorbed molecule may result in its sudden detachment from the wall, after which it becomes bulk. The reversibility of adsorption implies that the actual number of adsorbed molecules on the wall is governed by the balance between adsorption and desorption. We show that it satisfies a non-linear balance equation which is coupled to the equation of motion for the bond vector correlator of the adsorbed molecules via flow-induced chain stretch.

The equations of motion for the adsorbed and bulk polymer molecules together with the balance equation for the surface density of adsorbed molecules form a system of equations which lies at the heart of the model. This system describes the flow of the polymer melt in the die and contains information on the dynamics of both bulk and adsorbed molecules. The latter are found to have a significant influence on the polymer melt flow in the die via their entanglements with the bulk chains. We show that a decrease in the number of the entanglements (via detachement of adsorbed chains from the wall or disentanglement between adsorbed and bulk molecules) may lead to a significant increase in the interfacial fluid velocity between the melt and the wall. Both desorption and disentanglement can therefore be regarded as possible slip mechanisms.

In both slip scenarios (due to desorption or disentanglement), it is the dynamics of the adsorbed molecules that governs the boundary conditions at the polymer melt / die wall interface. The present model provides a detailed information about the dynamics of the adsorbed molecules, and therefore is able to describe and quantify the boundary conditions. The model predicts the onset of slip over a wide range of temperatures, polymer melts, and wall materials. For certain cases, the model predicts a "mixed" slip regime, in which desorption and disentanglement occur in parallel. The onset of slip receives a spatial attention in this work. In particular, the present model demonstrates a complex nonmonotonous dependence of the parameters of the stick-to-slip transition on the molecular parameters of the melt and material of the die wall. Besides that, the model exhibits a complicated nonlinear temperature dependence of the parameters of the transition, which has not been revealed in the earlier theories for wall slip.

In a real extrusion system, the polymer melt is normally polydisperse and therefore contains various fractions of polymer molecules with different molecular weights. In order to study the effect of polydispersity of bulk and adsorbed molecules on the onset of wall slip, the developed model has been extended. We found a strong dependence of the parameters of the stick-to-slip transition on the molecular weight distribution (MWD) of the melt. Specifically, we show that polydisperse melts can be much more resistant to the onset of slip than monodisperse ones.

Acknowledgement

The work presented in this thesis is the result of a three-year research project carried out within the group of Applied Analysis and Mathematical Physics at the University of Twente, The Netherlands. Here I would like to express my gratitude and my sincere thanks to those who have contributed to the completion of this thesis.

First of all, I would like to thank my supervisors Prof. Dr. Jaap Molenaar and Prof. Dr. Han Slot for giving me the opportunity to work on this project as well as for their constructive suggestions, critical reviews and constant support during the research. It was a honor for me to work with you. The completion of the thesis would not have been possible without your contributions. I would also like to say a word of thanks to Dr. Roman Stepanyan, Dr. Rudy Koopmans, Dr. Jaap den Doelder, and Dr. Markus Bulters for useful and productive discussions that helped shed some light on many aspects of polymer physics and polymer chemistry.

A special word of thanks should be addressed to my office-mates Chris, Sena, and Vijaya for making my office-life comfortable and pleasant as well as for their good and healthy sense of humor, a necessity for those who work full-time in the Netherlands ;o) Indeed, I would also like to thank all my colleagues from the AAMP and NACM group for nice and sometimes hilarious conversations during numerous lunch and coffee breaks.

Furthermore, I would like to thank my parents, my sister, and of course all my friends for their understanding, encouragement and solid support during the last three years, and for all the the fun we have had together.

In conclusion, I would like to thank the Technology Foundation STW, applied science division of NWO, and the technology programme of the Ministry of Economic Affairs of the Netherlands for the financial support of the project.

Enschede, The Netherlands — Mikhail Tchesnokov
March 15, 2005

Contents

Chapter 1

Introduction

The word POLYMER does not refer to a specific substance, but rather a phenomenon of molecular structure that is observed in nearly an infinite number of different materials. POLY is of the Greek origin and means many. MER means part or parts. A polymer is a chain-like molecule made up of many individual molecular components, called "monomers". Each monomer can in turn be a complex molecule. For example, let us take a look at the simple sketch below of a polypropylene molecule:

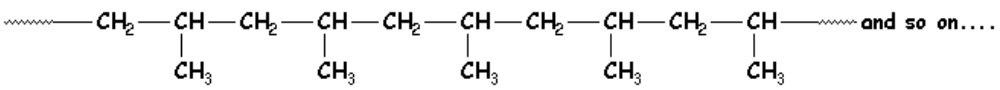

In this case, each monomer is a propylene molecule which consists of two carbon atoms. One carbon atom has two hydrogen atoms attached to it, and the other one has one hydrogen atom and one methyl group (CH3).

Polymers are abundant in nature (e.g. proteins, cellulose). Found to possess a unique variety of properties, they soon became an object of intensive research, encouraged by growing demands of industry. Insights in their molecular structure have led to the feasibility of designing and fabricating new materials with desired macroscopic properties. All this, together with the ease of processing, generated a vast market for polymers. As a consequence, in recent decades the number of available synthetic polymers has increased dramatically.

1.1 An industrial problem

Many fabrication processes of polymers involve an extrusion step, in which a molten polymer is forced to flow through a narrow shaping die, thereby acquiring the desired shape of the final product such as strand, tube or film. A simple sketch of an extruder is shown in Figure 1.1, in which the polymer

melt is conveyed into the die by a plunger. The final product, usually referred to as extrudate, has to fulfill specific requirements. For example, synthetic films, which are widely used in packing, must be transparent and smooth.

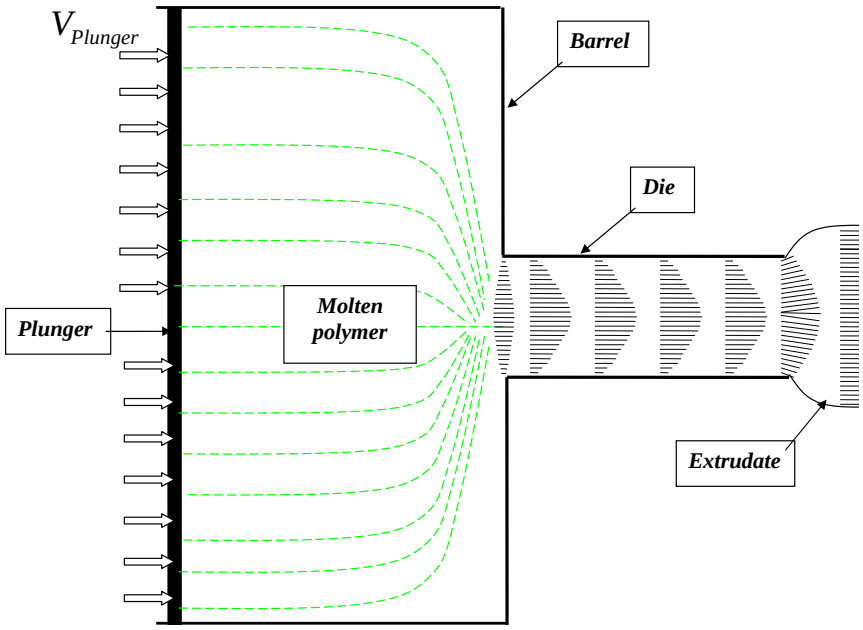

Figure 1.1: A simple extruder. The plunger moves at a constant speed, thus forcing the melt to flow through the shaping die. The thin lines indicate corresponding velocity profiles.

Economical stimuli demand fast operations with high extrusion rates. Unfortunately, it is observed that an increase in the extrusion speed often leads to a decrease in the quality of the extrudate. This phenomenon, visually observed as distortions and undulations of the extrudate, poses a serious problem for the polymer processing industry by limiting the production rates and technological opportunities of the polymeric materials. Different types of the extrudate distortions are commonly referred to as extrusion instabilities.

Classification of the extrusion instabilities could be based on the amplitude of the extrudate distortions. At low extrusion rates, no instabilities are observed and so the extrudate shows no distortions. When increasing the plunger speed, the first manifestation of the extrusion instabilities is often the appearance of distortions on the extrudate surface, which is usually referred to as "shark-skin". At higher extrusion rates, the extrudate emerges in periodic bursts, which is reflected in a pattern of pressure oscillations. This type of volume distortions is usually referred to as "spurt". At very high extrusion rates, no regular volumetric distortions are observed, and the extrudate is helically or chaotically disturbed. The sequence of the extrudate distortions during controlled flow rate extrusion of a linear low-density polyethylene (LLDPE) through a long stainless steel capillary is shown in Figure 1.2

1.2 Extrusion instabilities and wall slip

Extrusion instabilities were first observed during the Second World War [1] and afterwards reported by numerous authors. The recent experimental data on the extrusion instabilities can be found in the reviews [2, 3, 4]. Despite the fact that these phenomena are known for more than half a century, the understanding of their origin, together with the feasibility of predicting their occurrence during extrusion, is still a challenge. In order to explain the occurrence of the extrusion instabilities, various mechanisms were proposed, such as a nonmonotonous stress-strain relation, presence of an oscillating boundary layer, and wall slip. In the past, all these concepts evolved in parallel and had their own supporters.

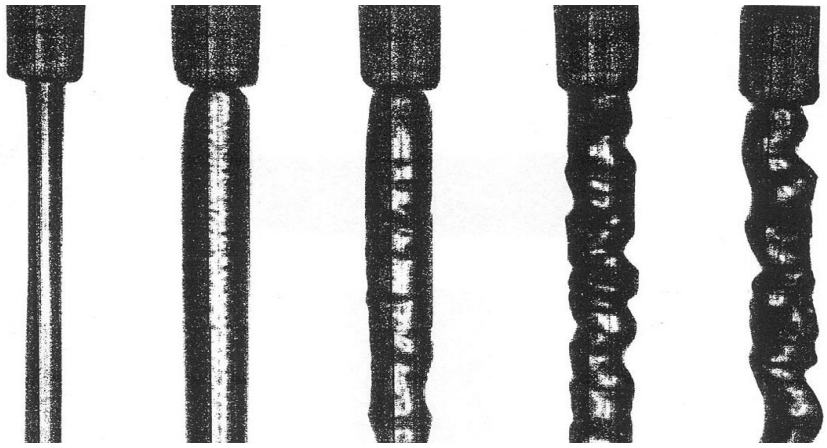

Figure 1.2: Five stages of a molten polyethylene flowing out of a die, visible at the top. The flow rate increases from left to right. Note that in the two leftmost photographs the extrudates are nice and smooth, while in the middle one undulations start to develop. As the flow rate increases even further towards the right, the amplitude of the undulations becomes stronger. When the flow rate is enhanced even more, the extrudate can break. From www.ilorentz.org

The latest developments in the experimental techniques made it possible to pinpoint the actual mechanism behind the extrusion instabilities. In particular, the recent experimental evidence suggests that some of the instabilities (e.g. spurt-like instabilities) originate from the violation of the no-slip boundary condition at the interface between the melt and the die wall. For example, Milner and coworkers [5] developed a novel technique, based on the Laser Doppler Velocimetry (LDV), which allows one to measure the velocity of the melt in close proximity to the die wall. They observed an apparent stick-to-slip transition prior to the onset of spurt oscillations. The experimentally observed connection between the wall slip and the extrusion instabilities has been recently reviewed in [6, 7, 8]. In contrast to polymer melts, the wall slip has never been observed for ordinary liquids (e.g. water).

The possibility of the wall slip for a polymer melt was first predicted by de Gennes [9]. He recognized that due to its high viscosity the melt should always show significant slippage when flowing over an ideal non-adsorbing surface,

whatever the flow rate. An ordinary liquid has a much smaller viscosity than the polymer melt and therefore does not show any measurable slip.

1.3 The Interfacial layer

In a real extrusion system, the polymer melt does not flow over the ideal non-adsorbing surface. In fact, due to the presence of attractive polymer-wall interaction, some of the molecules in the near-wall layer of the melt may become adsorbed on (or, equivalently, attached to) the wall (see Figure 1.3). In general, each of them makes several connections with the wall, thereby forming so-called loops and tails. The loop is a part of an adsorbed molecule between adjacent polymer-wall connection points. Both ends of the loop are attached to the wall. The tail is a part of an adsorbed molecule that has only one connection with the wall.

Every adsorbed chain has two tails. Despite they belong to the same molecule, their motions can be considered as being independent of each other. Hereafter, each tail will be regarded as a separate "tethered chain". The tethered chain is much more mobile than the loop. It can renew its spatial configuration via constraint release, retraction, or thermal fluctuations, whereas the loop by constraint release alone. Being severely restricted in motion, in the presence of flow loops will eventually be squeezed against the wall by the moving mesh of surrounding constraints, and thus will not interact with the flowing bulk. In this work, the dynamics of the loops is discarded, and instead the dynamics of the tethered chains is only considered.

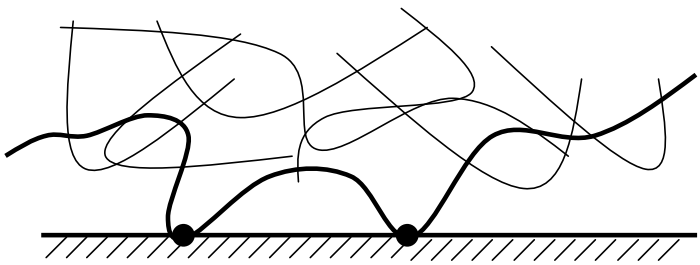

Figure 1.3: The interfacial layer. The thin and thick lines stand for bulk and surface molecules, respectively.

The adsorbed molecules (and accordingly the tethered chains) occupy a thin near-wall layer which separates the flowing bulk and the die wall. It will be referred to as the interfacial layer throughout the text. In the absence of flow, each tethered chain has its own length. However, as a first approximation, we will assume that at rest all the tethered chains in the interfacial layer have the same length equal to L_{0T}, their mean equilibrium length. We will also assume that unattached polymer molecules are monodisperse. Their equilibrium length will be denoted by L_{0B}. Later on, we will consider a more general

case in which the tethered chains and unattached molecules are allowed to have different molecular weights.

Attention must be paid to the fact that L_{0T} is not only a function of the molecular weight of the unattached polymer molecules, but also depends on the strength of the polymer-wall interaction. On a low surface energy wall, adsorbed molecules tend to have only one connection with the wall, so that $L_{0T} \approx L_{0B}/2$. In contrast, on a high surface energy wall, adsorbed molecules make on average several connections with the wall, and hence $L_{0T} << L_{0B}$.

The presence of the tethered chains in the near-wall layer implies that in the real extrusion system the polymer melt actually flows over a "polymer brush" made up of the tethered chains. Despite being attached to the wall, these tethered chains remain entangled with unattached polymer molecules in the polymer bulk. In what follows, the unattached molecules in the bulk will for short be referred to as "bulk molecules".

As shown by Brochard-Wyart and de Gennes [10], entanglements between bulk and tethered chains strongly reduce the interfacial fluid velocity at the polymer melt/die wall interface compared to the case of the melt flowing past the ideal non-adsorbing wall. On the basis of this observation, two mechanisms were proposed to explain the origin of slip. The first view, conceptualized by Bergem [11], suggests that slip stems from a sudden disentanglement between the adsorbed and bulk molecules at a certain critical stress. After the disentanglement, the polymer melt will slip on the die wall, covered by a "lubrication layer" of surface molecules smashed against the wall by the flow. Slip due to disentanglement is often referred to as "cohesive" slip.

The second view explains slip by adhesive failure of adsorbed polymer molecules on the die wall. Due to their entanglements with the bulk chains, in the presence of flow they undergo a certain flow-induced drag force which tends to detach them from the wall. A strong enough flow may cause a massive desorption of the adsorbed molecules after which the polymer melt slips over the "bare" die wall. This type of slip is usually referred to as "adhesive" slip.

1.4 Modeling of wall slip

In both slip scenarios, it is the dynamics of tethered chains that control the onset of slip. A number of theories have been proposed to model the behavior of the tethered chains and predict wall slip by either desorption or disentanglement. Theories that focus on the former can be found in [12, 13, 14, 15, 16, 17]. In particular, Lau and Schowalter [12] developed a simple model for adhesive slip, based on the activation rate kinetics of adsorption/desorption and Eyring's absolute rate theory. They argued that the wall shear stress σ_w alters

the activation energy of desorption and postulated a power law dependence of the slip velocity on σ_w above some critical stress for the onset of slip. A different perspective on adhesive slip was offered by Hill, Hasegawa, and Denn [13] who argued that normal stresses rather than shear stress control the onset of slip. Their relation between the slip velocity and wall shear stress is, however, virtually similar to that found by Lau and Schowalter. Stewart [14] further modified Lau and Showalter's theory by incorporating a proportionality of the bonding free energy to the polymer-wall work of adhesion. He proposed a simple linear relation between the critical wall shear stress for the onset of adhesive slip and work of adhesion at the melt /die wall interface.

Theories that predict slip via disentanglement can be found in [18, 19, 20, 21, 22]. The theoretical foundation for cohesive slip was developed by Brochard-Wyart and de Gennes [18] who proposed a scaling model for a polymer flow over a low-density brush of end-tethered chains of the same polymer. They imagined entanglements between these chains and nearby molecules in the bulk and postulated that the end-tethered chains undergo a coil-to-stretch transition at a critical shear stress. Since stretched chains cannot entangle with the bulk, this transition can be related to a transition to a strong slip. Further developments of this model can be found in Ajdari et al [19] and Mhetar and Archer [20]. Recently, Joshi et al [21, 22] proposed a molecular theory for cohesive slip based on the microscopic consideration of the near-wall layer and physical processes on the tethered chains. They argued that the tethered chains undergo a "suppressed" constraint release (SCR) whose strength determines the resistibility of the system to slip. Above a certain critical stress, the SCR is no longer able to prevent orientation of these chains by the flow which leads to a sudden disentanglement between the bulk and tethered chains.

In reality, both slip mechanisms occur in parallel and therefore should be studied simultaneously. Theories that include both disentanglement and desorption were proposed by Yarin and Graham [23] and Joshi et al [24]. The model of Yarin and Graham is based on a simplified description of the near-wall layer in which the tethered chains are represented as dumbbells that are rotated and stretched by the flow. The lifetime of a dumbbell is controlled by the amount of stretch gained by the dumbbell due to flow. The dumbbells are assumed to move independently of each other which restricts the scope of the model to rather low surface energy walls. Joshi and coworkers proposed an alternative way to the slip modeling based on the transient network theory, in which the entanglement network in the melt consists of junctions constantly created and annihilated due to the motion of the polymer chains. They show that with strain-dependent rates of formation f and loss g of junctions their model can predict the observed behavior of the stick-to-slip transition. However, a consistent derivation of the functional forms of f and g was not given, and instead some empirical forms were used.

The goal of the present work is to develop a molecular theory for slip which unites the two slip mechanisms into a single framework. The model must be valid over a wide range of wall materials and polymer melts including those for which desorption and disentanglement occur in parallel and thus must be considered self-consistently. The model must be applicable over a wide range of temperatures, in order to be able to interpret the observed rheological behavior. Finally, the model should be quantitative and contain only those parameters that can be measured directly or estimated from independent experimental data.

1.5 Thesis outline

This work is organized as follows: in chapter 2 we introduce a few basic concepts to represent flexible chains. These are the s_0 coordinates, the parameterized curve, and the bond vector. We also derive a "microscopic" equation of motion for the bond vectors of a tethered chain. In chapter 3, we introduce the bond vector correlator, an effective mathematical "tool" to describe the ensemble-averaged dynamics of tethered chains. Based on the microscopic equation of motion for the bond vectors of the tethered chain, the corresponding equation of motion for the bond vector correlator is derived, which accounts for all the major mechanisms for the tethered chains such as retraction, convection, constraint release, and contour length fluctuations. The contents of Chapter 2 and Chapter 3 is based on our previous work [25].

In chapter 4, the bond vector correlator of bulk chains is introduced. The equation of motion for this correlator is based on the microscopic equation of motion for the bond vectors of a bulk chain. The contents of Chapter 4 is based on our previous work [26]. In chapter 5, a molecular model for cohesive slip is formulated for the case of parallel plate geometry. This model does not allow for flow-induced detachment of adsorbed molecules, thus treating the surface density of tethered chains as a free parameter. In Chapter 6, this model is extended to include desorption. The contents of Chapter 5 and Chapter 6 is based on our earlier work [27] and [28], respectively. In Chapter 7, the effect of polydispersity of the bulk and tethered chains on the onset of wall slip is studied. The contents of Chapter 7 is partially developed in [29].

Chapter 2

Dynamics of tethered chains

As mentioned before, it is adsorbed molecules that play a key role in the polymer melt dynamics in the die. In this chapter, we will consider a case in which the polymer-wall interaction is strong enough to prevent their detachment. In this regime, tethered chains are considered to be grafted permanently on the wall, and slip only occurs via disentanglement. We will study all the major physical mechanisms inherent to tethered chains and derive an equation of motion for a single tethered chain in flow.

2.1 The tube concept

To begin with, let us first introduce the concept of the tube [30], applied for both tethered and bulk chains, which is widely used in modeling the behavior of entangled polymer melts. It was recognized that motions of a polymer chain in the melt orthogonal to its contour are severely restricted by the nearby molecules which impose topological constraints on the chain (see Figure 2.1). The Brownian motion of the chain implies fast oscillations of its contour within the mesh of the constraints. In a photograph of the chain taken with an exposure time much larger than the period of these oscillations, its Brownian motion will visualize as a "fuzzy" tube-like structure (see Figure 2.2). The diameter of this "tube" is of order the mean spacing between entanglements. The axis of the tube is often referred to as the primitive path of the polymer chain. Note that the length of the primitive path is normally much smaller than the actual length of the physical chain.

Photographing the chain with a finite exposure time is equivalent to time averaging over the corresponding time scale. This means that the motion of the primitive path only captures the time averaged behavior of the physical chain. In what follows, the motion of the physical chain will only be represented via the motion of its primitive path. Moreover, the primitive path of the chain will for short be referred to as "chain" throughout the text.

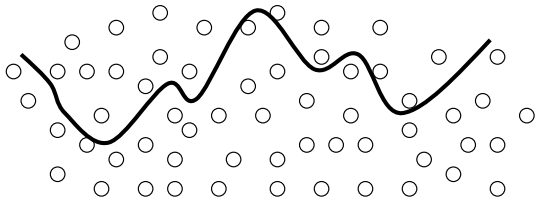

Figure 2.1: Chain in a melt. Open circles stand for surrounding molecules.

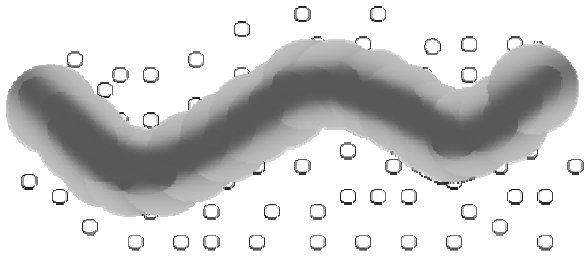

Figure 2.2: Tube.

2.2 Major physical mechanisms for tethered chains

On a microscopic level, as noticed by Joshi et al [21], the dynamics of tethered chains is governed by the following physical processes: convection, retraction, constraint release, and thermal fluctuations. Thermal fluctuations describe the Brownian motion of a tethered chain within the mesh of the surrounding constraints and can be visualized as fluctuations in the length of its primitive path. Convection describes the flow-induced deformation of a tethered chain by the moving constraints. It rotates the chain in the direction of the flow (see Figure 2.3). Convection tries to disentangle the tethered chain from the bulk and ultimately squeeze it against the die wall. Clearly, it is convection that causes wall slip in the absence of desorption.

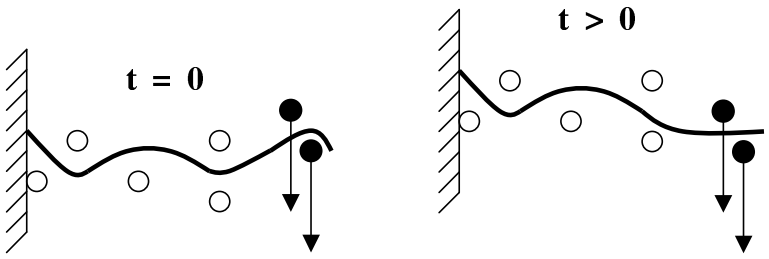

Figure 2.3: Convection.

Deformation of the tethered chain by the flow also implies that in the presence of flow the length of the primitive path may be larger than its equilibrium value. In other words, the flow stretches the primitive path of the chain. Due to the Brownian motion and the connectivity of the tethered chain, its primitive path tends to restore the equilibrium length by shrinking back within the mesh of constraints (see Figure 2.4). This mechanism will be referred to as retraction. Note that retraction works in parallel to convection.

Attention must be paid to the fact that the constraints on the tethered chain are not permanent. In fact, they are imposed by other polymer molecules whose motions may result in a sudden removal of one of them. After this, the chain contour can make a random local jump to a configuration which is

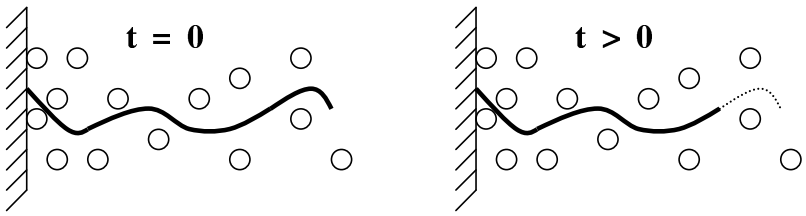

Figure 2.4: Retraction.

more favorable under the given conditions (see Figure 2.5). Each constraint release event permits the chain to move locally a distance of order the tube diameter, whereupon it finds itself once again constrained by the surrounding molecules. Constraint release "randomizes" configurations of tethered chains, thereby preventing their orientation by the flow. Whether slip will occur at a given flow rate in the absence of desorption is thus determined by the balance of convection and constraint release. The importance of constraint release in the dynamics of tethered chains was first recognized by Joshi et al [21].

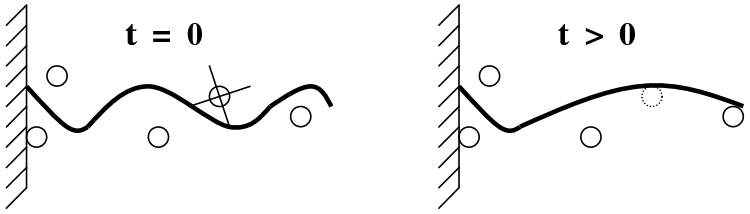

Figure 2.5: Constraint release.

2.3 The parameterized chain

Having introduced the concepts of tube and primitive path and established the major physical mechanisms for tethered chains, we now need a suitable coordinate system to address each segment of the primitive path of a tethered chain. One of the possible choices is to refer to it using its arclength $\hat{s}$ taken along the chain contour from the tethered end (see Figure 2.6). The description of the chain contour, that treats the arclength $\hat{s}$ as a curvilinear coordinate, is commonly used in the theory of monodisperse inextensible chains, for which the length of the primitive path always remains equal to its equilibrium value. Alternatively, the primitive path of the tethered chain can be presented as a three dimensional parameterized curve $\mathbf{R}(s_0, t)$ where parameter s_0 runs over a certain fixed interval $0...L_0$, the same for all tethered chains (see Figure 2.6). Here L_0 is an arbitrarily chosen number. The attached and free end of the tethered chain correspond to $s_0 = 0$ and $s_0 = L_0$, respectively.

The parameter s_0 "labels" the same physical segment of the primitive path at

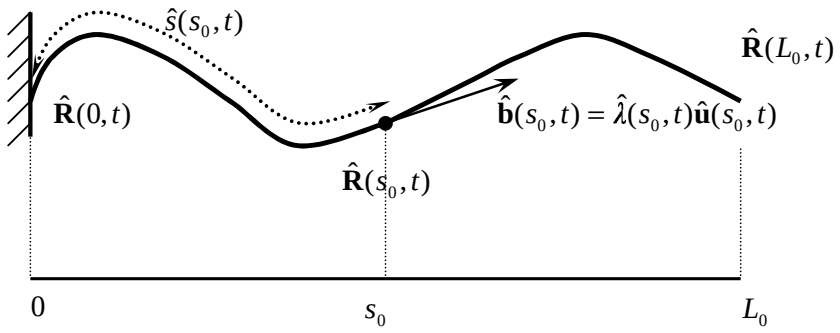

Figure 2.6: Parametrization of a tethered chain: $\hat{s}$ is the arclength of the segment s_0; $\hat{\mathbf{R}}(s_0,t)$ is the position vector at s_0 and time t; $\hat{\lambda}(s_0,t)$ and $\hat{\mathbf{u}}(s_0,t)$ are the local stretch and unit tangent vector at s_0 and time t, respectively.

all times, and therefore can be regarded as its coordinate. Note that different tethered chains "share" their parametrization interval with each other which implies that s_0 does not only address a certain segment of one tethered chain, but refers to alike segments of all the tethered chains. In contrast, $\mathbf{R}(s_0,t)$ specifies the spatial position of the segment of one particular tethered chain. Therefore, there are two types of variables present in the model: deterministic (i.e., fixed global variables such as s_0 and L_0) and stochastic (i.e., chain and time dependent variables such as $\mathbf{R}(s_0,t)$). Hereafter, in order to distinguish between them, the latter will be denoted by a hat sign.

Since we have freedom in choosing L_0, it is convenient to take L_0 as the equilibrium primitive path length of the tethered chain. So under the assumption that all the tethered chains have the same equilibrium length L_{0T}, parameter s_0 runs over the interval $0...L_{0T}$. With L_0 chosen as the equilibrium length of the primitive path, s_0 measures the equilibrium arclength of a chain segment along the primitive path. Its actual arclength $\hat{s}(s_0,t)$ (see Figure 2.6) is

$$\hat{s}(s_0,t)=\int_0^{s_0} dx\,\hat{\lambda}(x,t)\,,$$

where

$$\hat{\lambda}(s_0,t)=\frac{\partial\hat{s}(s_0,t)}{\partial s_0}\,. \tag{2.1}$$

Here $\hat{\lambda}(s_0,t)$ is local stretch of the primitive path of the chain at s_0 and time t. In the presence of flow, when polymer chains are stretched, $\hat{\lambda}(s_0,t)>1$ and therefore $\hat{s}\neq s_0$. At rest, $\hat{s}(s_0,t)\equiv s_0$ so that $\hat{\lambda}(s_0,t)\equiv 1$ along the chain contour. Note that in the presence of flow different polymer molecules show, in general, different amounts of stretch. In this case, both $\hat{s}(s_0,t)$ and $\hat{\lambda}(s_0,t)$ become chain-dependent and should be denoted by the hat sign.

Every tethered chain in the interfacial layer has its own parametrization function $\hat{\mathbf{R}}(s_0,t)$ which reflects the evolution of its primitive path in time. Once

$\hat{\mathbf{R}}(s_0,t)$ is known, the dynamics of the chain is completely defined. Alternatively, the spatial configuration of the primitive path can be described in terms of so-called "bond vectors" which are defined as follows

$$\hat{\mathbf{b}}(s_0,t) = \frac{\partial \hat{\mathbf{R}}(s_0,t)}{\partial s_0}\,. \tag{2.2}$$

As follows from eqn.(2.1) and eqn.(2.2), the modulus of $\hat{\mathbf{b}}(s_0,t)$ coincides with the local stretch $\hat{\lambda}(s_0,t)$ of the primitive path at s_0 and time t. The orientation of the bond vector $\hat{\mathbf{b}}(s_0,t)$ at a certain point along the chain contour is described by the unit vector $\hat{\mathbf{u}}(s_0,t)$ defined as

$$\hat{\mathbf{u}}(s_0,t) = \frac{\hat{\mathbf{b}}(s_0,t)}{|\hat{\mathbf{b}}(s_0,t)|}\,. \tag{2.3}$$

As shown in Figure 2.6, $\hat{\mathbf{u}}(s_0,t)$ coincides with the unit tangent to the primitive path at s_0 and time t and therefore specifies local orientation of the chain contour. Note that both the local stretch $\hat{\lambda}$ and local orientation $\hat{\mathbf{u}}$ pertain to a single tethered chain and hence carry a hat sign.

Once the parametrization function $\hat{\mathbf{R}}(s_0,t)$ of every tethered chain in the interfacial layer is known, the dynamics of the layer is completely defined. In practice, however, such a detailed description is not necessary. In fact, in order to calculate various macroscopic properties of the layer, such as the wall stress or layer thickness, we only need to know certain averages over the ensemble of tethered chains. The bond vector $\hat{\mathbf{b}}(s_0,t)$ of a tethered chain contains information on both its local stretch and local orientation, and therefore can also be used to describe the single tethered chain dynamics and ultimately to calculate the macroscopic properties of the layer. As will be shown later on, for the calculation of the macroscopic properties, which involves averaging over the ensemble of tethered chains, the description based on the bond vectors turns out to be the most convenient one. In the next chapter, we will demonstrate that using the bond vectors allows one to develop a simple, yet accurate, mathematical formalism able to represent the behavior of the ensemble of tethered chains in flow.

2.4 The equation of motion for the bond vector

Having introduced the coordinate system, we may now derive the equation of motion for a single tethered chain in a flow. We will first consider retraction and convection in the absence of constraint release and contour length fluctuations. Let us point out a tethered chain in the interfacial layer. Figure 2.7 shows two snapshots of the chain taken at time t and $t+\Delta t$ (where Δt

is small). Next, let us choose a segment on the chain contour, say s_0, and follow its trajectory between t and $t+\Delta t$. If $\hat{\mathbf{R}}(s_0,t)$ is the position vector of segment s_0 at time t, then that at time $t+\Delta t$ can be symbolically written as $(\bar{\bar{\mathbf{A}}}*\bar{\bar{\mathbf{B}}})\hat{\mathbf{R}}(s_0,t)$, where operators $\bar{\bar{\mathbf{A}}}$ and $\bar{\bar{\mathbf{B}}}$ describe the motion of the segment (between t and $t+\Delta t$) due to convection and retraction, respectively. Here operator $(\bar{\bar{\mathbf{A}}}*\bar{\bar{\mathbf{B}}})$ represents the combined action of retraction and convection.

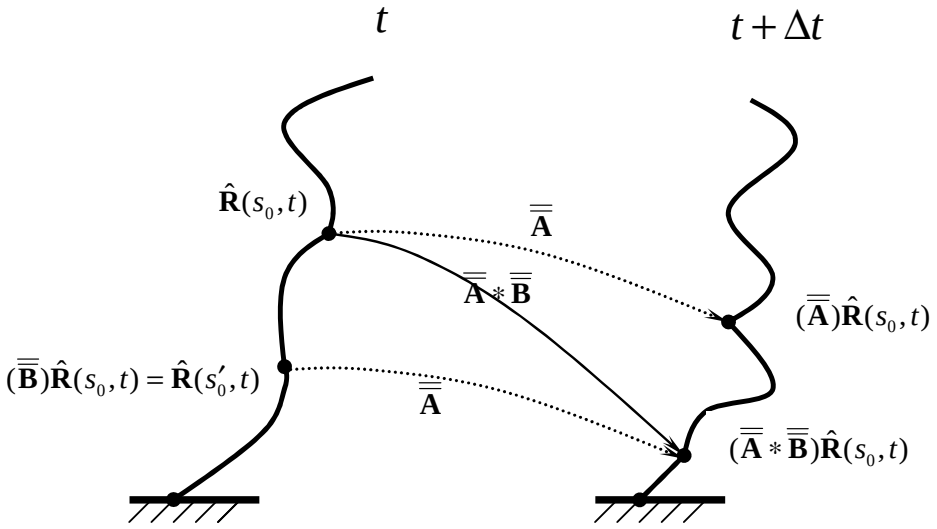

Figure 2.7: Time evolution of a tethered chain. The $\bar{\bar{\mathbf{A}}}$-operator determines how the primitive path is deformed by the flow. The $\bar{\bar{\mathbf{B}}}$-operator describes retraction of the test chain.

The complex motion of segment s_0 due to retraction and convection can be visualized as a two step process. First, it "slides along" the chain contour to a certain position s_0', which satisfies the following equation (see Figure 2.7)

$$\hat{\mathbf{R}}(s_0',t) = (\bar{\bar{\mathbf{B}}})\hat{\mathbf{R}}(s_0,t) = \hat{\mathbf{R}}(s_0+\Delta\hat{s}_0,t)\,, \tag{2.4}$$

where $\Delta\hat{s}_0 = s_0' - s_0$. Then, the chain is convected in the absence of retraction so that segment s_0' finally arrives at $(\bar{\bar{\mathbf{A}}}*\bar{\bar{\mathbf{B}}})\hat{\mathbf{R}}(s_0,t)$, as depicted in Figure 2.7. Comparison between the two snapshots of the test chain yields

$$\hat{\mathbf{R}}(s_0,t+\Delta t) = (\bar{\bar{\mathbf{A}}}*\bar{\bar{\mathbf{B}}})\hat{\mathbf{R}}(s_0,t) = (\bar{\bar{\mathbf{A}}})\hat{\mathbf{R}}(s_0',t) = (\bar{\bar{\mathbf{A}}})\hat{\mathbf{R}}(s_0+\Delta\hat{s}_0,t) \tag{2.5}$$

Note that $\Delta\hat{s}_0$ is not equal to the physical distance passed by segment s_0 along the chain contour due to retraction between t and $t+\Delta t$. It gives the distance between segment s_0 and virtual segment s_0' measured along the parametrization axis. $\Delta\hat{s}_0(s_0,t)$ can be written as a product $\hat{v}_0(s_0,t)\Delta t$, where $\hat{v}_0(s_0,t)$ is the velocity (at time t) at which segment s_0 moves along the axis due to retraction. The retraction velocity $\hat{v}_0(s_0,t)$ is defined by

$$\hat{v}_0(s_0,t) = \lim_{\Delta t\to 0}\frac{\Delta\hat{s}_0(s_0,t)}{\Delta t}\,. \tag{2.6}$$

According to [31], for small Δt the convection operator $\bar{\bar{\mathbf{A}}}$ can be expanded in powers of Δt as $\bar{\bar{\mathbf{A}}} = \bar{\bar{\mathbf{1}}} + \bar{\bar{\mathbf{K}}}^I\Delta t + O(\Delta t^2)$, where $\bar{\bar{\mathbf{1}}}$ is the unit tensor and

$\bar{\bar{\mathbf{K}}}^I$ the so-called gradient velocity tensor whose $\alpha\beta$ component is given by

$$K^I_{\alpha\beta}(\mathbf{r},t) = \frac{\partial V_\alpha(\mathbf{r},t)}{\partial r_\beta}\,, \tag{2.7}$$

where $\mathbf{V}(\mathbf{r},t)$ is the fluid velocity at position $\mathbf{r}$ in the interfacial layer. In general, $\mathbf{V}(\mathbf{r},t)$ can be written as $\overline{\mathbf{V}}(\mathbf{r},t) + \delta\mathbf{v}(\mathbf{r},t)$, where $\overline{\mathbf{V}}(\mathbf{r},t)$ is the "macroscopic" velocity of monomers induced by the flow and $\delta\mathbf{v}(\mathbf{r},t)$ pertains to their "microscopic" Brownian motions. $\delta\mathbf{v}(\mathbf{r},t)$ rapidly oscillates in time with the period T equal to that of the thermal oscillations. On the other hand, the primitive path of the tethered chain only captures its time-averaged behavior with the time scale much larger than T. Since in our case the tensor $\bar{\bar{\mathbf{K}}}^I$ describes the flow-induced deformation of the primitive path, the actual velocity profile $\mathbf{V}(\mathbf{r},t)$ in eqn.(2.7) must be replaced with macroscopic $\overline{\mathbf{V}}(\mathbf{r},t)$.

With the help of the gradient velocity tensor $\bar{\bar{K}}^I$, eqn.(2.5) now reads as

$$\hat{\mathbf{R}}(s_0, t+\Delta t) = [\bar{\bar{\mathbf{1}}} + \bar{\bar{\mathbf{K}}}^I(t)\Delta t + O(\Delta t^2)]\,\hat{\mathbf{R}}(s_0 + \hat{v}_0\,\Delta t, t)\,, \tag{2.8}$$

where the expression in square brackets determines the deformation of the contour of the tethered chain produced by the flow over the small time interval between t and $t+\Delta t$. Note that the interfacial layer is rather thin. Its thickness is normally much smaller than the length of bulk polymer chains. This implies that the velocity profile $\overline{\mathbf{V}}(\mathbf{r},t)$ in the layer can be approximated linear so that the spatial dependence in $\bar{\bar{K}}^I$ can be dropped. Furthermore, in a simple shear flow $\bar{\bar{K}}^I$ has only one non-zero component equal to the wall shear rate $\dot{\gamma}_w$.

According to eqn.(2.2), given an equation of motion for $\hat{\mathbf{R}}(s_0,t)$, one can readily find the one for $\hat{\mathbf{b}}(s_0,t)$. Namely, by differentiating both sides of eqn.(2.8) with respect to s_0 and taking the limit $\Delta t \to 0$, the equation of motion for the bond vector $\hat{\mathbf{b}}(s_0,t)$ takes the form

$$\frac{\partial\hat{\mathbf{b}}(s_0,t)}{\partial t} = \bar{\bar{\mathbf{K}}}^I(t)\cdot\hat{\mathbf{b}}(s_0,t) + \frac{\partial}{\partial s_0}\left(\hat{v}_0(s_0,t)\,\hat{\mathbf{b}}(s_0,t)\right). \tag{2.9}$$

Eqn.(2.9) has the form of a balance equation and contains two contributions on the RHS. The first one pertains to convection, and therefore describes affine "stretching" and "rotation" of the bond vector by the flow. The second term stems from retraction and describes "sliding" and "shrinking" of the bond vector along the chain contour. Multiplying both sides of eqn.(2.9) by the unit vector $\hat{\mathbf{u}}(s_0,t)$ and taking into account that $\hat{\mathbf{b}} = \hat{\lambda}\hat{\mathbf{u}}$, one finds that

$$\frac{\partial\hat{\lambda}(s_0,t)}{\partial t} = \bar{\bar{\mathbf{K}}}^I(t)\cdot\hat{\mathbf{b}}(s_0,t)\cdot\hat{\mathbf{u}}(s_0,t) + \frac{\partial}{\partial s_0}\left(\hat{v}_0(s_0,t)\,\hat{\lambda}(s_0,t)\right).$$

Next, integrating both sides of this equation over s_0 from 0 to x and taking into account that at the tethered end $\hat{v}_0 = 0$, we finally find that the retraction

velocity $\hat{v}_0(x,t)$ can be written as

$$\hat{v}_0(x,t) = \frac{1}{\hat{\lambda}(x,t)} \int_0^x ds_0\, \hat{\xi}(s_0,t) \;\;,\;\; \hat{\xi} = \frac{\partial \hat{\lambda}}{\partial t} - K^I_{\alpha\beta} \hat{u}_\alpha \hat{u}_\beta \hat{\lambda}\,. \tag{2.10}$$

Here summation is implied over the repeated indices. In eqn.(2.10), $\hat{\xi}(s_0,t)$ is the local retraction rate of the primitive path of the tethered chain at s_0 and time t. The integral in eqn.(2.10) gives the velocity at which segment x of the tethered chain slides along its contour due to retraction. It is in turn equal to $\partial \hat{s}(x,t)/\partial t$, where $\hat{s}(x,t)$ is the actual arclength of segment x. So eqn.(2.10) shows that the retraction velocity $\hat{v}_0(x,t)$ of segment x is equal to its velocity along the chain contour divided by the corresponding local stretch $\hat{\lambda}(x,t)$.

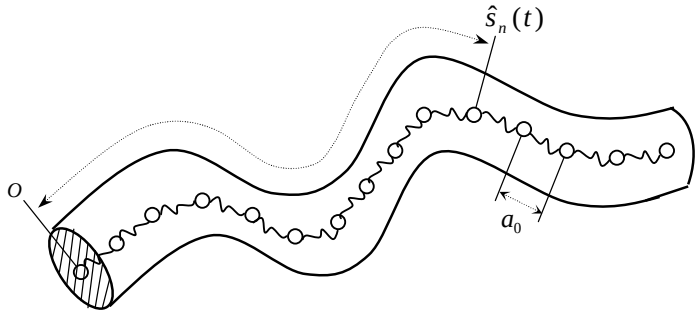

Figure 2.8: A tethered chain as a bead-spring system.

The local retraction rate $\hat{\xi}(s_0,t)$ describes relaxation of the local stretch of the primitive path due to the connectivity and the Brownian motion of the physical chain. According to eqn.(2.10), its explicit form can be found by studying relaxation of an initially stretched chain in the absence of flow (i.e., $\bar{\bar{K}}^I = 0$). In order to calculate $\hat{\xi}(s_0,t)$, let us first recall that the primitive path represents the time averaged behavior of the physical chain. Due to the presence of constraints and connectivity of the physical chain, motions of the neighboring segments of the primitive path are not independent [31]. Let a be the characteristic equilibrium correlation length between different segments of the primitive path. Then, motions of segments s_0 and s_0' for which $|s_0 - s_0'| > a$ can be considered as being independent of each other. Apparently, a is of order of the mean equilibrium distance between entanglements. In the literature, a is often referred to as the step length of the primitive path.

If L_{0T} is the equilibrium length of the primitive path, then the chain contour can be divided into $Z_T = L_{0T}/a$ discrete segments, each can "rotate" independently of its neighbors. Each of these segments contains on average $N_e = N_T/Z_T$ monomers, where N_T is the total number of monomers per tethered chain. So at equilibrium each tethered chain in the melt can be presented as a freely-jointed chain [31] which consists of $Z_T + 1$ beads connected by Z_T bonds. At rest, all the bonds have the same length a. In a flow, however, each

bond is allowed to have its own length. Due to the connectivity and the Brownian motion of the physical chain, the bonds are elastic. So in the flow they can be replaced by elastic springs (see Figure 2.8). Clearly, representation of the tethered chain by the bead-spring system allows to capture its flexibility and elasticity, as well as possible chain stretch induced by the flow.

The dynamics of the bead-spring system can readily be inferred from the Rouse model [31, 32]. Let $\hat{\mathbf{R}}_n(t)$ be the position vector of the n-th bead at time t. Following to Doi and Edwards [31], a microscopic force balance for the bead yields the following equation of motion for $\hat{\mathbf{R}}_n(t)$

$$m\frac{\partial^2\hat{\mathbf{R}}_n(t)}{\partial t^2} = -N_e\zeta\frac{\partial\hat{\mathbf{R}}_n(t)}{\partial t} + \frac{3k_BT}{a^2}\left[\hat{\mathbf{R}}_{n+1}(t) + \hat{\mathbf{R}}_{n-1}(t) - 2\hat{\mathbf{R}}_n(t)\right], \quad (2.11)$$

where m, k_B, T, and ζ are the mass of a bead, the Boltzmann constant, the absolute temperature, and the monomeric friction coefficient, respectively. In eqn.(2.11), we took into account that in our case the equilibrium length of each spring is equal to a and each bead contains approximately N_e monomers so that its friction coefficient is of order $N_e\zeta$. The first term on the RHS describes friction between the bead and the neighboring polymers. The second term stems from the elasticity of the springs, where $3k_BT/a^2$ is the spring constant. The term on the LHS is the inertial term. Since for a realistic polymer chain in a melt the mass of a bead and its accelerations are normally small, the inertia term can be neglected in comparison to the other contributions.

Note that for long enough tethered chains eqn.(2.11) can be written in terms of the s_0-coordinates introduced earlier. Namely, keeping in mind that $n \approx s_0/a$, the second term on the RHS of eqn.(2.11) can be approximated by a second derivative with respect to s_0. Therefore,

$$\frac{\partial\hat{\mathbf{R}}(s_0,t)}{\partial t} \approx \frac{3k_BT}{N_e\zeta}\frac{\partial^2\hat{\mathbf{R}}(s_0,t)}{\partial s_0^2}\,. \quad (2.12)$$

Eqn.(2.12) describes the trajectory of segment s_0 of the tethered chain due to retraction. In reality, it only slides along the chain contour whose local orientation is given by the unit tangent vector $\hat{\mathbf{u}}(s_0,t)$ (see eqn.(2.3)). Projection of eqn.(2.12) on the chain contour then yields

$$\hat{\mathbf{u}}\cdot\frac{\partial\hat{\mathbf{R}}}{\partial t} = \frac{3k_BT}{N_e\zeta}\frac{\partial\hat{\lambda}}{\partial s_0}\,. \quad (2.13)$$

where use was made of eqn.(2.1) and eqn.(2.2). The inner product on the LHS of eqn.(2.13) gives the actual velocity of segment s_0 along the chain contour equal to $\partial\hat{s}(s_0,t)/\partial t$. As discussed earlier, this velocity is in turn equal to the integral over the local retraction rate $\hat{\xi}$ in eqn.(2.10). Therefore, differentiation of both sides of eqn.(2.13) with respect to s_0 yields

$$\hat{\xi} = \frac{3k_BT}{N_e\zeta}\frac{\partial^2\hat{\lambda}}{\partial s_0^2}\,. \quad (2.14)$$

Eqn.(2.14) shows that relaxation of the local stretch can be visualized as one-dimensional diffusion of monomers along the chain contour. In other words, retraction originates from a fast local rearrangement of monomers along the primitive path. Finally, from eqn.(2.10) and eqn.(2.14), one may conclude that the equation of motion for the local stretch has the form of a diffusion equation with the source term given by $K^I_{\alpha\beta}\hat{u}_\alpha\hat{u}_\beta\hat{\lambda}$. The source term is proportional to the flow-induced velocity of segment s_0 along the chain contour towards the free end of the chain and therefore describes local stretching of the primitive path by the flow

Let us show now that in some cases the explicit form of $\hat{\xi}$ can be further simplified. As follows from eqn.(2.14), relaxation of the local stretch $\hat{\lambda}$ is governed by the following equation of motion

$$\frac{\partial\hat{\lambda}}{\partial t} = \frac{3k_BT}{N_e\zeta}\frac{\partial^2\hat{\lambda}}{\partial s_0^2}\,. \tag{2.15}$$

To solve it, we need to specify the boundary conditions for $\hat{\lambda}$. The relaxation time of segments of the tethered chain near the free end is of order τ_e, the Rouse time of one entanglement segment. According to Doi and Edwards [31], τ_e is equal to $3k_BT/a^2N_e\zeta$. Note that τ_e is of order the period of the Brownian oscillations of the physical chain. On the other hand, $\hat{\lambda}$ describes the local stretch of the primitive path. Therefore, due to fast retraction processes active at the free end of the physical chain, the corresponding stretch of the primitive path can be neglected so that $\hat{\lambda}(L_{0T},t)=1$. On the other hand, the segments near the tethered end have the largest relaxation time since their relaxation requires retraction of all other chain segments. This means that the local stretch at the tethered end is maximal, and so $\partial\hat{\lambda}/\partial s_0 = 0$ if $s_0 = 0$.

Applying standard techniques and taking into account the boundary conditions for $\hat{\lambda}$, the solution of eqn.(2.15) can be written in the form

$$\hat{\lambda}(s_0,t) = 1 + \sum_{p=1,3,5,\ldots}^{\infty} \hat{C}_p e^{-p^2t/T_{RT}}\,\cos\left(\frac{p\pi s_0}{2L_{0T}}\right), \tag{2.16}$$

where

$$T_{RT} = \frac{4\zeta N_e L_{0T}^2}{3\pi^2 k_BT}\,. \tag{2.17}$$

The coefficients $\hat{C}_p$ are determined by the initial condition for $\hat{\lambda}(s_0,t)$. As is seen from eqn.(2.16), relaxation of the local stretch is described by a set of relaxation times $T_p = T_{RT}/p^2$, where $p = 1,3,5,\ldots$. Hereafter, the longest relaxation time T_{RT} will be referred to as the Rouse time of tethered chains. In view of eqn.(2.16), T_{RT} is the decay time of the first mode ($p=1$) in the relaxation spectrum of $\hat{\lambda}$. The second mode has the decay time which is nearly

ten times smaller than T_{RT}. So on the time scale of T_{RT} the high order modes with $p = 3, 5, \ldots$ can be considered as relaxing instantaneously.

According to eqn.(2.15), the characteristic relaxation time of the local stretch for the "interior" segments of the tethered chain is of order $3k_BT/L_{0T}^2 N_e\zeta$, which is in turn of order T_{RT}. So for flows whose time scale is larger than T_{RT}, T_{RT} can be chosen as the smallest time scale for these segments. As a result, the high order modes in eqn.(2.16) can be neglected and only the first mode may be considered. Then, from eqn.(2.16) one can find that in this case the local retraction rate $\hat{\xi}$ can be approximated by

$$\hat{\xi} \approx -\frac{\hat{\lambda} - 1}{T_{RT}}\,. \tag{2.18}$$

Hereafter, this approximation will be referred to as the single relaxation time approximation. Note that it may not be applicable to segments of the tethered chain near the free end. As mentioned earlier, the characteristic relaxation time of these segments and accordingly the time scale associated with them is much smaller than T_{RT}. So the proper description of relaxation of the local stretch for these segments requires consideration of many modes in eqn.(2.16).

2.5 Constraint release (CR)

Until now, we have derived the equation of motion for the single tethered chain in flow which includes convection and retraction. In this section, we will study constraint release (CR) on the chain and extend this equation to include CR. As discussed earlier, every constraint release event allows the chain contour to "jump" locally over a distance of order the mean spacing a_0 between entanglements. Verdier and Stockmayer [33] developed a simple model which allows one to describe CR as a sequence of local random jumps, as depicted in Figure 2.9. Following their model, we again present the tethered chain as a system of $Z_T + 1$ beads connected by Z_T springs. Each spring has the equilibrium length equal to a, the equilibrium step length of the primitive path. In a small time interval Δt, internal beads make the following jumps:

$$\mathbf{R}_n \rightarrow (\mathbf{R}_{n+1} + \mathbf{R}_{n-1} - \mathbf{R}_n) \tag{2.19}$$

with probability $\nu_T \Delta t$, where ν_T is the characteristic frequency of constraint release on tethered chains. Here $\mathbf{R}_n$ is the position vector of the n-th bead. The probability for $\mathbf{R}_n$ not to jump during the time interval Δt is equal to $1 - \nu_T \Delta t$. From the above, the equation of motion for the position vector $\mathbf{R}_n$ due to constraint release can therefore be written as

$$\frac{\partial \mathbf{R}_n(t)}{\partial t} = \nu_T \Big[\mathbf{R}_{n+1}(t) + \mathbf{R}_{n-1}(t) - 2\mathbf{R}_n(t)\Big]\,. \tag{2.20}$$

Similar to eqn.(2.11), for long enough tethered chains eqn.(2.20) can be rewritten in terms of the s_0-coordinates. Taking into account that $n \approx s_0/a$, from eqn.(2.20) we finally arrive at

$$\frac{\partial \hat{\mathbf{R}}(s_0,t)}{\partial t} \approx \nu_T a^2 \frac{\partial^2 \hat{\mathbf{R}}(s_0,t)}{\partial s_0^2}\,. \tag{2.21}$$

As is seen, the equation of motion for the tethered chain due to CR has the form of a diffusion process with the coefficient proportional to the corresponding frequency ν_T of constraint release. The coefficient makes it explicit that the local jumps of the chain contour occur at the rate equal to ν_T and each jump is over a distance of order the mean entanglement spacing.

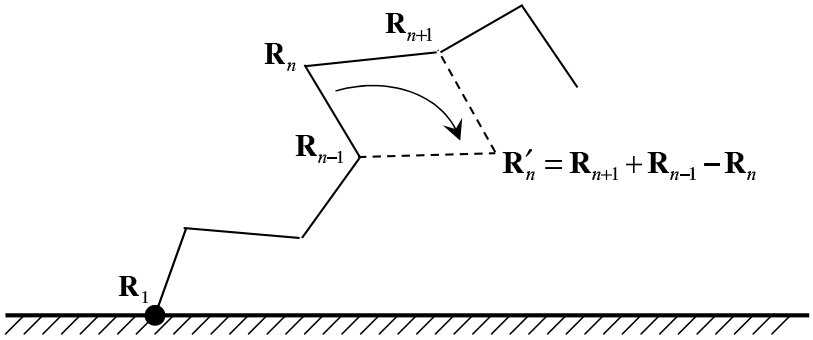

Figure 2.9: Local jump model.

A more rigorous approach to model CR was developed by Viovy et al [34]. They recognized that, as constraints are released at the same rate on all parts of the tube, CR yields a Brownian-like motion of the tube itself. This implies that the motion of the primitive path due to CR can be interpreted as a Rouse process [31]. Based on this observation, Milner et al [35] proposed the following equation of motion for a polymer chain in the melt due to CR

$$\frac{\partial \hat{\mathbf{R}}(s_0,t)}{\partial t} = \nu_T a_0^2 \frac{\partial \hat{\mathbf{R}}(s_0,t)}{\partial s_0^2} + \mathbf{g}(s_0,t)\,, \tag{2.22}$$

where a_0 is the mean entanglement spacing and $\mathbf{g}(s_0,t)$ a delta-correlated, zero-mean noise vector. Eqn.(2.22) has the form of a Langevin equation. Since $a \approx a_0$, it agrees well with the earlier result in eqn.(2.21) obtained from the simple bond-flip model. By the fluctuation-dissipation theorem, the components of $\mathbf{g}(s_0,t)$ are related to the frequency ν_T as follows

$$< g_\alpha(s_0,t) g_\beta(s_0',t') >= \frac{2}{3}\nu_T a_0^3 \delta(t-t')\delta(s_0-s_0')\delta_{\alpha\beta}\,. \tag{2.23}$$

where $< ... >$ denote averaging over tethered chains. Components of $\mathbf{g}(s_0,t)$ taken at different times or positions along the chain are uncorrelated, as is typical for the Rouse process. To conclude, eqns.(2.9, 2.22) describe the evolution of the single tethered chain in flow governed by convection, retraction, and constraint release. In the next chapter, these equations will further be used to derive the "macroscopic" equation of motion for the interfacial layer.

Chapter 3

Equation of motion for the interfacial layer

Based on the "microscopic" consideration of the interfacial layer, in the previous chapter we studied the dynamics of a single tethered chain in flow. In practice, however, we only need to know the behavior of the entire ensemble of tethered chains present in the layer. Here the dynamics of this ensemble will be studied and the corresponding constitutive equation will be derived.

3.1 The bond vector correlator

In order to quantify the dynamics of the ensemble of tethered chains, let us introduce the following tensor $\mathbf{S}^T(s_0,t)$ whose components are given by

$$S^T_{\alpha\beta}(s_0,t) =< \hat{b}_\alpha(s_0,t)\hat{b}_\beta(s_0,t) >_T , \tag{3.1}$$

where b_α is the α component of the bond vector of a tethered chain and $< \ldots >_T$ denote averaging over the ensemble. Parameter s_0 in eqn.(3.1) runs from 0 to L_{0T}, the equilibrium length of the tethered chains. The tensor $\mathbf{S}^T(s_0,t)$ will be referred to as the "bond vector correlator" throughout the text. The superscript T in $\mathbf{S}^T(s_0,t)$ indicates that this tensor pertains to tethered chains. Note that the averaging over the ensemble in eqn.(3.1) can be replaced with averaging over all possible values of the bond vector, that is

$$S^T_{\alpha\beta}(s_0,t) = \int\limits_{\mathbb{R}^3} d^3\mathbf{b}\, b_\alpha b_\beta\, f_T(\mathbf{b},s_0,t)\,. \tag{3.2}$$

Here $f_T(\mathbf{b},s_0,t)$ is the bond vector probability distribution function (BVPDF), a fraction of the tethered chains whose bond vector $\hat{\mathbf{b}}$ at s_0 and time t is equal

to $\mathbf{b}$. By definition, the BVPDF is normalized

$$\int_{\mathbb{R}^3} d^3\mathbf{b}\ f_T(\mathbf{b}, s_0, t) = 1\,.$$

At rest, tethered chains are not stretched so that $\hat{\mathbf{b}} = \hat{\mathbf{u}}$, where $\hat{\mathbf{u}}$ is the corresponding unit tangent vector to the chain contour (see Figure 2.6). By definition, every tethered chain has only one connection with the die wall (at $s_0 = 0$). The attractive potential of the wall is localized on its surface. The above implies that segments of the chain far from the tethered end do not "feel" the non-anisotropy of the melt caused by the presence of the wall. As a result, in the absence of flow all directions of the bond vector for these segments are equally probable, and $f_T(\mathbf{b}, s_0, t)$ is isotropic. From eqn.(3.2) it then follows that at equilibrium $S^T_{\alpha\beta}(s_0, t)$ for $s_0 > 0$ is diagonal and equal to

$$S^{(eq)}_{\alpha\beta}(s_0, t) = \frac{1}{3}\delta_{\alpha\beta}\,, \tag{3.3}$$

where we used that in the absence of stretch $S^T_{\alpha\alpha} = 1$.

As shown earlier, the bond vector $\hat{\mathbf{b}}$ can be written as the product $\hat{\lambda}\hat{\mathbf{u}}$, where $\hat{\lambda}$ is the local stretch and $\hat{\mathbf{u}}$ the local orientation of the chain contour. This means that the correlator $S^T_{\alpha\beta}(s_0, t)$ contains information on both the average local stretch and the average local orientation of the tethered chains. Note that in the absence of stretch (i.e., $\lambda = 1$), $S^T_{\alpha\beta}(s_0, t)$ boils down to the orientation tensor $< \hat{\mathbf{u}}\hat{\mathbf{u}} >_T$ similar to one introduced by Doi and Edwards [31] to describe the dynamics of bulk inextensible chains. Clearly, the bond vector correlator provides an extension of the original orientation tensor of Doi and Edwards to systems which allow chain stretch.

Once the correlator $S^T_{\alpha\beta}(s_0, t)$ of the ensemble of tethered chains is known, one can readily calculate various parameters of the ensemble. For example, following Doi and Edwards [31], the local stress $\sigma^I_{\alpha\beta}$ induced in the chains by the flow is proportional to the value of $S^T_{\alpha\beta}$ averaged along the chain contour:

$$\sigma^I_{\alpha\beta}(t) = \frac{G_{0I}}{L_{0T}} \int_0^{L_{0T}} ds_0\, S^T_{\alpha\beta}(s_0, t)\,. \tag{3.4}$$

Here G_{0I} is the elastic modulus of the interfacial layer. Later on, we will calculate G_{0I} in terms of the molecular parameters of the melt and the surface density of tethered chains. Eqn.(3.4) reveals that the equation of motion for $S^T_{\alpha\beta}$ is in fact the constitutive equation for the ensemble of tethered chains.

3.2 The equation of motion for the bond vector correlator

Let us first derive the equation of motion for the bond vector correlator $S^T_{\alpha\beta}(s_0,t)$ of tethered chains in the absence of constraint release and contour length fluctuations. By differentiating eqn.(3.1) with respect to time and taking into account eqn.(2.9), one can find (for $s_0 > 0$)

$$\frac{\partial S^T_{\alpha\beta}}{\partial t} = K^I_{\alpha\gamma} S^T_{\beta\gamma} + K^I_{\beta\gamma} S^T_{\alpha\gamma} + \frac{\partial}{\partial s_0} < \hat{b}_\alpha \hat{b}_\beta \hat{v}_0 >_T + < \hat{b}_\alpha \hat{b}_\beta \frac{\partial \hat{v}_0}{\partial s_0} >_T \ . \qquad (3.5)$$

Here the first two terms on the RHS pertain to convection. Since $S^T_{\alpha\beta}$ contains information on both the mean local stretch and the mean local orientation of the tethered chains, these terms make it explicit that convection stretches and rotates the tethered chains, as was discussed earlier. The last two terms stem from retraction. They are proportional to the local retraction velocity $\hat{v}_0$ introduced earlier in eqn.(2.10). According to eqn.(2.10), $\hat{v}_0(s_0,t)$ depends on the local stretch of segments x of the tethered chains which satisfy $0 \leq x \leq s_0$. This implies that the retraction terms in eqn.(3.5) are "nonlocal" with respect to s_0. In order to evaluate them, let us introduce the two-point BVPDF $f^{(2)}_T(\mathbf{b}, s_0 | \mathbf{b}', s_0', t)$, which is the probability for a tethered chain to have (at time t) bond vectors at s_0 and s_0' equal to $\mathbf{b}$ and $\mathbf{b}'$, respectively. In view of eqn.(2.10), the third term on the RHS of eqn.(3.5) can be evaluated as follows (for compactness' sake, we leave out the time arguments)

$$\begin{aligned} < \hat{b}_\alpha(s_0) \hat{b}_\beta(s_0) \hat{v}_0(s_0) >_T = \int_0^{s_0} dx < \hat{b}_\alpha(s_0) \hat{u}_\beta(s_0) \hat{\xi}(x) >_T = \\ \int_0^{s_0} dx \int_{\mathbb{R}^3} d^3\mathbf{b} \int_{\mathbb{R}^3} d^3\mathbf{b}' \, b_\alpha \, u_\beta \, \xi(\mathbf{b}') f^{(2)}_T(\mathbf{b}, s_0 | \mathbf{b}', x) \end{aligned} \qquad (3.6)$$

where u_β stands for $b_\beta/|\mathbf{b}|$. Notice that in eqn.(3.6) use has been made of the fact that the local retraction rate $\hat{\xi}(s_0,t)$ depends on position s_0 and time t only via the corresponding bond vector $\hat{\mathbf{b}}(s_0,t)$ (see eqn.(2.14) and eqn.(2.18)) so that $\hat{\xi}(s_0,t) = \xi(\hat{\mathbf{b}}(s_0,t))$, where $\xi(\hat{\mathbf{b}})$ is a deterministic function of $\hat{\mathbf{b}}$. Eqn.(3.6) shows that the first retraction term in eqn.(3.5) in fact depends on the two-point BVPDF $f^{(2)}_T(\mathbf{b}, s_0 | \mathbf{b}', s_0', t)$. On the other hand, as follows from eqn.(3.2), the convection terms in eqn.(3.5) can simply be expressed in terms of the one-point BVPDF $f_T(\mathbf{b}, s_0, t)$. The presence of the two-point BVPDF in eqn.(3.5) reveals that in general the equation of motion for the bond vector correlator $S^T_{\alpha\beta}$ (and also for the BVPDF $f_T(\mathbf{b}, s_0, t)$) is not closed, and involves higher order bond vector probability distribution functions.

In order to express $f_T^{(2)}$ in terms of f_T and thereby close eqn.(3.5), we need a reliable closure approximation. Note that $f_T^{(2)}(\mathbf{b}, s_0|\mathbf{b}', s_0', t)$ does not only describe the evolution of a certain segment (s_0 or s_0') of the primitive path, but also includes correlations between separate segments. The range of these correlations is described by a characteristic correlation length δ, the mean distance (along the parametrization axis) between separate segments of a tethered chain at which their motions can be considered as being independent of each other, and therefore

$$f_T^{(2)}(\mathbf{b}, s_0|\mathbf{b}', s_0', t) \approx f(\mathbf{b}, s_0, t) f(\mathbf{b}', s_0', t) \quad if \quad |s_0 - s_0'| > \delta \,. \tag{3.7}$$

At rest, the correlation length δ is equal to the step length a of the primitive path and therefore is of order the mean entanglement spacing a_0. Then, as discussed earlier, each tethered chain can be presented as a system of beads connected by stiff bonds, each bond having the length a. Every bond can point in any direction (except for the one attached to the wall), independently of others. However, in the presence of stretch motions of the neighboring bonds are no longer independent. To show this, let us point out a single tethered chain in the interfacial layer. For simplicity, we assume that the chain contour is fixed in space. Let us choose two different segments on the chain contour, say s_0 and s_0'. At time $t = 0$, we start stretching the chain contour locally at position s_0. Due to the chain connectivity, the segment s_0' will "slide" along the chain contour (see Figure 3.1). Clearly, its position (and orientation) at time Δt is determined by the corresponding amount of stretch at s_0. This simple example shows that the correlation between separate chain segments may become long-ranged (i.e., $\delta \approx L_{0T}$) when tethered chains are highly stretched, which is expected at flow rates much larger than T_{RT}^{-1} (T_{RT} is the characteristic relaxation time of the local stretch given by eqn.(2.17)).

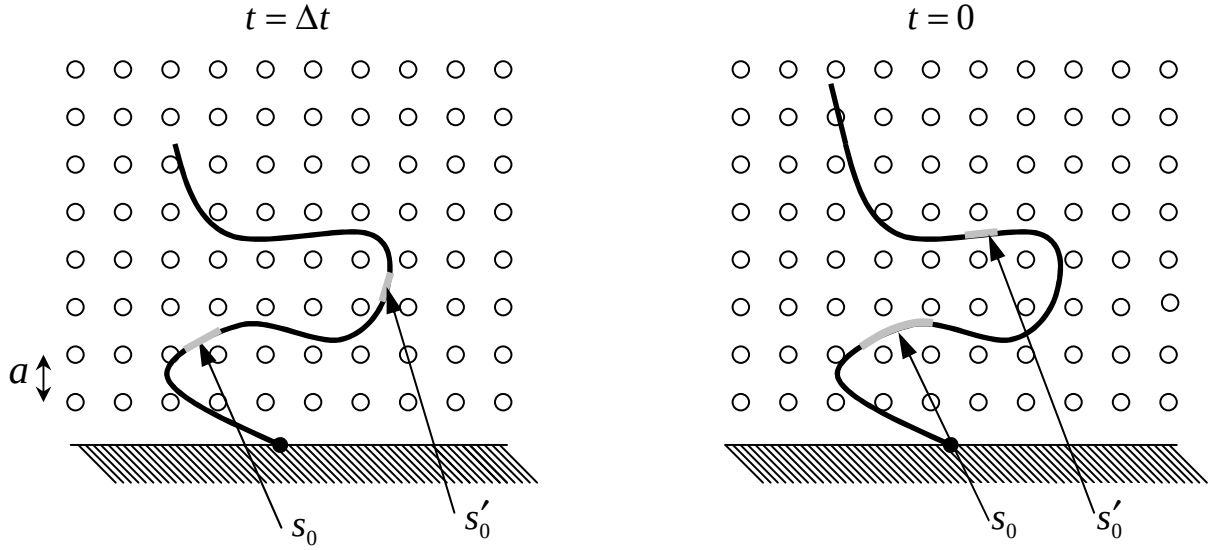

Figure 3.1: Correlation between separate chain segments.

In a flow whose rate is less than T_{RT}^{-1}, tethered chains are stretched only slightly. In this regime, the flow can still be considered as a perturbation on

the level of one chain segment so that one may expect that $\delta \approx a << L_{0T}$. Constraint release "randomizes" configurations of tethered chains and thus weakens the correlation. It "extends" the regime of small δ to even higher flow rates. Note that in the regime of small δ ($\delta << L_{0T}$), the two-point BVPDF $f_T^{(2)}(\mathbf{b}, s_0|\mathbf{b}', s_0', t)$ can be approximated through the following simple exponential interpolation formula (leave out the time arguments):

$$f_T^{(2)}(\mathbf{b}, s_0|\mathbf{b}', s_0') \cong \left(1 - e^{-\frac{|s_0 - s_0'|}{a}}\right) f_T(\mathbf{b}, s_0) f_T(\mathbf{b}', s_0') + e^{-\frac{|s_0 - s_0'|}{a}} f_T^{(2)}(\mathbf{b}, s_0|\mathbf{b}', s_0)\,, \tag{3.8}$$

where δ has been replaced with the step length a. Eqn.(3.8) assures that for $|s_0 - s_0'| > a$ the bond vector probability distributions at s_0 and s_0' become independent, and so eqn.(3.7) holds. In order to calculate $f_T^{(2)}(\mathbf{b}, s_0|\mathbf{b}', s_0, t)$, let us first recall eqn.(3.1) and eqn.(3.2). Their comparison yields that the one-point BVPDF $f_T(\mathbf{b}, s_0, t)$ can formally be defined as follows

$$f_T(\mathbf{b}, s_0, t) = < \delta(\mathbf{b} - \hat{\mathbf{b}}(s_0, t)) >_T\,, \tag{3.9}$$

where $< \ldots >_T$ denote averaging over the ensemble of tethered chains. Eqn.(3.9) shows that $f_T(\mathbf{b}, s_0, t)$ is normalized, as expected. Similarly, the two-point BVPDF $f_T^{(2)}$ can be defined as

$$f_T^{(2)}(\mathbf{b}, s_0|\mathbf{b}', s_0', t) = < \delta(\mathbf{b} - \hat{\mathbf{b}}(s_0, t))\, \delta(\mathbf{b}' - \hat{\mathbf{b}}(s_0', t)) >_T\ . \tag{3.10}$$

Eqn.(3.10) shows explicitly that $f_T^{(2)}(\mathbf{b}, s_0|\mathbf{b}', s_0', t)$ is symmetric with respect to interchanges of its arguments $(\mathbf{b}, s_0) \leftrightarrows (\mathbf{b}', s_0')$. Comparison of eqn.(3.9) with eqn.(3.10) then yields that

$$f_T^{(2)}(\mathbf{b}, s_0|\mathbf{b}', s_0, t) = \delta(\mathbf{b} - \mathbf{b}') f_T(\mathbf{b}, s_0, t)$$

So eqn.(3.8) becomes the closure approximation we were looking for:

$$\begin{aligned} f_T^{(2)}(\mathbf{b}, s_0|\mathbf{b}', s_0', t) \cong \left(1 - e^{-\frac{|s_0 - s_0'|}{a}}\right) f_T(\mathbf{b}, s_0, t) f_T(\mathbf{b}', s_0', t) + \\ e^{-\frac{|s_0 - s_0'|}{a}} f_T(\mathbf{b}, \frac{s_0 + s_0'}{2}, t) \delta(\mathbf{b} - \mathbf{b}')\,, \end{aligned} \tag{3.11}$$

where we have taken into account that the BVPDF $f_T^{(2)}(\mathbf{b}, s_0|\mathbf{b}', s_0', t)$ is symmetric with respect to interchanges of its arguments $(\mathbf{b}, s_0) \leftrightarrows (\mathbf{b}', s_0')$. The closure approximation in eqn.(3.11) is only valid in a flow regime where tethered chains are stretched only slightly. However, as we will see later on, in most cases this is the regime where the stick-to-slip transition occurs.

Once the closure approximation (3.11) is given, we may now explicitly evaluate the LHS of eqn.(3.6). Substitution of eqn.(3.11) into eqn.(3.6) yields (we again

leave out the time arguments)

$$< \hat{b}_\alpha(s_0)\hat{b}_\beta(s_0)\hat{v}_0(s_0) >_T = < \hat{b}_\alpha(s_0)\hat{u}_\beta(s_0) >_T \int_0^{s_0} dx\, \bar{\xi}_T(x) + \int_0^{s_0} dx\, e^{-\frac{s_0-x}{a}} \times$$
$$\left[< \hat{b}_\alpha(\frac{s_0+x}{2})\hat{u}_\beta(\frac{s_0+x}{2})\hat{\xi}(\frac{s_0+x}{2}) >_T - < \hat{b}_\alpha(s_0)\hat{u}_\beta(s_0) >_T \bar{\xi}_T(x) \right], \tag{3.12}$$

where $\bar{\xi}_T(x)$ stands for $< \hat{\xi}(x) >_T$. Note that $exp\big[-(s_0 - x)/a\big]$ in the second term on the RHS is a sharp function of x. It is maximal for $x = s_0$ and decreases rapidly with x when $x < s_0 - a$. In contrast, the expression in square brackets in the second term is a smoothly varying function of x. Therefore, by expanding it in a Taylor series in the vicinity of $x = s_0$, we find that eqn.(3.12) can be presented as the following series (for $s_0 > a$)

$$< \hat{b}_\alpha(s_0)\hat{b}_\beta(s_0)\hat{v}_0(s_0) >_T = < \hat{b}_\alpha(s_0)\hat{u}_\beta(s_0) >_T \int_0^{s_0} dx\, \bar{\xi}_T(x) +$$
$$a\Big\{ < \hat{b}_\alpha(s_0)\hat{u}_\beta(s_0)\hat{\xi}(s_0) >_T - < \hat{b}_\alpha(s_0)\hat{u}_\beta(s_0) >_T \bar{\xi}_T(s_0) \Big\} + \ldots \tag{3.13}$$

The first term on the RHS is of order $\bar{\xi}_T L_{0T}$, whereas the second of order $\bar{\xi}_T a$. So the series in eqn.(3.13) is in fact in powers of a/L_{0T}. The closure approximation (3.11) is only valid in the regime of small stretch (i.e., the local stretch $\lambda \approx 1$), which implies that eqn.(3.13) can further be simplified. To this end, let us present $\hat{\lambda}$ in the form $\hat{\lambda} = 1+\hat{\alpha}$, where $\hat{\alpha}$ is small. Expansion of the first term on the RHS of eqn.(3.13) in powers of $\hat{\alpha}$ yields

$$< \hat{b}_\alpha(s_0)\hat{u}_\beta(s_0) >_T \int_0^{s_0} dx\, \bar{\xi}_T(x) \;= < \hat{b}_\alpha(s_0)\hat{b}_\beta(s_0) >_T \int_0^{s_0} dx\, \bar{\xi}_T(x) + O\left(\frac{\bar{\alpha}_T^2 L_{0T}}{T_{RT}}\right), \tag{3.14}$$

where $\bar{\alpha}_T$ stands for $< \hat{\alpha} >_T$. In eqn.(3.14), we have taken into account that the local retraction rate $\hat{\xi}$ can be written as $-\hat{\alpha}/T_{RT}$ (see eqn.(2.18)), where T_{RT} is the Rouse time of tethered chains. Note that the first term on the RHS of eqn.(3.14) is of order $L_{0T}\bar{\alpha}_T/T_{RT}$, whereas the second one of order $L_{0T}\bar{\alpha}_T^2/T_{RT}$. Next, from eqn.(3.1) and the fact that the bond vector $\hat{\mathbf{b}}$ can be written as a product $\hat{\lambda}\hat{\mathbf{u}}$, where $\hat{\mathbf{u}}$ is a unit vector, we have that for small $\hat{\alpha}$

$$\sqrt{< \hat{\lambda}^2 >_T} =< \hat{\lambda} >_T + O(\bar{\alpha}_T^2)\,. \tag{3.15}$$

At rest, tethered chains are not stretched, that is $\hat{\lambda}(s_0, t) \equiv 1$ for any s_0. In terms of the BVPDF, this implies that $f_T(\mathbf{b}, s_0, t) \propto \delta(|\mathbf{b}| - 1)$. Eqn.(3.15)

indicates that for small $\hat{\alpha}$ the mean square deviation of the local stretch remains small, and so the stretch distribution function is still narrow peaked. Taking this into account and recalling eqn.(2.18), we then have

$$\begin{aligned} < \hat{b}_\alpha(s_0)\hat{u}_\beta(s_0)\hat{\xi}(s_0) >_T = & < \hat{b}_\alpha(s_0)\hat{u}_\beta(s_0) >_T < \hat{\xi}(s_0) >_T + O(\bar{\alpha}_T^2 T_{RT}^{-1}) = \\ & < \hat{b}_\alpha(s_0)\hat{b}_\beta(s_0) >_T < \hat{\xi}(s_0) >_T + O(\bar{\alpha}_T^2 T_{RT}^{-1}) \,. \end{aligned} \tag{3.16}$$

With the help of eqn.(3.14) and eqn.(3.16), eqn.(3.13) now reads as

$$< \hat{b}_\alpha(s_0)\hat{b}_\beta(s_0)\hat{\upsilon}_0(s_0) >_T = < \hat{b}_\alpha(s_0)\hat{b}_\beta(s_0) >_T \int_0^{s_0} dx\, \bar{\xi}_T(x) + O(\bar{\alpha}_T^2 L_{0T} T_{RT}^{-1}) \,. \tag{3.17}$$

Upon differentiating both sides of eqn.(3.17) with respect to s_0 and neglecting terms of order $\bar{\alpha}_T^2 L_{0T} T_{RT}^{-1}$, the third term on the RHS of eqn.(3.5) becomes

$$\frac{\partial}{\partial s_0} < \hat{b}_\alpha \hat{b}_\beta \hat{\upsilon}_0 >_T = \bar{\xi}_T S^T_{\alpha\beta} + \left[\int_0^{s_0} dx\, \bar{\xi}_T(x) \right] \frac{\partial S^T_{\alpha\beta}}{\partial s_0} \,. \tag{3.18}$$

In view of eqn.(2.10), the last term on the RHS of eqn.(3.5) reads as

$$< \hat{b}_\alpha \hat{b}_\beta \frac{\partial \hat{\upsilon}_0}{\partial s_0} >_T = < \hat{b}_\alpha \hat{u}_\beta \left[\hat{\xi} - \frac{1}{\hat{\lambda}} \frac{\partial \hat{\lambda}}{\partial s_0} \int_0^{s_0} dx\, \hat{\xi}(x) \right] >_T \,. \tag{3.19}$$

The first term on the RHS is of order $\bar{\alpha}_T T_{RT}^{-1}$, whereas the second one of order $\bar{\alpha}_T^2 T_{RT}^{-1}$ (since $\partial\hat{\lambda}/\partial s_0$ is of order $\hat{\alpha}/L_{0T}$). Therefore, after neglecting terms of order $\bar{\alpha}_T^2 T_{RT}^{-1}$, eqn.(3.19) reduces to

$$< \hat{b}_\alpha \hat{b}_\beta \frac{\partial \hat{\upsilon}_0}{\partial s_0} >_T = \bar{\xi}_T S^T_{\alpha\beta} \,. \tag{3.20}$$

where use has been made of eqn.(3.16). Finally, combination of eqns.(3.5, 3.18, 3.20) results in the following equation of motion for the bond vector correlator $S^T_{\alpha\beta}(s_0, t)$ (for $s_0 > a$)

$$\begin{aligned} \frac{\partial S^T_{\alpha\beta}(s_0,t)}{\partial t} = & \; K^I_{\alpha\gamma} S^T_{\beta\gamma}(s_0,t) + K^I_{\beta\gamma} S^T_{\alpha\gamma}(s_0,t) + 2\,\bar{\xi}_T(s_0,t) S^T_{\alpha\beta}(s_0,t) \\ & + \left[\int_0^{s_0} dx\, \bar{\xi}_T(x,t) \right] \frac{\partial S^T_{\alpha\beta}(s_0,t)}{\partial s_0} \,. \end{aligned} \tag{3.21}$$

As is seen, $S^T_{\alpha\beta}(s_0, t)$ satisfies an integro-partial differential equation. Notice that the equations of motion for different components of $S^T_{\alpha\beta}$ are coupled

through the gradient velocity tensor $K^I_{\alpha\beta}$ (see eqn.(2.7)). Therefore, in general, the dynamics of tethered chains is actually governed by a system of nine coupled equations, one for each component of $S^T_{\alpha\beta}$. In a shear flow, where $K^I_{\alpha\beta}$ has only one nonzero component, the number of equations reduces to four. In contrast, in a description based on the parametrization functions $\hat{\mathbf{R}}(s_0,t)$ (see Figure 2.6), in order to quantify the evolution of the ensemble of tethered chains in flow, we have to deal with a macroscopically large system of Langevin equations. The number of equations in this system is equal to the number of tethered chains present in the interfacial layer.

In view of eqn.(2.18), the mean local retraction rate $\bar{\xi}_T$ is given by

$$\bar{\xi}_T(s_0,t) = -\frac{\bar{\lambda}_T(s_0,t)-1}{T_{RT}}\,, \tag{3.22}$$

where $\bar{\lambda}_T(s_0,t)$ is the mean local stretch of tethered chains at position s_0 and time t. As follows from eqn.(3.1) and eqn.(3.15), in a flow regime where tethered chains are stretched only slightly, $\bar{\lambda}_T(s_0,t)$ can in turn be expressed in terms of the correlator $S^T_{\alpha\beta}$ as follows

$$\bar{\lambda}_T = \sqrt{S^T_{\alpha\alpha}}\,, \tag{3.23}$$

where summation is implied over the repeated indices. Eqn.(3.23) reveals that eqn.(3.21) is nonlinear. Eqn.(3.21) describes the dynamics of the ensemble of tethered chains in the presence of flow. It accounts for convection and retraction. However, it does not include constraint release and contour length fluctuations, other possible relaxation mechanisms for tethered chains. In the next section, we will further discuss eqn.(3.21) and derive the corresponding contributions due to constraint release and contour length fluctuations.

3.3 Constraint release

In order to calculate the contribution of constraint release to the equation of motion for $S^T_{\alpha\beta}(s_0,t)$ derived earlier, let us first study the following correlator

$$\Phi_{\alpha\beta}(s_0,s_0',t) = \left\langle \frac{\partial \hat{R}_\alpha(s_0,t)}{\partial s_0}\frac{\partial \hat{R}_\beta(s_0',t)}{\partial s_0'} \right\rangle_T\,, \tag{3.24}$$

where $\hat{R}_\beta(s_0,t)$ is the β component of the position vector $\hat{\mathbf{R}}(s_0,t)$ of segment s_0 of a tethered chain at time t. As was recognized by Viovy et al [34], motion of the primitive path of the tethered chain due to CR can be modelled as a Rouse process (see the discussion after Figure 2.9). Based on this observation, Milner et al [35] proposed an equation of motion for $\hat{\mathbf{R}}(s_0,t)$ due to

CR which has the form of a Langevin equation (see eqn.(2.22)). Substitution of eqn.(2.22) into eqn.(3.24) yields the following equation of motion for the correlator $\Phi_{\alpha\beta}(s_0, s_0', t)$ (for $s_0 \neq s_0'$)

$$\frac{\partial \Phi_{\alpha\beta}}{\partial t} = \nu_T a_0^2 \left(\frac{\partial^2}{\partial s_0^2} + \frac{\partial^2}{\partial s_0'^2} \right) \Phi_{\alpha\beta} \,, \tag{3.25}$$

where use has been made of the fact that $\mathbf{g}(s_0, t)$ in eqn.(2.22), which represents a random force acting on segment s_0, is uncorrelated with motions of other segments of the chain (see eqn.(2.23)). In eqn.(3.25), ν_T is the frequency of constraint release on tethered chains and a_0 is the mean distance between entanglements. As follows from eqns.(2.2, 3.10, 3.24), the correlator $\Phi_{\alpha\beta}(s_0, s_0', t)$ can be expressed via the second moment of the BVPDF $f_T^{(2)}(\mathbf{b}, s_0|\mathbf{b}', s_0', t)$ as

$$\Phi_{\alpha\beta}(s_0, s_0', t) = \int\limits_{\mathbb{R}^3} d^3\mathbf{b} \int\limits_{\mathbb{R}^3} d^3\mathbf{b}' \, b_\alpha b_\beta' \, f_T^{(2)}(\mathbf{b}, s_0|\mathbf{b}', s_0', t) \,. \tag{3.26}$$

Eqn.(3.26) shows that the two-point BVPDF $f_T^{(2)}$ should also satisfy eqn.(3.25). Note that for $s_0 \neq s_0'$, the BVPDF $f_T^{(2)}(\mathbf{b}, s_0|\mathbf{b}', s_0', t)$ can be written as a product of two one-point BVPDF's (see eqn.(3.7)). Therefore, substituting eqn.(3.7) into eqn.(3.25) and separating variables, one finds the corresponding equation of motion for the one-point BVPDF $f_T(\mathbf{b}, s_0, t)$

$$\frac{\partial f_T(\mathbf{b}, s_0, t)}{\partial t} - \nu_T a_0^2 \frac{\partial^2 f_T(\mathbf{b}, s_0, t)}{\partial s_0^2} = \chi(t) f_T(\mathbf{b}, s_0, t) \,, \tag{3.27}$$

where $\chi(t)$ is a function of time alone. Integrating both sides of eqn.(3.27) over all possible values of the bond vector and taking into account that $f_T(\mathbf{b}, s_0, t)$ is normalized, we have that $\chi(t) = 0$. Next, by multiplying both sides of eqn.(3.27) by $b_\alpha b_\beta$ and integrating over all possible values of the bond vector, we arrive at the following equation of motion for $S_{\alpha\beta}^T$ due to CR

$$\left[\frac{\partial S_{\alpha\beta}^T}{\partial t} \right]_{CR} = \nu_T a_0^2 \frac{\partial^2 S_{\alpha\beta}^T}{\partial s_0^2} \,, \tag{3.28}$$

where use was made of eqn.(3.2). Since constraint release works independently of and in parallel to convection and retraction, eqn.(3.28) explicitly specifies the contribution of CR to the equation of motion for the correlator $S_{\alpha\beta}^T$ (see eqn.(3.21)). As is seen, it has the form of a diffusion process with the coefficient proportional to the CR frequency ν_T. The diffusion form of eqn.(3.28) implies that constraint release leads to relaxation of initially oriented configurations of tethered chains towards the isotropic one described by the tensor $S_{\alpha\beta}^{(eq)}$ in eqn.(3.3). In particular, according to eqn.(3.28), the characteristic relaxation

time of the overall configuration of a tethered chain is of order Z_T^2/ν_T (Z_T is the mean number of constraints per tethered chain), in agreement with the earlier predictions of Verdier and Stockmayer [33]. This implies that after a sequence of Z_T^2 jumps most of the tethered chains in the ensemble will completely renew their tubes, and so their initial configurations will be "forgotten".

Attention must be paid to the fact that the correlator $S_{\alpha\beta}^T$ does not only describe the mean local orientation of the tethered chains, but also contains information on their mean local stretch (see eqn.(3.23)). Therefore, the diffusion form of eqn.(3.28) suggests that constraint release also leads to relaxation of the local stretch via removal of a constraint on a "tout" piece of the tethered chain. Apparently, in the presence of CR, each tethered chain can restore its equilibrium length by either retraction or by constraint release.

3.4 Contour length fluctuations

Due to its Brownian motion, a physical chain in the melt rapidly oscillates within the mesh of the surrounding constraints. Since the tube (and so the primitive path) of the chain only captures its time averaged behavior, the Brownian oscillations lead to fluctuations in the length of the chain primitive path. These fluctuations can be visualized as if the free end of the path "moved" inwards and outwards the tube. When the end moves inwards the corresponding portion of the initial tube near the end is vacated. When the end moves outwards again, it is free to choose its direction so that the portion of the initial tube is forgotten. Clearly, such an "inward-outward" motion results in a fast local relaxation of the initial tube near the end towards the isotropic nonstretched configuration described by the tensor $S_{\alpha\beta}^{(eq)}$ in eqn.(3.3).

Milner and McLeish [36] developed a quantitative molecular theory for the dynamics of star polymer melts, for which contour length fluctuations (CLF) are the principal mode of stress relaxation. Since each tethered chain can be considered as an "arm" of a larger star polymer molecule, their results can directly be used here to calculate the contribution of CLF to the equation of motion for $S_{\alpha\beta}^T$. According to [36], the characteristic relaxation time $\tau_T(s_0)$ of segment s_0 of the tube due to CLF is equal to the corresponding mean first passage time needed to retract the end of the primitive path inside the tube a distance equal to $L_{0T} - s_0$. Milner and McLeish showed that for segments s_0 which satisfy $L_{0T} - s_0 > a$ the relaxation time $\tau_T(s_0)$ increases exponentially with the square of the distance from the chain end

$$\tau_T(s_0) \approx \tau_{0T}\, e^{1.5\, Z_T\, (1-s_0/L_{0T})^2}\,, \tag{3.29}$$

where use has been made of the fact that due to fast retraction of the primitive path at the free end, the corresponding stretch can be neglected so that the

actual arclength $\hat{s}(s_0,t) = s_0$. For the time constant τ_{0T} we take the Rouse time T_{RT} of tethered chains (see eqn.(2.17)). A more accurate prefactor, which depends on s_0, can be found in [36]. Given $\tau_T(s_0)$, the equation of motion for the correlator $S^T_{\alpha\beta}$ due to CLF can be written as (for $s_0 < L_{0T} - a$)

$$\left[\frac{\partial S^T_{\alpha\beta}(s_0,t)}{\partial t}\right]_{CLF} = -\frac{1}{\tau_T(s_0)}\left[S^T_{\alpha\beta}(s_0,t) - S^{eq}_{\alpha\beta}\right], \tag{3.30}$$

Since contour length fluctuations work independently of other processes for tethered chains, eqn.(3.30) explicitly specifies their contribution to the equation of motion for the bond vector correlator $S^T_{\alpha\beta}$. Eqn.(3.30) shows that CLF are especially important for segments of the tethered chains near the free end. Besides that, eqn.(3.30) indicates that CLF may give a significant contribution to the stress relaxation for short (small Z_T) tethered chains, whereas for long ones they can be neglected.

3.5 Results and discussion

Combination of all the contributions from eqns.(3.21, 3.28, 3.30) leads to the following final equation of motion for the correlator $S^T_{\alpha\beta}$ of tethered chains

$$\begin{aligned}\frac{\partial S^T_{\alpha\beta}}{\partial t} &= K^I_{\alpha\gamma}S^T_{\beta\gamma} + K^I_{\beta\gamma}S^T_{\alpha\gamma} + \nu_T a_0^2\frac{\partial^2 S^T_{\alpha\beta}}{\partial s_0^2} \\ &\quad + 2\,\bar{\xi}_T S^T_{\alpha\beta} + \left[\int_0^{s_0} dx\,\bar{\xi}_T(x,t)\right]\frac{\partial S^T_{\alpha\beta}}{\partial s_0} - \frac{1}{\tau_T}\left[S^T_{\alpha\beta} - S^{eq}_{\alpha\beta}\right].\end{aligned} \tag{3.31}$$

This equation describes the evolution of the tethered chains in flow. It includes all the major mechanisms inherent to the tethered chains in the melt, such as convection, retraction, constraint release, and contour length fluctuations. Attention must be paid to the fact that in the strict sense eqn.(3.31) is only applicable to the "inner" segments of the tethered chains which satisfy $a < s_0 < L_{0T} - a$, where a is the step length of the primitive path. Despite the fact that these segments do not feel the non-anisotropy caused by the wall, their relaxation behavior is affected by the presence of the wall. Namely, due to the fact that each tethered chain is attached to the wall, eqn.(3.31) does not contain reptation, another stress relaxation mode inherent to unattached linear polymer chains. In other words, due to the presence of the wall reptation is prohibited for the tethered chains and thus do not enter eqn.(3.31).

The effect of the wall is especially strong for segments of the tethered chains near the tethered end ($s_0 = 0$). For these segments, eqn.(3.31) may contain additional terms which arise from the non-anisotropy of the melt near the

wall. The non-anisotropy should be taken into account for those segments of the tethered chains which satisfy $0 < s_0 < a$, where a is the step length of the primitive path or, in other words, the characteristic correlation length between different segments of the chain contour (see the discussion after eqn.(3.7)). As we will see later on, in order to quantify the stick-to-slip transition at the polymer melt/die wall interface we only need to know the value of the correlator $S^T_{\alpha\beta}$ averaged along the chain contour. This implies that in practice, since a is much smaller than the chain length L_{0T}, we can neglect the anisotropy effects in the equation of motion for segments with $0 < s_0 < a$ and still use eqn.(3.31).

In contrast to the inner segments of the tethered chains, relaxation of segments which satisfy $L_{0T} - a < s_0 < L_{0T}$ is mainly controlled by fast contour length fluctuations and retraction. As discussed earlier, the single relaxation time approximation (see eqn.(2.18)) used in the derivation of eqn.(3.31) may not be applicable for these segments. However, similar to the non-anisotropy effects considered above, in practice we can neglect the high order relaxation modes of the local stretch in the equation of motion for these segments and still use eqn.(3.31).

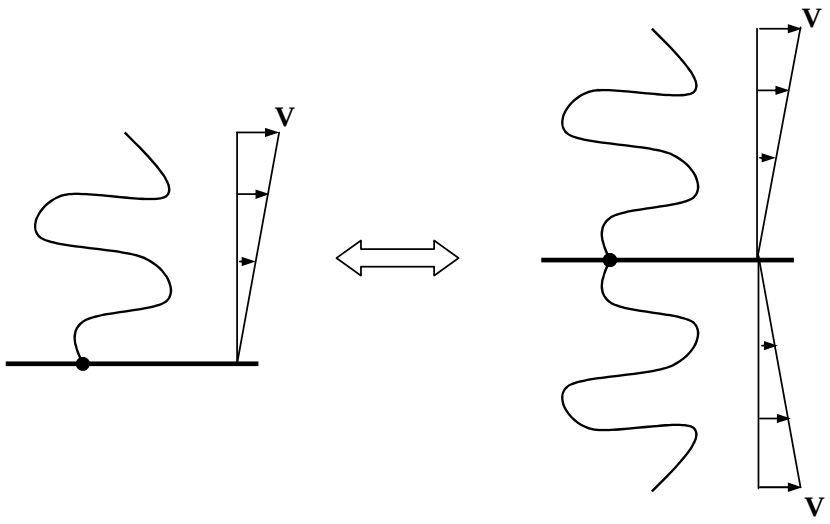

Figure 3.2: Symmetrizing the flow.

In order to solve eqn.(3.31), we must also specify the boundary conditions for $S^T_{\alpha\beta}$. First, due to fast CLF motions of the free end of the tethered chains, the corresponding average local configuration of the primitive path is isotropic and non-stretched, and therefore the BVPDF $f_T(\mathbf{b}, L_{0T}, t) = \delta(|\mathbf{b}| - 1)/4\pi$. On the other hand, each tethered chain can be imagined as an "arm" of a larger polymer molecule attached to the wall in the middle and subjected to a symmetric flow (see Figure 3.2). Then, as follows from symmetry arguments, $S^T_{\alpha\beta}(s_0, t)$ can be thought of as being an even function of s_0. Notice that in a case where the flow is antisymmetric one would receive that $S^T_{\alpha\beta}(0, t)$ is zero, which is unphysical since the trace of $S^T_{\alpha\beta}(s_0, t)$ is always equal to or larger

than unity. From the above, we find that

$$S^T_{\alpha\beta}(s_0 = L_{0T}, t) = \frac{1}{3}\delta_{\alpha\beta} \qquad \left.\frac{\partial S^T_{\alpha\beta}(s_0, t)}{\partial s_0}\right|_{s_0=0} = 0\,. \tag{3.32}$$

By recalling eqn.(3.23), one may conclude that the mean local stretch at the attached end of the tethered chains is maximal, as expected.

Eqn.(3.31) extended with the boundary conditions for the correlator $S^T_{\alpha\beta}$ in eqn.(3.32) forms a system of equations that enables us to calculate the local stress in the interfacial layer (see eqn.(3.4)), provided that the corresponding gradient velocity tensor $\bar{\bar{K}}^I$ and the molecular parameters of the melt are known. Another outcome of the model is the thickness h of the interfacial layer. In order to calculate h, we again present each tethered chain in the layer as a system of $Z_T + 1$ beads connected by Z_T bonds (see Figure 3.3). At equilibrium, tethered chains are not stretched, and all the bonds have the same length equal to the step length a. In a flow, however, each bond may have its own length which can be written as $a\hat{\lambda}$, where $\hat{\lambda}$ is the stretch of the bond. The orientation of the bond is described by its unit vector $\hat{\mathbf{u}}$. As follows from Figure 3.3, if $\hat{\mathcal{R}}_y$ is the y component of the end-to-end vector $\hat{\mathcal{R}}$ of a tethered chain then the layer thickness h can be estimated as

$$h \approx \sqrt{< \hat{\mathcal{R}}_y \hat{\mathcal{R}}_y >_T}\,. \tag{3.33}$$

Note that $\hat{\mathcal{R}}$ can be presented as

$$\hat{\mathcal{R}} = a_0 \sum_{i=1}^{Z_T} \hat{\mathbf{b}}(i)\,, \tag{3.34}$$

where $\hat{\mathbf{b}}(i)$ is the bond vector of the i-th bond given by $\hat{\lambda}(i)\hat{\mathbf{u}}(i)$, where $\hat{\lambda}(i)$ is stretch and $\hat{\mathbf{u}}(i)$ orientation of the bond. From eqns.(3.33, 3.34) we have

$$h^2 \approx \sum_{i=1}^{Z_T}\sum_{j=1}^{Z_T} < \hat{b}_y(i)\hat{b}_y(j) >_T\,, \tag{3.35}$$

where $\hat{b}_y(i)$ is the y component of $\hat{\mathbf{b}}(i)$. At equilibrium, there are no correlations between neighboring bonds, and the bonds move independently of each other (see the discussion after eqn.(3.7)). Recalling that in this case the BVPDF f_T is isotropic and all the bonds have the same length a, one can find that at rest the correlator $< b_y(i)b_y(j) >_T = a^2\delta_{ij}/3$. From eqn.(3.35), the equilibrium thickness h_0 of the interfacial layer is then given by

$$h_0 \approx \sqrt{\frac{Z_T a^2}{3}}\,. \tag{3.36}$$

In the presence of flow, the correlator $< b_y(i)b_y(j) >_T$ does not vanish for $i \neq j$. However, in a regime where the tethered chains are stretched only slightly it decreases very rapidly with $|i-j|$, the distance between segments. Therefore, neglecting long-range correlations in eqn.(3.35), the thickness h of the interfacial layer can finally be written as

$$h^2(t) \approx \sum_{i=1}^{Z_T} < b_y(i)b_y(i) >= \frac{3h_0^2}{L_{0T}} \int_0^{L_{0T}} ds_0 \, S_{yy}^T(s_0,t)\,, \tag{3.37}$$

where a transition has been made from the discrete to the continuous description of the tethered chains. The coefficient before the integral assures that at rest $h = h_0$. Eqn.(3.37) shows explicitly that the thickness h, similar to the wall stress $\sigma_{\alpha\beta}^I$ (see eqn.(3.4)), is a function of the bond vector correlator $S_{\alpha\beta}^T$ averaged along the chain contour. This in turn implies that both $\sigma_{\alpha\beta}^I$ and h can be expressed via second order moments of the BVPDF $f_T(\mathbf{b}, s_0, t)$.

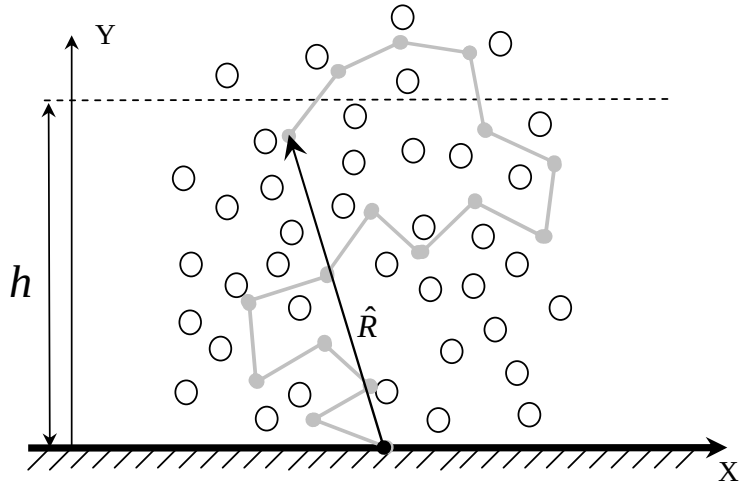

Figure 3.3: Thickness of the interfacial layer.

To demonstrate the developed theory, eqn.(3.31) has been analyzed numerically for a simple case of steady shear flow. The direction of the flow will be denoted by the X-axis, whereas the normal to the wall by the Y-axis. In this case, the gradient velocity tensor $K_{\alpha\beta}^I$ has only one non-zero component K_{xy}^I, which is equal to the shear rate $\dot{\gamma}_w$ in the interfacial layer. The model parameters are: the mean number Z_T of constraints per tethered chain, the Rouse time T_{RT} of tethered chains, the mean entanglement spacing a_0, the equilibrium primitive path length L_{0T}, the elastic modulus G_{0I} of the layer, and the frequency ν_T of constraint release. Since we have not yet specified an explicit form of ν_T, in this section it will be regarded as a free parameter.

As discussed earlier, eqn.(3.31) is a nonlinear integro-partial differential equation. The procedure that were used to solve eqn.(3.31) is briefly discussed below. First, the parametrization interval $[0, L_{0T}]$ of the tethered chains is discretized into N steps. For each pair of $\alpha\beta$, eqn.(3.31) extended with the

boundary conditions (3.32) then turns into a nonlinear system of coupled algebraic equations for the components of the bond vector correlator $\{S^T_{\gamma\delta}(x_i)\}^{i=N}_{i=1}$ $(\gamma, \delta = x, y, z)$. This system can be symbolically written in the following form

$$F_{\alpha\beta}\left(\{S^T_{\gamma\delta}(x_i)\}^{i=N}_{i=1}\right) = 0 \quad , \quad \gamma, \delta = x, y, z \tag{3.38}$$

In general, $F_{\alpha\beta}$ has $9N$ arguments. In the shear flow, the number of independent variables reduces to $4N$. In the presence of flow, components of the bond vector correlator $S^T_{\alpha\beta}$ (and accordingly functionals $F_{\alpha\beta}$) are coupled via the gradient velocity tensor $K^I_{\nu\mu}$, which implies that equations (3.38) must be solved simultaneously. A solution of the system of equations for $F_{\alpha\beta}$ is found by the conventional Newton method with an adjustable step. The obtained solution is then integrated along the chain contour, in order to calculate the components of the wall stress tensor and the layer thickness h. The steady shear model predictions for the thickness h and the wall shear stress σ^I_{xy} are shown in Figure 3.4 and Figure 3.5, respectively.

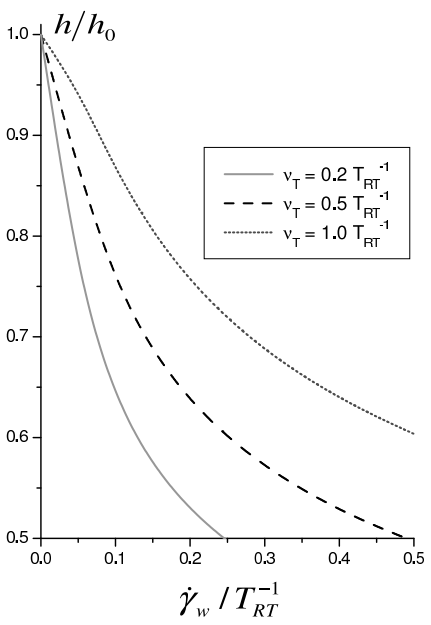

Figure 3.4: Layer thickness vs wall shear rate for $Z_T = 20$.

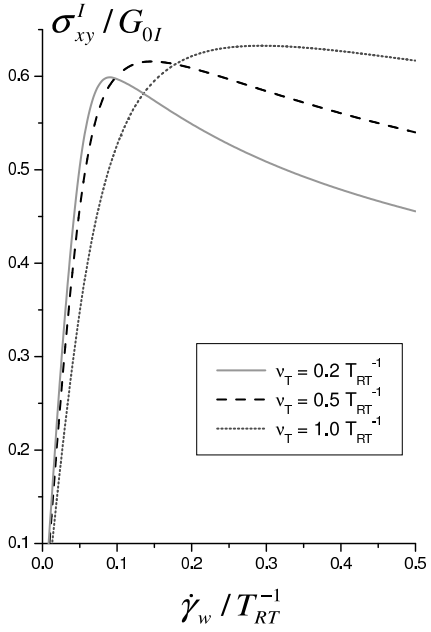

Figure 3.5: Wall shear stress vs wall shear rate for $Z_T = 20$.

In Figure 3.4, the model predictions for the thickness h are shown versus the wall shear rate $\dot{\gamma}_w$ for different values of ν_T. As seen, h decreases monotonically with $\dot{\gamma}_w$. Clearly, a strong enough flow may cause a significant orientation of the tethered chains, which is visualized as a decrease in h. An increase in the frequency ν_T of constraint release decreases the amount of chain orientation and therefore leads to an increase in h. Apparently, it is the strength of constraint release, as measured by the frequency ν_T, that determines the resistibility of the tethered chains to the flow.

In Figure 3.5, the wall shear stress σ_{xy}^I is presented versus the wall shear rate $\dot{\gamma}_w$ for different values of ν_T. As is seen, σ_{xy}^I is a nonmonotonous function of $\dot{\gamma}_w$. At small shear rates, an increase in $\dot{\gamma}_w$ results in an increase in the drag force exerted on the tethered chains by the flow, which in turn leads to an increase in the corresponding tensile force acting along the contour of the tethered chains. The stress σ_{xy}^I induced in the tethered chains is proportional to this tensile force and therefore also increases with $\dot{\gamma}_w$.

At higher shear rates, constraint release is no longer able to resist strong convection so that the tethered chains begin to align with the flow. In this case, the flow starts to lose its "grip" on the tethered chains. This amounts to a decreases in the drag force on the chains, and ultimately leads to a decrease in σ_{xy}^I. The maximum of σ_{xy}^I in Figure 3.5 then corresponds to a shear rate $\dot{\gamma}_w^*$ at which convection and constraint release balance each other. As a consequence, an increase in the frequency ν_T shifts the maximum to higher shear rates, as shown in Figure 3.5. For shear rates $\dot{\gamma}_w > \dot{\gamma}_w^*$, σ_{xy}^I monotonically decreases with $\dot{\gamma}_w$. The non-monotonicity of the dependence of σ_{xy}^I on $\dot{\gamma}_w$ was also confirmed by direct numerical simulations in [37].

So far, the frequency ν_T of constraint release was regarded as a free parameter. In reality, ν_T is a function of the flow rate and the molecular parameters of the melt. To show this, let us consider a single tethered chain in the interfacial layer. In general, it has entanglements with other tethered and bulk chains present in the layer. This implies two sorts of constraints on the chain (see Figure 3.6). Those of the first sort are imposed by the bulk chains, and can be released via their reptation (the so-called thermal CR) or retraction (the so-called convective CR). Constraints of the second sort are imposed by other tethered chains and can only be released via thermal fluctuations of their free ends (the so-called arm retraction).

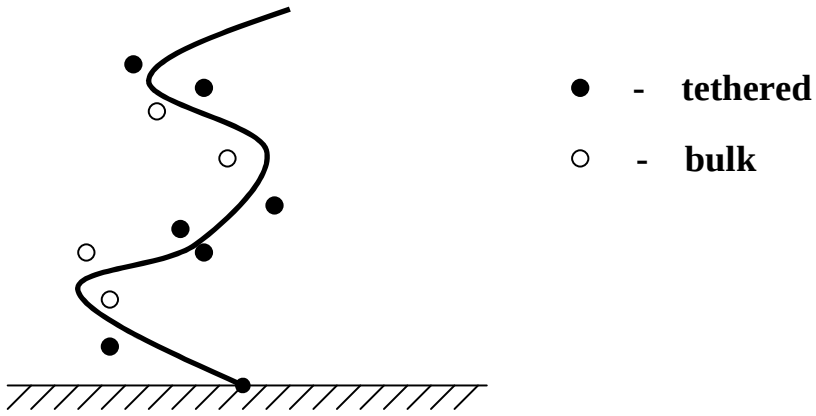

Figure 3.6: Two sorts of constraints on a tethered chain.

Let τ_B and τ_T be the mean lifetime of a bulk and a tethered constraint, respectively. As mentioned in the previous chapter, the thickness of the interfacial layer is normally much smaller than the length of bulk molecules. This means that most of the bulk chains present in the layer are actually short fragments of

unattached polymer molecules from the bulk. Since the bulk and the tethered constraints are imposed by different sorts of polymer chains and therefore relax independently, the CR frequency ν_T of tethered chains can finally be written as

$$\nu_T = \tau_B^{-1}\phi_Z + \tau_T^{-1}(1 - \phi_Z)\,, \tag{3.39}$$

where ϕ_Z is the mean fraction of bulk constraints per tethered chain. Note that τ_B is determined by the motion of polymer molecules in the bulk and therefore is a function of the bulk flow rate. The explicit dependence of the frequency ν_T on τ_B implies that the dynamics of the tethered chains is strongly coupled to the dynamics of the polymer molecules in the bulk. Therefore, in order to calculate ν_T explicitly and thus complete eqn.(3.31), we must also study the dynamics of unattached polymer molecules subjected to a flow. This is the subject of the next chapter.

Chapter 4

Dynamics of bulk molecules

In this chapter, the dynamics of molecules in the bulk is studied in the presence of flow. As in the case of tethered chains, the dynamics of an ensemble of bulk chains will be described by the corresponding bond vector correlator. The resulting equation of motion for this correlator accounts for such mechanisms for the bulk chains as convection, retraction, constraint release, contour length fluctuations, and reptation. Based on a simple geometrical analysis, we also calculate the frequency of constraint release in the bulk.

4.1 Bond vector correlator of bulk chains

Similar to tethered chains, the dynamics of an ensemble of bulk molecules will be described by the corresponding bond vector correlator $S^B_{\alpha\beta}$ given by

$$S^B_{\alpha\beta}(s_0,t) =< \hat{b}_\alpha(s_0,t)\hat{b}_\beta(s_0,t) >_B \tag{4.1}$$

where $\hat{b}_\alpha(s_0,t)$ is the α component of the bond vector $\hat{\mathbf{b}}(s_0,t)$ of a bulk chain and $< \ldots >_B$ denote averaging over the ensemble. The equilibrium primitive path length of the bulk molecules will be denoted as L_{0B}. Note that in the case of bulk chains, it is convenient to choose the parametrization interval as $-L_{0B}/2 \le s_0 \le L_{0B}/2$. Then, as follows from symmetry arguments and the fact that $S^B_{\alpha\beta}(s_0,t)$ involves averaging over the ensemble, $S^B_{\alpha\beta}(s_0,t)$ is an even function of s_0. In this case, segments $s_0 = \pm L_{0B}/2$ and $s_0 = 0$ correspond to the free ends and the center of the chain, respectively. Once the correlator $S^B_{\alpha\beta}$ of the ensemble is known, the local stress induced in the bulk chains by the flow can be written as (compare with eqn.(3.4))

$$\sigma^B_{\alpha\beta}(t) = \frac{G_{0B}}{L_{0B}} \int_{-L_{0B}/2}^{L_{0B}/2} ds_0\, S^B_{\alpha\beta}(s_0,t)\,, \tag{4.2}$$

where G_{0B} is the elastic modulus of the bulk. Its explicit form can be found in eqn.(5.10).

4.2 Reptation

Like tethered chains, bulk ones undergo convection, retraction, constraint release, and contour length fluctuations (CLF). In addition, they can "reptate". As well as CLF, reptation stems from the Brownian motion of the physical chain in the melt. Since the lateral motions of the physical chain are severely restricted by its neighbors, its fast Brownian oscillations will eventually lead to a curvilinear diffusion of the primitive path along itself (see Figure 4.1). This motion, called reptation, is the principal stress relaxation mode for linear entangled polymers in the linear viscoelastic regime. The notion of reptation was first introduced by de Gennes [38] for the diffusion of a linear polymer inside a strongly cross-linked gel, and afterwards has been extended by Doi and Edwards [31] to polymer melts and highly concentrated solutions.

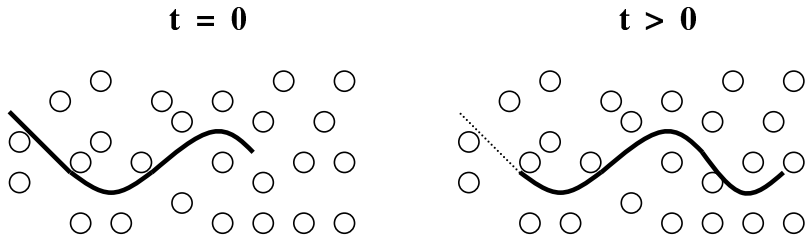

Figure 4.1: Reptation.

4.3 Equation of motion for the correlator $S^B_{\alpha\beta}$

Since bulk chains undergo the same mechanisms as tethered ones, in the absence of reptation the equation of motion for $S^B_{\alpha\beta}(s_0,t)$ has exactly the same form as the one for $S^T_{\alpha\beta}$ (see eqn.(3.31)). Reptation "works" independently of and in parallel to other processes for bulk chains. This implies that in order to calculate the contribution of reptation to the equation of motion for $S^B_{\alpha\beta}(s_0,t)$, we may study reptation separately. Following the ideas proposed by de Gennes [38], we will describe reptation as the one-dimensional diffusion of the primitive path. Let $\Delta\hat{\zeta}(s_0,t)$ be the physical shift of segment s_0 of a bulk chain along the chain contour over a small time interval Δt due to reptation. Due to the Brownian nature of reptation, $\Delta\hat{\zeta}(s_0,t)$ is stochastic and can be modelled by a diffusion process. Therefore, we have

$$\langle\Delta\hat{\zeta}\rangle = 0 \quad \langle\Delta\hat{\zeta}^2\rangle = 2D_c\Delta t\,, \tag{4.3}$$

where D_c is the diffusion coefficient of reptation. The Brownian motion of a physical chain in a dilute solution is known to be successfully modelled by a Rouse chain [31] undergoing local random forces. The Rouse chain consists of a series of beads connected by elastic springs. The springs represent the connectivity of the physical chain. Apart from elastic forces imposed by adjacent springs, each bead experiences a stochastic force which describes the effect of motions of other chains on the bead. The amplitudes and orientations of the stochastic force on different beads are assumed to be uncorrelated with each other. Reptation of the primitive path corresponds to the overall translation of the physical chain along the tube, and therefore can be interpreted as an one-dimensional Rouse process. So the parameter D_c in eqn.(4.3) can be identified with the diffusion coefficient of the Rouse motion in one dimension, and therefore is given by (see, for example, Doi and Edwards [31])

$$D_c = \frac{k_B T}{N\varsigma}\,, \tag{4.4}$$

where N, ς and T are the number of monomers per polymer chain, the monomeric friction coefficient, and the melt temperature, respectively.

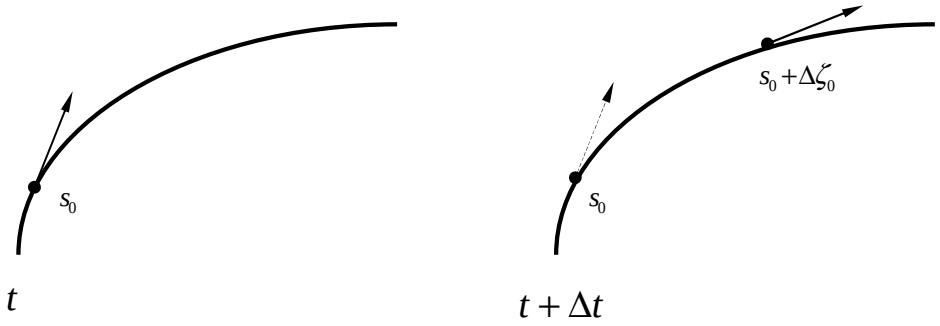

Figure 4.2: Motion of a bulk chain due to reptation.

As follows from Figure 4.2, the position vector $\hat{\mathbf{R}}(s_0,t)$ of segment s_0 of a reptating bulk chain satisfies the following equation of motion

$$\hat{\mathbf{R}}(s_0, t+\Delta t) = \hat{\mathbf{R}}\big(s_0 + \Delta\hat{\zeta}_0, t\big)\,, \tag{4.5}$$

where $\Delta\hat{\zeta}_0$ is a shift of segment s_0 along the parametrization axis due to reptation over the time interval between t and $t+\Delta t$. According to eqn.(2.1), for small Δt the shift $\Delta\hat{\zeta}_0(s_0,t)$ is related to the corresponding physical shift $\Delta\hat{\zeta}(s_0,t)$ along the chain contour (see eqn.(4.3)) via

$$\Delta\hat{\zeta}_0(s_0,t) = \frac{\Delta\hat{\zeta}(s_0,t)}{\hat{\lambda}(s_0,t)}\,,$$

where $\hat{\lambda}(s_0,t)$ is the local stretch at position s_0 and time t. Differentiating both sides of eqn.(4.5) with respect to s_0 and taking into account eqn.(2.2),

one can find that the equation of motion for the bond vector $\hat{\mathbf{b}}(s_0,t)$ of the bulk chain due to reptation is given by

$$\hat{\mathbf{b}}(s_0,t+\Delta t)=\left[1+\frac{\partial\Delta\hat{\zeta}_0}{\partial s_0}\right]\hat{\mathbf{b}}(s_0+\Delta\hat{\zeta}_0,t)\,. \tag{4.6}$$

According to eqn.(4.3), the characteristic time T_{Rept} needed for the bulk chain to reptate a distance of order its length L_{0B} is of order L_{0B}^2/D_c. On the other hand, the retraction time T_{RB} of bulk chains is given by eqn.(2.17) with L_{0T} replaced with $L_{0B}/2$. From eqn.(2.17) and eqn.(4.4) it then follows that $T_{RB}/T_{Rept}\propto N_e/N=1/Z_B$, where N is the number of monomers per bulk chain, N_e the mean number of monomers between constraints, and Z_B the mean number of constraints per bulk chain. Since for a real polymer melt Z_B is usually rather large, the characteristic time scale of retraction is much smaller than that of reptation. Therefore, in the presence of retraction, reptation can be considered as a simultaneous and coordinated motion of all the segments of the chain, so the chain moves in the melt as a whole. This implies that on the time scale of reptation $\hat{\zeta}_0$ is independent of s_0 so that the second term in the square brackets on the RHS of eqn.(4.6) can be neglected. Moreover, reptation is the dominant relaxation mechanism for the bulk chains in the absence of flow or for flows whose rate is smaller than T_{Rept}^{-1}. In flows whose rate is larger than T_{RB}^{-1} (where chain stretch becomes essential), it gives only a minor contribution to the stress relaxation compared to constraint release and retraction, and can be neglected. So in flow regimes where reptation is important the local stretch $\hat{\lambda}\approx 1$ and $\Delta\hat{\zeta}_0$ in eqn.(4.6) can be replaced with $\Delta\hat{\zeta}$. Finally, substitution of eqn.(4.6) into eqn.(4.1) yields

$$\begin{aligned}S^B_{\alpha\beta}(s_0,t+\Delta t)=S^B_{\alpha\beta}(s_0,t)+&<\Delta\hat{\zeta}\,\frac{\partial\hat{b}_\alpha}{\partial s_0}\hat{b}_\beta>_B+\frac{1}{2}<(\Delta\hat{\zeta})^2\frac{\partial^2\hat{b}_\alpha}{\partial s_0^2}\hat{b}_\beta>_B+\\&<\Delta\hat{\zeta}\,\frac{\partial\hat{b}_\beta}{\partial s_0}\hat{b}_\alpha>_B+<(\Delta\hat{\zeta})^2\frac{\partial\hat{b}_\alpha}{\partial s_0}\frac{\partial\hat{b}_\beta}{\partial s_0}>_B+\frac{1}{2}<(\Delta\hat{\zeta})^2\frac{\partial^2\hat{b}_\beta}{\partial s_0^2}\hat{b}_\alpha>_B\,,\end{aligned}$$

where terms of order $\Delta\hat{\zeta}^3$ and higher were neglected. Taking the limit $\Delta t\to 0$ and keeping in mind that $\Delta\hat{\zeta}$ is a zero-mean noise uncorrelated with the corresponding bond vector at the same point, one can find that the equation of motion for $S^B_{\alpha\beta}$ due to reptation has the form

$$\left[\frac{\partial S^B_{\alpha\beta}}{\partial t}\right]_{rept}=D_c\frac{\partial^2 S^B_{\alpha\beta}}{\partial s_0^2}\,. \tag{4.7}$$

It is seen that the contribution of reptation to the equation of motion for $S^B_{\alpha\beta}$ has the form of a diffusion process with the coefficient D_c defined in eqn.(4.4). The diffusion form of eqn.(4.7) implies that, similar to constraint release, reptation leads to relaxation of initially oriented configurations of bulk

chains towards the isotropic one described by the tensor $S^{(eq)}_{\alpha\beta}$ in eqn.(3.3). Specifically, reptation constantly "destroys" and "creates" again portions of the tube near the chain ends, and thereby constantly renews the tube.

In order to solve eqn.(4.7), we also need to specify the boundary conditions for the correlator $S^B_{\alpha\beta}(s_0,t)$. As found earlier for tethered chains (see the discussion after eqn.(3.31)), due to fast CLF motions of the free end of a polymer chain, the corresponding BVPDF is isotropic and the local stretch is relaxed. Therefore, $S^B_{\alpha\beta}(s_0,t)$ satisfies the following boundary conditions

$$S^B_{\alpha\beta}(\pm\, L_{0B}/2,t) = \frac{1}{3}\delta_{\alpha\beta}\,. \tag{4.8}$$

From eqns.(4.7, 4.8) it follows that reptation is described by the set of relaxation times T_p:

$$T_p = \frac{L^2_{0B}}{\pi^2 D_c p^2} \quad , \quad p = 1,3,5,\ldots \tag{4.9}$$

The longest of them ($p=1$) is usually referred to as the reptation time and will be denoted by T_{DB}. According to eqn.(4.7), T_{DB} can be regarded as the characteristic time necessary for a bulk chain to completely renew its tube by reptation. In other words, T_{DB} is the characteristic time needed for the bulk chain to reptate a distance of order its length L_{0B}.

Finally, taking into account eqns.(3.31, 4.7), we can write down the equation of motion for the correlator $S^B_{\alpha\beta}$ of bulk chains (for $0 < s_0 < L_{0B}/2$)

$$\begin{aligned}\frac{\partial S^B_{\alpha\beta}}{\partial t} &= K^B_{\alpha\gamma}S^B_{\beta\gamma} + K^B_{\beta\gamma}S^B_{\alpha\gamma} + \Big[D_c + \nu_B a_0^2\Big]\frac{\partial^2 S^B_{\alpha\beta}}{\partial s_0^2} \\ &+ 2\bar{\xi}_B S^B_{\alpha\beta} + \Big[\int\limits_0^{s_0} dx\,\bar{\xi}_B(x,t)\Big]\frac{\partial S^B_{\alpha\beta}}{\partial s_0} - \frac{1}{\tau_B}(S^B_{\alpha\beta} - S^{eq}_{\alpha\beta})\,.\end{aligned} \tag{4.10}$$

Here $K^B_{\alpha\beta}$ is the gradient velocity tensor for the polymer bulk. In a shear flow, $K^B_{\alpha\beta}$ has only one non-zero component equal to the bulk shear rate $\dot{\gamma}_b$. The third term on the RHS includes both reptation and constraint release. Despite having a different origin, both contributions have the form of a diffusion process. The diffusion due to reptation corresponds to the axial motion of the chain along the tube, whereas the diffusion due to CR represents the lateral motion. The last term on the RHS of eqn.(4.10) arises from contour length fluctuations (CLF). In addition to reptation, which describes the overall translation of the physical chain along the tube, CLF allow a more detailed description of its Brownian motion in the melt. As discussed earlier, CLF lead to local relaxation of the tube near the free ends of the chain towards the isotropic nonstretched configuration described by the tensor tensor $S^{(eq)}_{\alpha\beta}$

in eqn.(3.3). Following eqn.(3.29), the mean relaxation time $\tau_B(s_0)$ of segment s_0 of the tube is given by (for $s_0 < L_{0B}/2 - a$)

$$\tau_B(s_0) \approx \frac{1}{4} T_{RB}\, e^{0.75\, Z_B\, (1-2s_0/L_{0B})^2}\,, \tag{4.11}$$

where Z_B is the mean number of constraints per bulk chain. In eqn.(4.11), for the time constant we used a quarter of the Rouse time T_{RB} of bulk molecules (see eqn.(2.17) where L_{0T} is replaced with $L_{0B}/2$). A more accurate prefactor, which depends on s_0, can be found in [39].

The forth and fifth terms on the RHS of eqn.(4.10) pertain to retraction where $\bar{\xi}_B(s_0,t)$ is the mean local retraction rate of the primitive path at s_0 and time t. In the single relaxation time approximation (see eqn.(2.18)), $\bar{\xi}_B(s_0,t)$ can be written as follows

$$\bar{\xi}_B(s_0,t) \approx -\frac{\bar{\lambda}_B(s_0,t)-1}{T_{RB}} \quad , \quad T_{RB} = \frac{\varsigma N_e L_{0B}^2}{3\pi^2 k_B T}\,. \tag{4.12}$$

Here $\bar{\lambda}_B$ is the mean local stretch and T_{RB} is the Rouse time of bulk molecules. From eqn.(2.17) and (4.12) it follows that the Rouse T_{RB} of a bulk molecule is four times larger than the Rouse time T_{RT} of a tethered chain with the same number of monomers. As was mentioned earlier, the bond vector correlator $S^B_{\alpha\beta}$ contains information on both the mean local stretch and mean local orientation of the bulk molecules. In fact, as follows from eqn.(3.23), in a flow regime where the bulk molecules are stretched only slightly we have that $\bar{\lambda}_B \approx \sqrt{S^B_{\alpha\alpha}}$, where summation is implied over the repeated indices. So eqn.(4.10) is a nonlinear integro-partial differential equation. As was discussed earlier, the single relaxation time approximation may not hold for segments of the bulk chain near the free ends. However, as we will see later on, in practice we are only interested in the value of the correlator $S^B_{\alpha\beta}$ averaged along the chain contour. This implies that we can neglect high order relaxation modes of the local stretch in the equation of motion for these segments and instead use eqn.(4.10). A further discussion of eqn.(4.10) and its comparison with the existing constitutive theories for the bulk chains can be found in [26].

4.4 Constraint release in the bulk

In order to complete eqn.(4.10), we must provide an explicit expression for ν_B, the frequency of constraint release of bulk chains. In the absence of flow, constraint release is driven by reptation. In what follows, it will be referred to as thermal constraint release (TCR). In the presence of flow, another mechanism may give a contribution to constraint release. In this case, each bulk chain undergoes a certain flow-induced drag force which deforms and stretches it. Due to its connectivity, the chain constantly retracts back, in order to restore

its equilibrium length. A simple way to visualize this motion is to imagine a polymer chain pulled by one of its ends through the melt. If one of the chain ends moves (within the mesh of constraints) over a distance of order the mean entanglement spacing a_0, it will release one (if entanglements are pairwise contacts) or more constraints on other chains. Flow-induced constraint release driven by retraction of polymer chains is commonly referred to as convective constraint release (CCR). The importance of CCR in the dynamics of polymer melts was recognized by Marrucci [40].

Let us first calculate the mean lifetime τ of an entanglement in the melt in the absence of flow. For certainty, we assume that all the entanglements in the melt are pairwise contacts between separate polymer chains. At rest, the entanglements are destroyed by reptation of polymer chains. Let δt be the average time needed for a bulk chain to reptate in the melt a distance equal to the mean entanglement spacing a_0. In the absence of CLF, reptation of the bulk chain during the time interval $0...\delta t$ will release (on average) one constraint on another chain. The number $N(t = \delta t)$ of entanglements per unit volume of the melt at time $t = \delta t$ is then given by

$$N(t = \delta t) = N(t = 0) - n\,, \tag{4.13}$$

where the entanglements "creation" mechanism has been ignored. In Eq. (4.13), n is the concentration of the bulk chains in the melt and $N(t = 0) = nZ_B/2$ is the number of the entanglements per unit volume of the melt at time $t = 0$. On the other hand, if τ is the mean lifetime of an entanglement in the melt, then we have that

$$N(t = \delta t) = N(t = 0) \cdot e^{-t/\tau}\,. \tag{4.14}$$

By comparing Eq. (4.13) with Eq. (4.14), one may conclude that

$$\tau = \frac{Z_B}{2}\,\delta t\,. \tag{4.15}$$

According to eqn.(4.3), $\delta t \approx a_0^2/2D_c$, so that finally we have

$$\tau \approx \frac{Z_B}{2}\,\frac{a_0^2}{2D_c}\,. \tag{4.16}$$

Once τ is known, one can readily calculate the frequency ν_B of thermal constraint release in the melt. Eqn.(4.16) specifies the average lifetime of a constraint on a bulk molecule imposed by another bulk chain. Note that some of the bulk molecules may have entanglements with tethered chains and therefore may have constraints which correspond to the tethered chains. However, since the thickness of the interfacial layer is much smaller than the length of the bulk molecule, the average fraction of the "tethered" constraints on each bulk chain is small and can be neglected. Therefore, from eqn.(4.16) the frequency ν_B of TCR can be written as

$$\nu_B = \frac{4D_c}{Z_B a_0^2} \tag{4.17}$$

Substitution of eqn.(4.17) into eqn.(4.10) yields that the corresponding diffusion coefficient of TCR is Z_B times smaller than the one of reptation. So for long monodisperse polymer chains thermal constraint release plays only a minor role in the melt dynamics compared to reptation.

In a flow, constraints on bulk chains can also be released via retraction of surrounding molecules (CCR). CCR works in parallel to and independently of thermal constraint release. To calculate the mean lifetime of an entanglement in the melt due to CCR, let us recall eqn.(4.15). In the case of CCR, δt is the average time necessary for the end of a bulk chain to move (along the chain contour) a distance a_0 due to retraction. If υ is the average velocity between the chain end and the tube, then $\delta t = a_0/\upsilon$. The velocity υ is equal to the retraction velocity of the end along the chain contour and therefore can be expressed in terms of the corresponding mean local retraction rate $\bar{\xi}_B(s_0, t)$ as follows (see also the discussion after eqn.(2.10))

$$\upsilon = \int_0^{L_{0B}/2} ds_0 \, |\bar{\xi}_B(s_0, t)| \,, \tag{4.18}$$

where we took into account that $\bar{\xi}(s_0, t) < 0$. From eqn.(4.18) we then find

$$\delta t = a_0 \left[\int_0^{L_{0B}/2} ds_0 \, |\bar{\xi}_B(s_0, t)| \right]^{-1} . \tag{4.19}$$

By substituting eqn.(4.19) into eqn.(4.15) and taking into account that thermal and convective constraint release work independently of each other, we finally have that in the presence of flow the mean lifetime τ of an entanglement in the melt can be written as follows

$$\tau^{-1} = \frac{2}{Z_B} \left[\frac{2D_c}{a_0^2} + 2\frac{1}{a_0} \int_0^{L_{0B}/2} ds_0 \, |\bar{\xi}_B(s_0, t)| \right] , \tag{4.20}$$

where the extra prefactor 2 before the CCR term stems from the fact that every bulk chain has two free ends which independently contribute to convective constraint release. Finally, from eqn.(4.20) the frequency of constraint release in the melt in the presence of flow is given by

$$\nu_B \approx \frac{4D_c}{Z_B a_0^2} + 2\frac{2}{L_{0B}} \left[\int_0^{L_{0B}/2} dx \, |\bar{\xi}_B(x, t)| \right] , \tag{4.21}$$

where we used that $a_0 \approx a$, where a is the step length of the primitive path equal to L_{0B}/Z_B. The frequency ν_B in eqn.(4.21) represents a combined action

of thermal and convective constraint release. Note that eqn.(4.21) does not account for a possible effect of CLF on thermal constraint release in the melt. Namely, CLF enhance reptation of polymers in their tubes and consequently decrease the lifetime τ of an entanglement in the melt in comparison to the original reptation picture. Following Doi and Edwards [31], inclusion of CLF into eqn.(4.21) amounts to an increase of the reptation diffusion coefficient D_c by the factor $(1 + C/\sqrt{Z_B})^2$, where C is a constant. Direct numerical simulation of reptation and CLF by Likhtman and McLeish [41] give $C \approx 1.52$ (where the difference in the notations has been taken into account).

According to eqn.(4.21), the frequency of CCR is proportional to the mean retraction rate of the bulk chains averaged along the chain contour. Eqn.(4.21) shows explicitly that CCR originates from retraction and vanishes in the absence of flow, where the chains are not stretched. Note that the single relaxation time approximation (see eqn.(4.12)) may not be applicable for chain segments near the free ends (see the discussion after eqn.(2.18)). Since it is these segments that give the major contribution to the integral in eqn.(4.21), in eqn.(4.21) one has to use the exact expression for the retraction rate $\bar{\xi}_B(s_0, t)$ which accounts for the fast relaxation modes of the local stretch. As follows from eqn.(2.14) and eqn.(4.4), $\bar{\xi}_B(s_0, t)$ is given by

$$\bar{\xi}_B = 3Z_B D_c \frac{\partial^2 \bar{\lambda}_B}{\partial s_0^2}\,, \tag{4.22}$$

where $\bar{\lambda}_B$ is the mean local stretch of a bulk chain. In the linear viscoelastic regime, i.e., at flow rates less than the reciprocal reptation time T_{DB} (see eqn.(4.9)), bulk chains are hardly stretched. From eqn.(4.22) and eqn.(4.21) it then follows that the CCR frequency is small. Clearly, in this regime CCR plays only a minor role in the melt dynamics compared to reptation and convection, and can be ignored. However, at higher flow rates, when chain stretch becomes essential, the CCR frequency can be of order or even larger than T_{BD}^{-1}. In this regime, CCR becomes an important relaxation mechanism for bulk chains. The important role of CCR in the dynamics of polymer melts was first recognized by Marrucci [40]. He pointed out that in slow flows convective constraint release is a slow, and perhaps not important, mechanism for monodisperse polymer melts. However, in flows with a rate larger than T_{DB}^{-1}, constraints imposed on a bulk chain may be swept away rapidly by the flow. In view of eqn.(2.10), we can rewrite the CCR frequency as

$$\nu_B = 2\frac{2}{L_{0B}} \int_0^{L_{0B}/2} dx \left[K_{\alpha\beta} < \hat{u}_\alpha \hat{u}_\beta \hat{\lambda} >_B - \frac{\partial \bar{\lambda}_B}{\partial t} \right]. \tag{4.23}$$

As is seen, ν_B contains two contributions. In order to explain their origin, let us imagine a chain which is pulled by one of its ends through the melt. If the chain is inextensible, then the average velocity between the chain and the melt

is equal to $K_{\alpha\beta}\overline{< \hat{u}_\alpha \hat{u}_\beta >}_B$ (where the bar denotes averaging along the chain contour), which is the projection of the mesh velocity on the chain contour. This corresponds to the first term on the RHS. In the presence of stretch, this motion is also accompanied by retraction which provides an additional velocity between the chain and the melt (the second term).

4.5 Results and discussion

Eqn.(4.10) extended with eqn.(4.21) was analyzed numerically using the conventional Newton method for solving systems of nonlinear equations. The numerical procedure of solving nonlinear integro-partial differential equations similar to eqn.(4.10) was discussed earlier in Chapter 3. Attention must be paid, however, to the fact that in eqn.(4.10) the frequency ν_B of constraint release is now a function of the bond vector correlator $S^B_{\alpha\beta}$ (via the mean local stretch in eqn.(4.23)), and is not a free parameter. The model predictions for various flow histories are presented in Figs.(4.3-4.6).

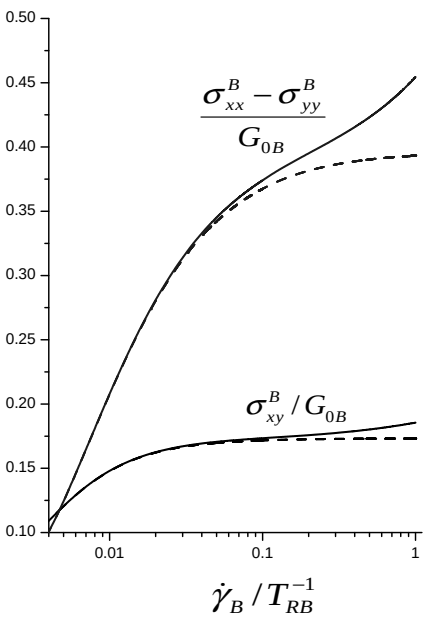

Figure 4.3: Shear stress and first normal stress difference vs shear rate for $Z_B = 30$. The dotted lines are predictions for inextensible chains.

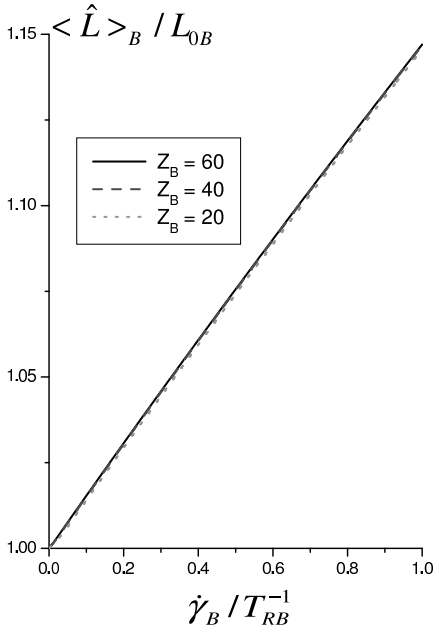

Figure 4.4: Mean chain lengthening vs shear rate for different Z_B.

In Figure 4.3 and Figure 4.4, the steady shear predictions are shown. In Figure 4.3, we plot the bulk shear stress σ^B_{xy} and the first normal stress difference $N_1 = \sigma^B_{xx} - \sigma^B_{yy}$ as functions of the shear rate in the bulk $\dot{\gamma}_B$. It is seen that both σ^B_{xy} and N_1 increase monotonically with $\dot{\gamma}_B$, and have three different regimes, in accordance with experimental observations [42, 43]. At low shear

rates $\dot{\gamma}_B < T_{DB}^{-1}$, there is a linear viscoelastic regime in which $\sigma_{xy}^B \propto \dot{\gamma}_B$ and $N_1 \propto \dot{\gamma}_B^2$, similar to the behavior predicted by the reptation model for inextensible chains of Doi and Edwards [31]. In this regime, it is convection and reptation that govern the dynamics of the bulk chains, whereas the contribution of constraint release is small. Moreover, in this regime polymer chains are hardly stretched so that the predictions of the "full" theory with chain stretch and a theory for inextensible chains (eqn.(4.10) where $T_{RB} \to 0$) coincide. In the nonlinear regime $T_{DB}^{-1} < \dot{\gamma}_B < T_{RB}^{-1}$, the shear stress σ_{xy}^B increases only slightly with $\dot{\gamma}_B$, whereas N_1 continues to grow rapidly. As mentioned earlier, in this regime CCR starts to play an important role in the dynamics of the bulk chains, preventing their orientation by the flow. Omission of CCR leads to an excessive chain alignment with the flow and therefore to the unrealistic behavior in which $\sigma_{xy}^B \propto \dot{\gamma}_B^{-0.5}$ and N_1 approaches a constant value (see, for example, Doi and Edwards [31] and Marrucci and Grizzuti [44]). In the nonlinear regime, omission of stretch leads to an underestimate of the actual values of σ_{xy}^B and N_1. Near the shear rate $\dot{\gamma}_B \approx T_{RB}^{-1}$ the slopes of both curves in Figure 4.3 again become steep due to significant chain stretch. The system enters the third regime in which stretch effects become dominant.

Figure 4.4 shows the mean chain lengthening $\lambda =< \hat{L} >_B / L_{0B}$ versus the bulk shear rate $\dot{\gamma}_B$ for different molecular weights M of bulk chains (we remind that Z_B is proportional to M). In the linear viscoelastic regime, the bulk chains are hardly stretched. As follows from eqn.(4.10), in this regime $\lambda = 1 + O(\dot{\gamma}_B^2 T_{RB}^2)$. In the nonlinear regime $T_{DB}^{-1} < \dot{\gamma}_B < T_{RB}^{-1}$, the shear stress σ_{xy}^B is nearly independent of $\dot{\gamma}_B$ (see Figure 4.3). From eqn.(4.10) it then follows that in this regime λ increases linearly with $\dot{\gamma}_B$, as depicted in Figure 4.4. Written as functions of the dimensionless shear rate $\dot{\gamma}_B T_{BR}$, all the curves corresponding to different molecular weights superimpose to a single one. Since $T_{RB} \propto Z_B^2$ (see eqn.(4.12)), this implies that $\lambda \propto Z_B^2$, and for a given $\dot{\gamma}_B$ longer chains are more stretched, as expected. Figure 4.4 shows explicitly that the chain stretch becomes especially important as $\dot{\gamma}_B$ approaches the reciprocal Rouse time T_{RB}^{-1}. Note that at $\dot{\gamma}_B = T_{RB}^{-1}$ the bulk chains have approximately 15% stretch, whatever the molecular weight.

In Figure 4.5 and Figure 4.6, the model predictions are shown for transient flows. In this case, one has to solve time dependent equation (4.10) with appropriate initial conditions. To do so, an implicit time integration scheme has been implemented. At each time step, this scheme requires a solution of a system of nonlinear integro-partial differential equations similar to that obtained in steady shear flows. Figure 4.5 shows early time relaxation of the bulk shear stress σ_{xy}^B after the cessation of a steady shear flow. The initial conditions for σ_{xy}^B are thus given by the corresponding values of the steady-shear stress. As found, the curves corresponding to initial shear rates $\dot{\gamma}_B$ much smaller than T_{RB}^{-1} nearly merge which implies that the stress relaxation is independent of the "prior" shear rate. In this regime, bulk chains are not

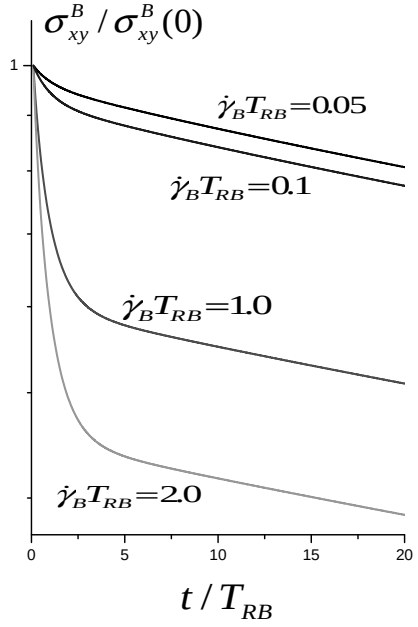

Figure 4.5: Early time relaxation of shear stress, normalized by its initial value at steady state, versus time after cessation of steady-state shear flow for different prior shear rates. $Z_B = 30$.

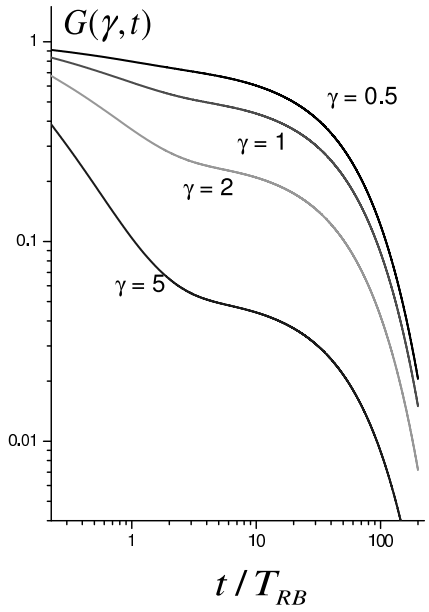

Figure 4.6: Relaxation of dimensionless shear modulus $G = 3\sigma^B_{xy}/(\gamma G_{0B})$ versus time after step shear strains of different magnitudes γ. $Z_B = 30$.

stretched so that relaxation of σ^B_{xy} can only be associated with relaxation of configurations of the bulk chains initially aligned by the flow due to reptation. Note that after the reptation time T_{DB} most of the bulk chains will "renew" their tubes by reptation. Due to the Brownian nature of reptation, "new" configurations of the bulk chains are uncorrelated with those at time $t = 0$ so that the corresponding BVPDF at $t = T_{DB}$ becomes isotropic. The isotropic BVPDF corresponds to the diagonal bond vector correlator (see eqn.(3.3)) and thus zero shear stress (see eqn.(4.2)). Therefore, after T_{DB} the initial shear stress σ^B_{xy} in the melt is completely relaxed.

At higher shear rates, when the bulk chains are stretched prior to the cessation of the flow, the relaxation of the shear stress is a two step process. First, on the time scale of order T_{RB}, it is only governed by retraction. In other words, the bulk chains shrink to acquire their equilibrium length. Note that in this time interval the rate of stress relaxation increases with $\dot\gamma_B$, similar to the behavior observed in experiments [45]. That is to say, the more chains are stretched, the faster they relax their stress. This is due to the influence of chain stretch on the rate of CCR. According to eqn.(4.23), the CCR frequency ν_B is proportional to the mean local stretch $\bar\lambda_B$, which is in turn proportional to the bulk shear rate $\dot\gamma_B$ (see Figure 4.4).

Attention must be paid to the fact that due to more effective constraint release, after time T_{RB} chains that initially were more stretched are less oriented

than those at smaller shear rates, and therefore show smaller amounts of the shear stress. After time T_{RB}, the shear stress decays at the same rate for all the curves with different $\dot{\gamma}_B$. Clearly, in this regime the chain stretch has completely relaxed so that the bulk chains continue to randomize their orientations via reptation alone. Note that in the case of inextensible chains one would expect that the stress relaxation rate via CCR is independent of the bulk shear rate $\dot{\gamma}_B$ prior the cessation.

In Figure 4.6, the model predictions are shown for a case of step shear deformation. Figure 4.6 shows relaxation of the shear modulus $G = 3\,\sigma^B_{xy}/(\gamma G_{0B})$ after a step shear of various magnitudes γ. The melt is assumed to be at equilibrium prior to the onset of deformation. After a small strain step, the bulk chains are hardly stretched so that the shear stress relaxes via reptation. In contrast, after a large strain step the bulk chains are stretched significantly so that at first the shear stress decays via relaxation of stretch. At larger times the stress relaxation is again governed by reptation. Such a "reptational" regime of the stress relaxation has been successfully described by the reptation model for inextensible chains of Doi and Edwards [31]. They found that for $t > T_{RB}$ all the curves $G(\gamma, t)$ pertaining to different values of the strain γ (see Figure 4.6) can be superposed into a single one by dividing $G(\gamma, t)$ by the corresponding value of the so-called damping function $h(\gamma)$ [31]. Figure 4.6 shows that an explicit form of the dumping function $h(\gamma)$ can readily be inferred from the model predictions.

Eqn.(4.21) shows that in the presence of flow the frequency ν_B of constraint release in the bulk is not only a function of the molecular parameters of the melt, but also a function of the bond vector correlator $S^B_{\alpha\beta}$ of bulk chains (via the local stretch). This implies that calculation of ν_B amounts to solving the equation of motion for $S^B_{\alpha\beta}$ given by eqn.(4.10). On the other hand, as we discussed earlier, ν_B is the entry parameter for the equation of motion of tethered chains given by eqn.(3.31). From the above, one may conclude that in order to quantify the dynamics of the tethered chains both eqn.(4.10) and eqn.(3.31) must be solved simultaneously. In the next chapter, we will further discuss this system and its possible applications.

Chapter 5

Slip due to disentanglement

In the previous chapters, we derived the equations of motion for bulk and tethered chains and established that in reality they are coupled through constraint release. These equations constitute of a system of equations which governs the overall flow in the die, including the polymer bulk and the interfacial layer. This system contains information about the polymer flow in the vicinity of the wall and therefore can further be used to calculate the fluid velocity at the polymer melt/die wall interface. In this chapter, this system will be solved in a case of parallel plate geometry for which precise experimental data on slip are available. Hereafter, we will ignore possible desorption of the tethered chains from the wall.

5.1 Parallel plate rheometer

A simple sketch of a parallel plate rheometer is shown in Figure 5.1. It is a controlled shear rate apparatus in which a homogeneous polymer melt is confined between two metal plates. The lower plate is fixed and will be referred to as "wall" throughout the text. The upper plate is moving at a certain constant velocity V_p. No slippage is assumed between the upper plate and the melt. The movement of the upper plate creates a linear velocity profile in the melt. However, as is seen in Figure 5.1, there are two different flow regions that must be distinguished. The first one is the polymer bulk. It only contains bulk polymer chains and has a shear rate $\dot{\gamma}_b$. The second region is the interfacial layer. It may contain both tethered and bulk molecules. The shear rate in this layer will be denoted by $\dot{\gamma}_w$.

Since the bulk and the interfacial layer contain different sorts of polymer molecules, the corresponding shear rates $\dot{\gamma}_b$ and $\dot{\gamma}_w$ are also different. Attention must be paid to the fact that the shear rates $\dot{\gamma}_b$ and $\dot{\gamma}_w$ are not independent, but certain functions of the upper plate velocity V_p. Therefore, in order to find their explicit dependence on V_p, we need two more equations. The first

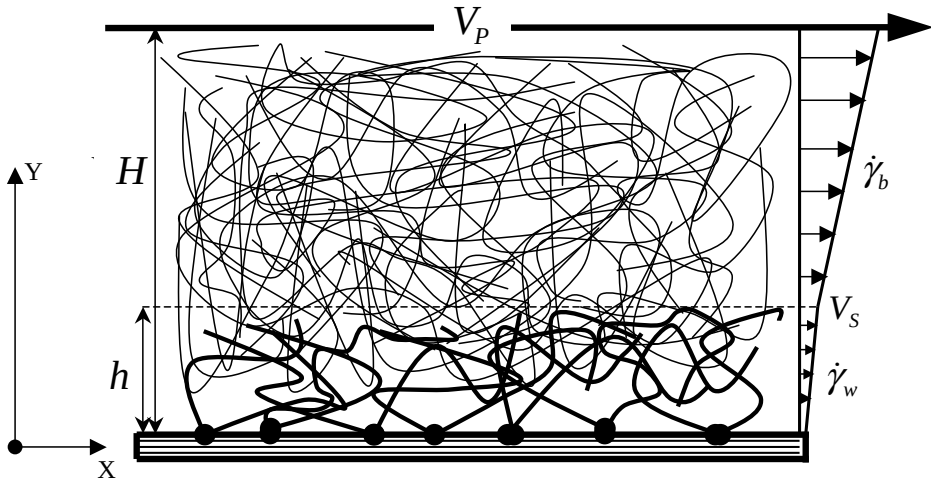

Figure 5.1: The parallel plate geometry (not on scale): H is the distance between plates; h is the thickness of the interfacial layer; $\dot\gamma_w$ and $\dot\gamma_b$ are the shear rates in the layer and the bulk, respectively. The slip velocity V_s is defined as the average velocity of monomers at the top of the layer.

equation stems from the continuity of the average velocity of monomers in the melt at the interface between the bulk and the interfacial layer, which can be written in the following form

$$h\dot\gamma_w + \dot\gamma_b(H-h) = V_p\,, \tag{5.1}$$

where H is a distance between the plates and h the thickness of the interfacial layer. The first term on the LHS gives the slip velocity V_s, defined as the average velocity of monomers at the top of the interfacial layer, whereas the second represents a change in the melt velocity over the bulk. According to Figure 3.4, the thickness h is a nonlinear function of the wall shear rate $\dot\gamma_w$. Moreover, as follows from eqn.(3.38), h may also depend on $\dot\gamma_b$ via the frequency ν_T of constraint release of tethered chains. So for a given $\dot\gamma_b$, eqn.(5.1) is a nonlinear equation for $\dot\gamma_w$. The second equation which relates $\dot\gamma_b$ and $\dot\gamma_w$ stems from the force balance at the interface between the bulk and the layer. It can be written as the continuity of the shear stress:

$$\sigma^B_{xy}(\dot\gamma_b) = \sigma^I_{xy}(\dot\gamma_w)\,, \tag{5.2}$$

where we took into account that the polymer melt is homogeneous and so neglected the spatial dependence of the shear stress. The wall shear stress σ^I_{xy} and the shear stress in the bulk σ^B_{xy} are given by eqn.(3.4) and eqn.(4.2), respectively. According to Figure 3.5, σ^I_{xy} is a nonlinear nonmonotonous function of $\dot\gamma_w$. It may also depend on $\dot\gamma_b$ via the frequency of constraint release ν_T. So eqn.(5.2) yields another nonlinear relation between $\dot\gamma_b$ and $\dot\gamma_w$.

For a given velocity V_p of the upper plate, eqn.(5.1) and eqn.(5.2) enable us to calculate the corresponding shear rates $\dot\gamma_b$ and $\dot\gamma_w$. The shear stress in the bulk and in the layer which enter eqn.(5.2) are calculated by solving the equations of motion for the bulk (4.10) and tethered (3.31) chains, which in

turn contain $\dot{\gamma}_b$ and $\dot{\gamma}_w$ as input parameters. This implies that eqns.(3.31, 4.10) extended with eqns.(5.1, 5.2) form a closed system of equations which governs the dynamics of the overall polymer flow in the die. To be able to solve this system, we must specify explicitly the frequency ν_T of constraint release of tethered chains which enters eqn.(3.31) as well as the elastic moduli of the bulk and interfacial layer in eqn.(3.4) and eqn.(4.2).

5.2 Constraint release on tethered chains

According to Figure 3.6, in general, each tethered chain has two sorts of constraints: bulk and tethered ones. Bulk constraints are imposed by polymer molecules from the bulk, and can be released via their reptation or retraction. Tethered constraints are imposed by nearby tethered chains, and are released via their contour length fluctuations. Let τ_B and τ_T be the mean lifetime of the bulk and tethered constraints, respectively. Then, ν_T is given by eqn.(3.39). In the previous chapter, when studying the dynamics of bulk molecules in the presence of flow, we found an explicit form of τ_B as a function of the molecular parameters of bulk chains (see eqn.(4.21)). Therefore, in order to make eqn.(3.39) explicit, we need to calculate the mean lifetime τ_T as well as the mean fraction ϕ_{iZ} of bulk constraints per tethered chain.

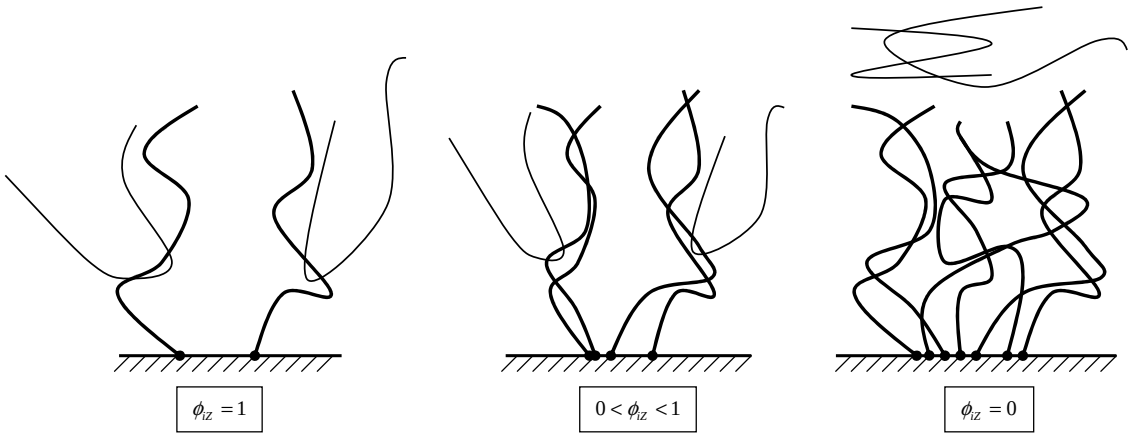

Figure 5.2: Grafting regimes. From left to right: mushroom regime, intermediate regime, and dry-brush regime. Thick and thin lines stand for tethered and bulk chains, respectively.

The lifetime τ_T of the tethered constraints was estimated by Ajdari et al [46]. They found that τ_T increases exponentially with the molecular weight of tethered chains and can be written as

$$\tau_T \approx T_{DB}(Z_T)\, Z_T^{-1}\, exp(1.5 Z_T)\,, \tag{5.3}$$

where $T_{DB}(Z_T)$ is the reptation time of a bulk chain with Z_T constraints. On the other hand, according to eqns.(4.9, 4.17), the mean lifetime of a bulk constraint due to TCR is of order $T_{DB}(Z_B)/Z_B$. So for long enough tethered

chains ($Z_T > 5$ if $Z_B < 100$) the mean lifetime of a tethered constraint is much larger than that of a bulk one. Thus, one may think that only the bulk constraints are released on a tethered chain, so eqn.(3.39) boils down to

$$\nu_T \approx \nu_B \phi_{iZ} \,, \tag{5.4}$$

where ν_B is the CR frequency in the bulk and ϕ_{iZ} the mean fraction of bulk constraints per tethered chain. Note that ϕ_{iZ} is a function of the surface density of the tethered chains. At low surface densities, entanglements between neighboring tethered chains are unlikely so that $\phi_{iZ} = 1$ (see Figure 5.2). This regime is often referred to as the mushroom regime. At very high surface densities, bulk chains are expelled from the interfacial layer so that it is only populated by the tethered chains. In this regime (usually referred to as the dry-brush regime), the tethered chains have only tethered constraints so that $\phi_{iZ} = 0$. There is also an intermediate grafting regime in which a tethered chain has both bulk and tethered constraints, and so $0 < \phi_{iZ} < 1$.

5.3 Model of half-entanglements

Let Σ_T be the surface density of the tethered chains, that is the number of the tethered chains per unit area of the die wall. In order to find an explicit dependence of the fraction ϕ_{iZ} on Σ_T, we will assume that all the entanglements in the melt are pairwise contacts between separate polymer chains. Then, the entanglement network in the layer can be imagined as consisting of interacting "half-entanglements" (see Figure 5.3). Every tethered chain contributes to $Z_T/2$ entanglements, or equivalently, provides Z_T "tethered" half-entanglements. Every bulk chain present in the layer may provide up to Z_B "bulk" half-entanglements.

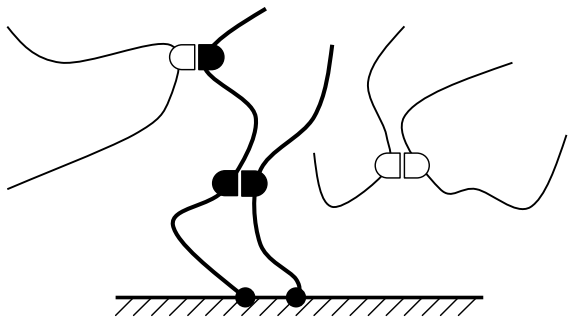

Figure 5.3: The entanglement network in the interfacial layer.

Each half-entanglement "interacts" with another tethered or bulk one available in the interfacial layer. Two half-entanglements build an entanglement of one of the three types: tethered-tethered (T-T), bulk-bulk (B-B), or bulk-tethered (B-T). Let W_T and W_B be a fraction of tethered and bulk half-entanglements per unit volume of the layer, respectively. Since half-entanglements

are distributed homogeneously in the layer, the corresponding volume fractions of entanglements of each type are given by

$$W_{BB} = W_B W_B \quad W_{TT} = W_T W_T \quad W_{BT} = 2W_B W_T \tag{5.5}$$

The factor 2 in the expression for W_{BT} is due to the fact that $W_{BT} = W_{TB}$. Since each tethered chain provides Z_T tethered half-entanglements, the number of the tethered half-entanglements per unit area of the wall in the layer is $Z_T\Sigma_T$, where Σ_T is the surface density of tethered chains. On the other hand, the total number of half-entanglements per unit area of the wall in the layer is equal to $2h/a_0^3$, where h is the layer thickness and a_0 the mean entanglement spacing. So the volume fractions of half-entanglements W_T and W_B are

$$W_T = a_0^3 \frac{Z_T \Sigma_T}{2h} \ , \ W_B = 1 - a_0^3 \frac{Z_T \Sigma_T}{2h} \, , \tag{5.6}$$

where we used that $W_T + W_B = 1$. As follows from eqn.(5.6), if the surface density Σ_T of the tethered chains is equal to the following critical value

$$\Sigma_T^* = \frac{2h}{a_0^3} \frac{1}{Z_T} \, , \tag{5.7}$$

the volume fraction W_B of the bulk half-entanglements vanishes, which means that the layer no longer contains bulk chains. In other words, the layer is only populated by the tethered chains. So Σ_T^* can be associated with the surface density of the dry-brush regime (see Figure 5.2).

In terms of the volume fractions of bulk and tethered half-entanglements, the mean fraction ϕ_{iZ} of bulk constraints per tethered chain can be written as

$$\phi_{iZ} = \frac{W_{BT}}{W_{TT} + W_{BT}} = \frac{2W_B}{W_T + 2W_B} \, , \tag{5.8}$$

where use was made of eqn.(5.5). According to eqn.(5.8), in the dry-brush regime $\phi_{iZ} = 0$ so that all the constraints on the tethered chains are tethered, as expected. In the mushroom regime, for which $\Sigma_T \to 0$, from eqn.(5.6) it follows that $\phi_{iZ} = 1$. Hence, all the constraints on the tethered chains are bulk, as expected. Let Σ_T^{**} be the critical surface density at which the layer enters the intermediate grafting regime. The mushroom regime then corresponds to surface densities $\Sigma_T < \Sigma_T^{**}$. The critical surface density Σ_T^{**} is a surface density of the tethered chains at which each tethered chain has on average only one tethered constraint, and so $\phi_{iZ} = 1 - 1/Z_T$. Therefore, from eqn.(5.6) and eqn.(5.8) one can find that

$$\Sigma_T^{**} \approx \frac{4h}{a_0^3} \frac{1}{Z_T^2} \, . \tag{5.9}$$

Comparison of eqn.(5.9) with eqn.(5.7) yields that the critical surface density of the intermediate regime is approximately $Z_T/2$ times smaller than the surface density of the dry brush regime.

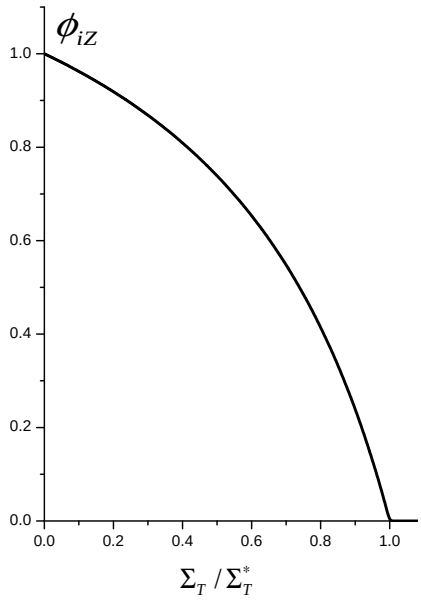

Figure 5.4: Mean fraction of bulk constraints per tethered chain vs surface density of tethered chains.

The behavior of ϕ_{iZ} (see eqn.(5.8)) as a function of Σ_T is shown in Figure 5.4. It is seen that ϕ_{iZ} is a monotonically decreasing function of Σ_T, which implies that the role of interactions between neighboring tethered chains increases with Σ_T. In the mushroom regime $\phi_{iZ} \approx 1$ so that the frequency ν_T of constraint release on the tethered chains (see eqn.(5.4)) is equal to the corresponding frequency ν_B of constraint release in the polymer bulk, calculated in the previous chapter (see eqn.(4.21)). However, at higher surface densities, where interactions between neighboring tethered chains become essential and thus $\phi_{iZ} < 1$, ν_T can be much smaller than ν_B. Clearly, in this regime constraint release on the tethered chains is "suppressed" by interactions between separate tethered chains. Note that it is constraint release that prevents orientation of the tethered chains by the flow. Therefore, one may expect that by increasing the surface density of the tethered chains we "ease" their alignment by the flow and thus facilitate slip via disentanglement. So, at high surface densities, due to the suppressed constraint release, wall slip via disentanglement may occur earlier than in the mushroom regime.

5.4 Elastic modulus of the interfacial layer

To solve eqn.(5.2), we only need to know the ratio between the elastic moduli of the layer G_{0I} and the bulk G_{0B}. Let us show that by using the half-entanglements model developed earlier, it can readily be expressed in terms of the molecular parameters of the melt and the surface density Σ_T of the

tethered chains. According to Doi and Edwards [31], G_{0B} is given by

$$G_{0B} = \frac{nMk_BT}{M_e}\,, \tag{5.10}$$

where n is the concentration of the bulk chains in the melt, M their molecular weight, and M_e the average molecular weight between entanglements. Note that eqn.(5.10) can rewritten in terms of the mean equilibrium entanglement spacing a_0. To show this, let us point out a unit volume in the bulk. If all the entanglements in the melt are pairwise contacts between separate polymers, then the total number N of entanglements per this volume is given by

$$N = \frac{n}{2}Z_B = \frac{1}{a_0^3}\,, \tag{5.11}$$

where Z_B is the the mean number of constraints per bulk chain. Notice that Z_B is equal to M/M_e. Then, from eqn.(5.10) and eqn.(5.11) one can find that

$$G_{0B} = \frac{2k_BT}{a_0^3}\,. \tag{5.12}$$

Since a_0^3 specifies the average volume "occupied" by one entanglement, eqn.(5.12) explicitly shows that the elastic modulus G_{0B} of the bulk is proportional to the equilibrium number of entanglements per unit volume of the melt, in accordance with earlier predictions of the rubber elasticity theory (see, for example, de Gennes [47]). An expression similar to eqn.(5.12) can also be written for the elastic modulus G_{0I} of the interfacial layer. However, as was recognized by Joshi et al [22], it is mostly entanglements between bulk and tethered chains that are active in transferring stress from the flowing bulk to the interfacial layer. Thus, G_{0I} can be written as

$$G_{0I} \approx \frac{2k_BT}{a_0^3}\psi_{BT}^0\,, \tag{5.13}$$

where ψ_{BT}^0 is the equilibrium fraction of bulk-tethered (B-T) entanglements per unit volume in the interfacial layer. According to eqns.(5.5, 5.6, 5.7), ψ_{BT}^0 has the form

$$\frac{G_{0I}}{G_{0B}} = \psi_{BT}^0 = \frac{W_{BT}^0}{W_{BB}^0 + W_{BT}^0 + W_{TT}^0} = 2\,\frac{\Sigma_{0T}}{\Sigma_{0T}^*}\left[1 - \frac{\Sigma_{0T}}{\Sigma_{0T}^*}\right]. \tag{5.14}$$

Here Σ_{0T}^* is the equilibrium surface density of the dry-brush regime (see eqn.(5.7) where h is replaced with its equilibrium value h_0). Σ_{0T} is the equilibrium surface density of the tethered chains. We remind that in the absence of desorption Σ_{0T} is constant and equal to the actual surface density Σ_T in eqn.(5.6). An expression for ψ_{BT}^0 was also proposed by Joshi et al [22]. Based on phenomenological arguments, they found that $\psi_{BT}^0 \propto \phi_Z^0\,\Sigma_{0S}\,a_0^2$, where ϕ_Z^0 is the mean equilibrium fraction of bulk constraints per tethered chains (see

eqn.(5.8)). This relation was further used to calculate the stick-slip law over a wide range of surface densities. However, as follows from eqn.(5.8) and eqn.(5.14), it only holds in the vicinity of the dry-brush regime, and thus cannot be applied in the mushroom or intermediate grafting regimes.

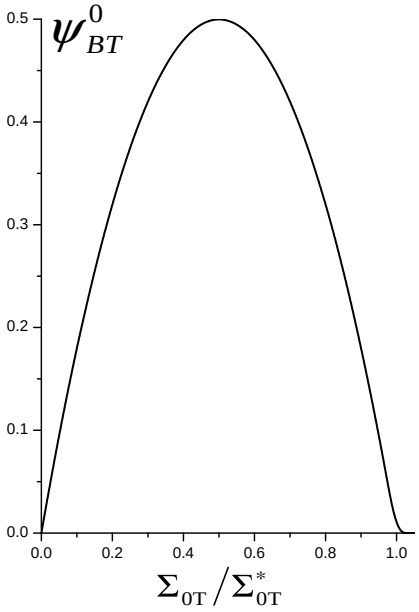

Figure 5.5: Equilibrium fraction of B-T entanglements per unit volume in the interfacial layer vs surface density of tethered chains.

The behavior of ψ^0_{BT} as a function of Σ_{0T} is shown in Figure 5.5. As seen, ψ^0_{BT} is a nonmonotonous function of Σ_{0T}. At small Σ_{0T}, neighboring tethered chains do not overlap and contribute independently to ψ^0_{BT}. According to eqn.(5.14), in this regime $\psi^0_{BT} \propto \Sigma_{0T}$, which implies that addition of one tethered chain to the interfacial layer will create Z_T new bulk-tethered entanglements. At the critical surface density Σ^{**}_{0T} (see eqn.(5.9)), neighboring tethered chains start to overlap. In this regime, addition of one tethered chain to the layer will create both tethered-tethered and bulk-tethered entanglements. At $\Sigma_{0T} \approx 0.5\,\Sigma^*_T$ the number of the bulk-tethered entanglements in the layer is maximal and equal to half of the total amount of entanglements in the layer. In this regime, all the bulk chains present in the layer are already entangled with the tethered ones so that addition of one tethered chain to the layer will "replace" Z_T bulk-tethered and bulk-bulk entanglements with Z_T tethered-tethered ones. By increasing Σ_{0T}, we increase the number of entanglements between the tethered chains, which results in a gradual "exclusion" of the bulk molecules from the interfacial layer and consequently leads to a decrease in ψ^0_{BT}. At $\Sigma_{0T} = \Sigma^*_{0T}$ the layer is in the dry-brush regime and no longer contains bulk-tethered entanglements, and thus $\psi^0_{BT} = 0$. Note that the nonmonotonous behaviour of ψ^0_{BT} was also predicted in [22].

According to eqn.(3.4) and eqn.(5.14), the wall shear stress σ^I_{xy} is proportional to the equilibrium volume fraction ψ^0_{BT} of the bulk-tethered entanglements in the layer. In the absence of these entanglements, we have that $\sigma^I_{xy} = 0$ and

therefore $\dot{\gamma}_w = 0$ (see Figure 3.5), irrespective the value of the upper plate velocity V_p. In this case, the bulk and the tethered chains do not interact with each other so that the polymer bulk slips freely over the interfacial layer. In reality, in the absence of the bulk-tethered entanglements the bulk and the tethered chains may still interact via monomer-monomer friction, a mechanism which is not included in eqn.(3.4). In the presence of the monomer-monomer friction both σ^I_{xy} and $\dot{\gamma}_w$ will have small, but finite, values proportional to the velocity of the bulk chains near the interface between the bulk and the interfacial layer [37]. However, in the presence of the bulk-tethered entanglements the contribution of the monomer-monomer friction to eqn.(3.4) is small and can be neglected.

5.5 Results and Discussion

Having specified the CR frequency ν_T of tethered chains and the elastic moduli of the bulk and interfacial layer, we are now able to describe quantitatively the polymer flow in the die. In fact, the equation of motion for the interfacial layer (see eqn.(3.31)) and for the bulk (see eqn.(4.10)) extended with eqns.(5.1, 5.2) form a closed system of equations which governs the dynamics of the whole polymer flow in the die and therefore can provide quantitative predictions for the stick-slip boundary conditions at the die wall. The independent input parameters for this system are: the mean number Z_B of constraints per bulk chain, the mean number Z_T of constraints per tethered chain, the Rouse time T_{RB} of bulk chains, the mean entanglement spacing a_0, the step length a of the primitive path, and the surface density Σ_T of tethered chains.

The final system was analyzed numerically using the procedure described earlier in Chapter 3 and 4. Attention must be paid to the fact that eqn.(3.31) and eqn.(4.10) are not independent. Namely, as was discussed earlier, eqn.(3.31) is coupled to eqn.(4.10) via the frequency ν_T of constraint release of the tethered chains. This implies that in general eqn.(3.31) depends on both the bulk $\dot{\gamma}_b$ and the wall $\dot{\gamma}_w$ shear rates. In contrast, since the average fraction of "tethered" constraints on the bulk chains is small, one can neglect the dependence of eqn.(4.10) on $\dot{\gamma}_w$ and so consider eqn.(4.10) as a function of $\dot{\gamma}_b$ alone. This is an important property of the obtained system which allows one to simplify remarkably the numerical algorithm.

The procedure of solving the system of eqns.(3.31, 4.10, 5.1, 5.2) is given below. First, for a certain bulk shear rate $\dot{\gamma}_b$ we solve eqn.(4.10). Its solution gives us the corresponding values of the CR frequency ν_B of the bulk chains and the bulk shear stress σ^B_{xy}. The obtained values of ν_B and σ^B_{xy} are then substituted into eqn.(3.31) and eqn.(5.2), respectively. Next, eqn.(5.2) is solved using a simple iterative search algorithm to compute the wall shear rate $\dot{\gamma}_w$ pertaining to the given $\dot{\gamma}_b$. Each step of this algorithm requires a solution of

eqn.(3.31). For the found $\dot{\gamma}_w$, eqn.(3.31) gives the corresponding thickness h of the interfacial layer. Finally, the found values of $\dot{\gamma}_b$, $\dot{\gamma}_w$, and h are substituted into eqn.(5.1) to calculate the velocity V_p of the upper plate. After this, the procedure is repeated again for a larger $\dot{\gamma}_b$ until a certain critical point is reached after which the system has only the trivial solution, that is $\dot{\gamma}_w = 0$, $\dot{\gamma}_b = 0$. As we mentioned before, such a trivial solution corresponds to a regime of complete disentanglement between the bulk and the tethered chains. So the critical point can be associated with a point at which the bulk and the tethered chains fully disentangle and cohesive slip occurs.

Let V_p^{cr} be the velocity of the upper plate at the critical point. As we will see later, at V_p^{cr} the near wall layer jumps from the "entangled" to the "fully disentangled" state, which in turn leads to a jump in the melt velocity at the wall. After the jump, the tethered chains are squeezed against the wall by the strong flow. They occupy a very thin near-wall layer of thickness of order a_0, the mean entanglement spacing. The polymer bulk slips freely over the layer of the smashed tethered chains, which implies that the velocity of monomers in the melt is no longer continuous at the interface between the bulk and this layer. In this case, the slip velocity V_s can be defined as the velocity of monomers in the bulk near the interface. Clearly, after the disentanglement we have that $V_s = V_p$ (if we neglect the monomer-monomer friction between the bulk and the tethered chains). In what follows, we will mostly focus on flow regimes prior to the transition point, and discuss the exact mechanics of the stick-to-slip transition initiated by the flow. The trivial slip regime after the transition point will be discussed only briefly.

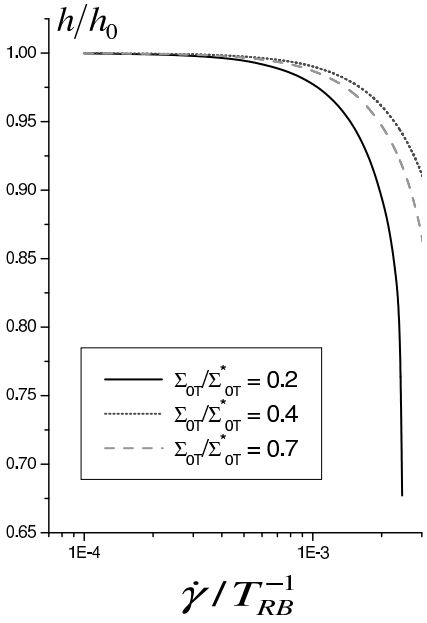

Figure 5.6: Thickness of the interfacial layer vs global shear rate for different surface densities of tethered chains. For $Z_B = 30, Z_T = 10$.

The steady state model predictions for the polymer flow in the die are presented in Figs.(5.6 - 5.13). In Figure 5.6, the thickness h of the interfacial layer

(see eqn.(3.37)) is shown as a function of the "global" shear rate $\dot{\gamma} = V_p/H$ up to the critical point for different surface densities of the tethered chains. As is seen, h is a monotonically decreasing function of $\dot{\gamma}$. At small $\dot{\gamma}$, both the shear rate $\dot{\gamma}_w$ in the layer and the shear rate $\dot{\gamma}_b$ in the bulk increase with V_p. The bulk shear rate $\dot{\gamma}_b$ determines the strength of constraint release on the tethered chains, measured by the frequency ν_T. So an increase in V_p also leads to an increase in ν_T. At small $\dot{\gamma}$, the actual thickness of the layer is determined by the balance of convection and constraint release on the tethered chains. As a result, the decrease of h when increasing $\dot{\gamma}$ indicates that the rate of convection for the tethered chains increases with V_p faster than ν_B.

At larger $\dot{\gamma}$, due to the increased imbalance between convection and constraint release, the slope of the curves in Figure 5.6 becomes so steep that even a small increase in $\dot{\gamma}$ leads to a sharp decrease in h. In this regime, a strong deviation of the thickness h from its equilibrium value h_0 suggests a severe orientation of the tethered chains by the flow. The alignment of the tethered chains with the flow direction results in a decrease in the number of the bulk-tethered entanglements in the interfacial layer. At the critical shear rate $\dot{\gamma}_{cr} = V_p^{cr}/H$, constraint release is no longer able to resist strong convection and prevent further alignment of the tethered chains. As a result, at $\dot{\gamma}_{cr}$ the bulk and the tethered chains suddenly disentangle and so the system enters the strong slip regime. As mentioned earlier, after the disentanglement the tethered chains occupy a very thin near-wall layer of thickness a_0.

The presented picture is consistent with the original idea of Bergem [11], who proposed a sudden loss of entanglements between bulk and tethered chains at a critical stress as the mechanism of wall slip. The imbalance between CR and convection at a critical shear rate as a cause for the disentanglement between the bulk and tethered chains was also suggested by Joshi et al [21]. In the slip model of Brochard and de Gennes [18], the mechanism for the disentanglement is a coil-to-stretch transition of the tethered chains at a critical stress. They argue that a fast enough flow deforms the tethered chains into cigar shaped coils. The diameter D of the cigar, determined by the balance between entropic and friction forces acting on the tethered chains, decreases if the wall shear rate is increased. When D decreases below the entanglement spacing, the entropic and friction forces can no longer balance each other so that bulk and tethered chains suddenly disentangle. Since the entropic and friction forces in Brochard and de Gennes' model can be associated with constraint release and convection, their model provides a virtually similar picture of the chain disentanglement to that proposed here.

As is seen in Figure 5.6, for a given shear rate $\dot{\gamma}$, the layer thickness h is a non-monotonous function of the surface density Σ_{0T} of the tethered chains. This can be explained as follows. At large Σ_{0T}, where interactions between separate tethered chains "suppress" constraint release in the layer, the tethered chains are more easily oriented by the flow than at medium surface densities. On

the other hand, in the mushroom regime the tethered chains undergo a larger flow-induced drag force compared to higher surface densities, where this force is distributed among a larger number of tethered chains. So for a given $\dot{\gamma}$, the tethered chains are less oriented in the intermediate grafting regime (see Figure 5.2) in comparison to other regimes.

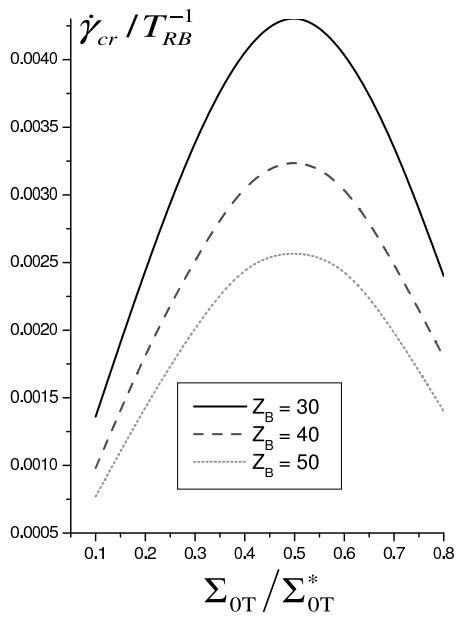

Figure 5.7: Critical shear rate vs surface density for different Z_B and $Z_T = 10$.

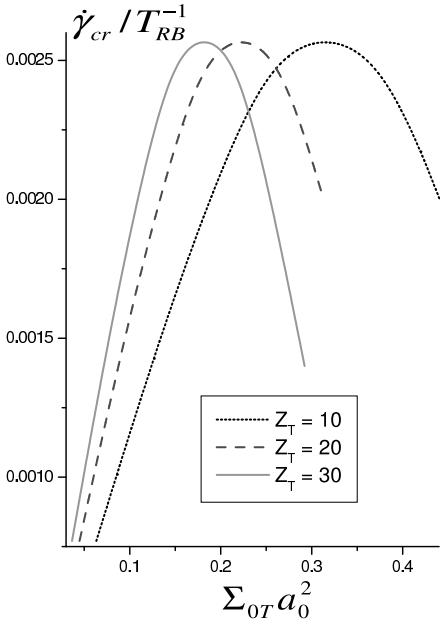

Figure 5.8: Critical shear rate vs surface density for different Z_T and $Z_B = 50$.

In Figure 5.7 and Figure 5.8, the critical shear rate $\dot{\gamma}_{cr}$ is shown versus the surface density Σ_{0T} of tethered chains for different molecular weights of the bulk and tethered chains. Intuitively, one would expect that the more tethered chains in the layer we have, the larger is the friction between the melt and the wall, and therefore the harder it is to make the melt slip. This suggests that $\dot{\gamma}_{cr}$ would monotonically increase with Σ_{0T}. However, it is seen in Figure 5.7 that such argumentation only works for small surface densities. In fact, the predicted dependence of $\dot{\gamma}_{cr}$ on Σ_{0T} is nonmonotonous. Earlier, when studying constraint release on tethered chains, we found that an increase in Σ_{0T} "strengthens" the interactions between separate tethered chains in the interfacial layer. Since these interactions suppress constraint release on the tethered chains and therefore ease their orientation by the flow, $\dot{\gamma}_{cr}$ is expected to decrease with Σ_{0T} at high surface densities of tethered chains, as is illustrated in Figure 5.7 and Figure 5.8.

At small Σ_{0T}, constraint release on tethered chains is much stronger than at high surface densities. However, as mentioned earlier, in this regime the chains may undergo strong convection even at rather small shear rates $\dot{\gamma}$. As a result, the corresponding critical shear rate $\dot{\gamma}_{cr}$ for the onset of disentanglement is small. The maximal $\dot{\gamma}_{cr}$ in Figure 5.7 and Figure 5.8 corresponds to intermediate surface densities, as expected. In this regime, tethered chains

are harder to orient so that the system has a larger resistibility to the flow.

By comparing Figures 5.7 and 5.8 with Figure 5.5, one may conclude that the critical shear rate $\dot{\gamma}_{cr}$ can be related to the number of the bulk-tethered (B-T) entanglements in the layer. At small Σ_{0T}, both $\dot{\gamma}_{cr}$ and the equilibrium fraction ψ^0_{BT} of the B-T entanglements (see eqn.(5.14)) are small, which indicates that a small number of the B-T entanglements is insufficient to prevent the onset of slip at high shear rates. In this regime, $\dot{\gamma}_{cr}$ and ψ^0_{BT} are proportional to Σ_{0T}, which implies that separate tethered chains move independently of each other. As a result, each tethered chain gives a separate contribution to $\dot{\gamma}_{cr}$. Addition of one tethered chain to the interfacial layer will create Z_T new B-T entanglements and therefore will "improve" the resistibility of the system to slip. At the critical surface density $\Sigma^{(cr)}_{0T} \approx 0.5\,\Sigma^*_{0T}$, the number of the B-T entanglements in the layer is maximal and so is the resistibility of the system to slip. As a consequence, in this case $\dot{\gamma}_{cr}$ is also maximal, as is shown in Figure 5.7. $\Sigma^{(cr)}_{0T}$ marks a grafting regime in which tethered-tethered entanglements start to play an important role in the dynamics of the interfacial layer (see the discussion after Figure 5.4). A further increase in Σ_{0T} decreases the number of the B-T entanglements in the melt and so $\dot{\gamma}_{cr}$ also decreases.

Figure 5.7 shows that an increase in the molecular weight of the bulk chains leads to a decrease in $\dot{\gamma}_{cr}$ for a fixed Σ_{0T}. In particular, the amplitude of the maximum in Figure 5.7 is nearly proportional to $T^{-1}_{RB} Z^{-1}_B$. On the other hand, the position of the maximum, as determined by the critical surface density $\Sigma^{(cr)}_T$, is insensitive to Z_B and given by

$$\Sigma^{(cr)}_T \approx 0.5\,\Sigma^*_{0T}\,, \tag{5.15}$$

where Σ^*_{0T} is the equilibrium surface density of the dry-brush regime (see eqn.(5.14)). In contrast, as is seen in Figure 5.8, the critical shear rate $\dot{\gamma}_{cr}$ can be a decreasing, increasing, or even nonmonotonous function of Z_T, depending on the value of the surface density Σ_{0T}. The amplitude of the maximum in Figure 5.8 is independent of Z_T, whereas its position scales as $1/\sqrt{Z_T}$, in agreement with eqn.(5.7) and eqn.(3.36). The nonmonotonous dependence of the critical shear rate for the onset of disentanglement on the surface density of tethered chains was also predicted by Joshi et al [22] and reported by Lèger and coworkers [8, 48]. Similar to the critical shear rate $\dot{\gamma}_{cr}$, the corresponding critical shear stress σ_{cr}, i.e., the shear stress in the melt prior to the transition point, is found to be a nonmonotonous function of Σ_{0T}. At low surface densities, σ_{cr} scales linearly with Σ_{0T} and can be written as

$$\sigma_{cr} = C_1 G_{0B} \Sigma_{0T}\,, \tag{5.16}$$

where C_1 is a constant independent of Σ_{0T}. According to eqn.(5.10), the elastic modulus G_{0B} of the bulk is proportional to the melt temperature T. Therefore, eqn.(5.16) can be written in a form similar to that proposed by Brochard

and de Gennes [18]. Specifically, based on phenomenological arguments, they found that in the mushroom regime

$$\sigma_{cr} \propto \Sigma_{0T} k_B T \,, \tag{5.17}$$

where k_B is the Boltzmann constant. In the absence of desorption, Σ_{0T} is constant so that σ_{cr} increases linearly with T over the whole range of melt temperatures, in agreement with the experimental data of Wang and Drda [49]. On the other hand, according to eqn.(4.12), the Rouse time of bulk chains $T_{RB} \propto T^{-1}$. Therefore, from Figure 5.7 one may infer that in the absence of desorption the critical shear rate $\dot{\gamma}_{cr}$ is also proportional to the melt temperature T.

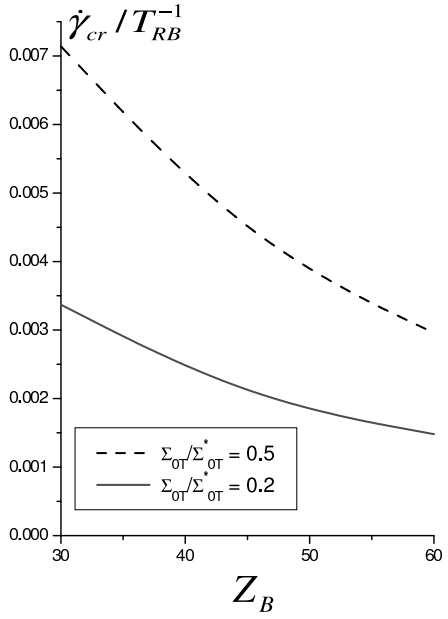

Figure 5.9: Critical shear rate vs molecular weight of bulk molecules for two different surface densities of tethered chains and $Z_T = 15$.

In Figure 5.9, the critical shear rate $\dot{\gamma}_{cr}$ is presented as a function of the molecular weight of bulk chains for different grafting regimes. Since the Rouse time T_{RB} of bulk chains is proportional to Z_B^2 (see eqn.(4.12)), Figure 5.9 shows that at small surface densities $\dot{\gamma}_{cr}$ scales as $Z_B^{-3.4}$, that is as the reciprocal reptation time T_{DB} (see eqn.(4.9)). A similar result was found by Joshi et al [18]. At higher surface densities Σ_{0T}, $\dot{\gamma}_{cr}$ becomes more sensitive to Z_B. Durliat and coworkers [48] reported that $\dot{\gamma}_{cr}$ scales as $M_w^{-3.1\pm0.5}$ at surface densities up to the critical value $\Sigma_T^{(cr)}$, which agrees well with the predictions of the present model. Contrary to the critical shear rate $\dot{\gamma}_{cr}$, the model predicts only a weak dependence of the critical shear stress σ_{cr} on Z_B, in agreement with the behavior reported by Wang and Drda [50].

In Figure 5.10, the slip velocity V_s is shown versus the shear rate $\dot{\gamma}$ up to the transition point. It is seen that two different regimes can be discerned. At small $\dot{\gamma}$, V_s is small compared to the upper plate velocity V_p (see Figure 5.1)

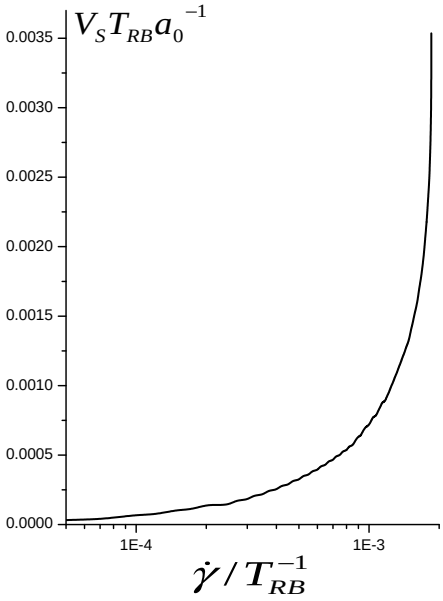

Figure 5.10: Slip velocity vs global shear rate. $Z_B = 40, Z_T = 10$.

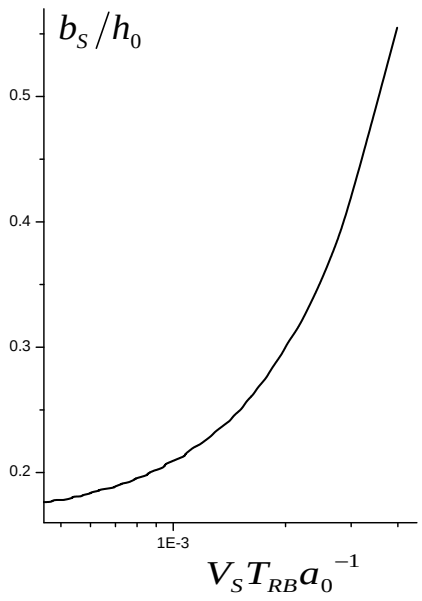

Figure 5.11: Slip length vs slip velocity. $Z_B = 40, Z_T = 10$.

and slowly increases with $\dot{\gamma}$. This regime will be referred to as the weak slip regime throughout the text. When $\dot{\gamma}$ approaches the critical shear rate $\dot{\gamma}_{cr}$, the slope of the curve $V_s(\dot{\gamma})$ becomes so steep that even a small increase in $\dot{\gamma}$ leads to a dramatic increase in V_s. At $\dot{\gamma}_{cr}$, a sudden disentanglement between the bulk and the tethered chains occurs after which V_s "jumps" up to V_p. The flow regime prior to $\dot{\gamma}_{cr}$ will be referred to as "stick-to-slip" transition. Above $\dot{\gamma}_{cr}$, a third regime is expected in which V_s is macroscopic. This regime will be referred to as the strong slip regime.

Note that in a real extrusion die V_p (defined as the melt velocity at the die axis) is not always constant, but determined by the mass flux leaving the die. The "jump" in V_s enhances the mass transfer through the die, whereas the incoming mass flux is constant (at a constant piston speed). The incompressibility of the melt in the die then yields that after the jump V_p may drop below the critical level so that entanglements between the tethered and bulk chains can be restored. After this, the stress in the layer will "build up" again and the cycle will repeat itself. So for the real extrusion die at the constant piston speed the strong slip regime is characterized by unstable flow with periodical alternations of the boundary conditions at the polymer/wall interface between the "no-slip" and "slip" limit. As was shown in [51, 52, 53], combination of the oscillating boundary conditions together with conservation of mass and momentum over the die allows one to explain the origin of the infamous spurt oscillations of the extrudate.

The existence of the three regimes in the curve $V_s(\dot{\gamma})$ was first predicted by Brochard and de Gennes [18] for cohesive slip and reported by Lèger and coworkers [8, 5, 48]. Figure 5.10 shows that V_s is non-zero even at small

shear rates $\dot{\gamma}$, in agreement with the precise measurements of Migler et al [5]. However, V_s remains small compared to V_p up to the transition point $\dot{\gamma}_{cr}$, which implies that the weak slip regime can hardly be inferred from macroscopic behavior, such as a change in the slope of the experimentally measured strain-stress curves. At $\dot{\gamma}_{cr}$, the transition from weak to strong slip occurs after which V_s is no longer microscopic. Such a transition can be detected via a significant pressure drop in controlled shear rate experiments or even visually. As is seen in Figure 5.10, this transition is rather sharp, that is initiated within a narrow interval of shear rates prior to $\dot{\gamma}_{cr}$. Note that at shear rates prior to $\dot{\gamma}_{cr}$, the bulk and tethered chains are just at the limit of being disentangled. Brochard and de Gennes [18] called this regime the marginal regime. In contrast to Brochard and de Gennes' model, the present theory is able to describe quantitatively the polymer flow in the marginal regime.

In Figure 5.11, the slip length $b_s = V_s/\dot{\gamma}_b$ is shown as a function of the slip velocity V_s. At small V_s, b_s is microscopic and almost independent of V_s. Such a behavior has been predicted earlier by Brochard and de Gennes [18] and Joshi and coworkers [21]. The value of b_s at small V_s is often referred to as the zero-slip-length b_0. Note that b_0 is a function of the molecular parameters of the melt and the surface density Σ_{0T} of tethered chains. We found that b_0 increases as Σ_{0T} is decreased, similar to the behavior predicted by Joshi et at [22]. In particular, in the mushroom regime we found that $b_0 \propto 1/\Sigma_{0T}$, in accordance with the earlier predictions of Brochard and de Gennes [18]. In the vicinity of the critical point, b_s starts to grow rapidly with V_s. After the transition to strong slip, a regime of nearly constant b_s is expected [18] in which b_s is macroscopically large and equal to $\beta\eta$, where η is the melt viscosity and β the friction coefficient between the melt and the layer of tethered chains squeezed against the wall. The three regimes in the curve $b_s(V_s)$ were observed experimentally by Migler et al [5].

In the rest of this section, the model predictions will be compared with the available experimental data on slip. Lèger et al [8] and Durliat et al [48] performed a series of experiments on monodisperse polydimethylsiloxane (PDMS) chains of molecular weight $96\,kg/mol$ adsorbed on a silica wall with a controlled surface density. These chains form a polymer brush which is in contact with a monodisperse PDMS melt of molecular weight $970\,kg/mol$. The size and molar mass of the monomer are reported to be $0.5\,nm$ and $0.074\,kg/mol$, respectively. Using the molecular data of Fetters et al [54], from eqn.(5.10) the mean entanglement spacing a_0 is estimated to be $4.8\,nm$. The distance H between parallel plates in the rheometer (see Fig. 5.1) is reported to be $8\,\mu m$. Based on independent molecular measurements, in [27] the parameters of the model Z_T, Z_B, and Σ^*_{0T} were estimated to be 10, 100, and $1.95 \cdot 10^{16}$ $(chains/m^2)$, respectively. The equilibrium thickness h_0 of the interfacial layer was estimated to be around $18\,nm$. By fitting the data of [8, 48], in [27] the value of the Rouse time T_{RB} of bulk PDMS chains was

found to be around $1.5 \times 10^{-4} s$.

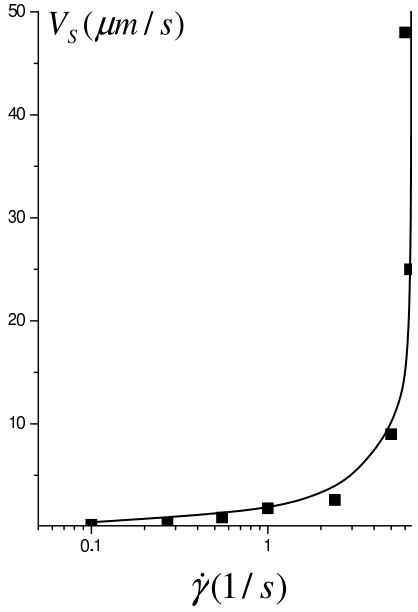

Figure 5.12: Slip velocity vs global shear rate. The solid line is the model prediction.

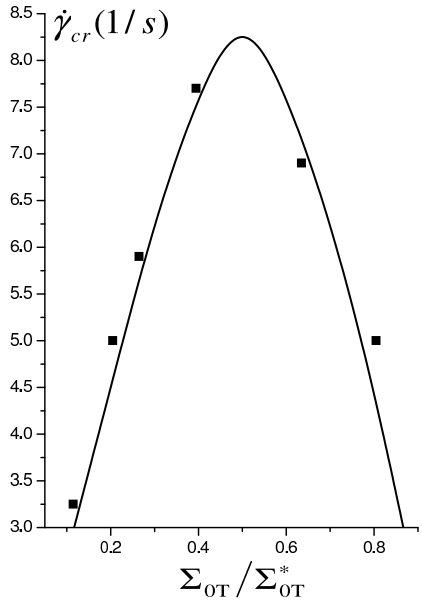

Figure 5.13: Critical shear rate vs grafting density. The solid line is the model prediction.

In Figure 5.12, the model predictions for the slip velocity V_s as a function of the global shear rate $\dot{\gamma}$ are compared with the microscopic slip data of Lèger et el [8]. The surface density Σ_{0T} is reported in [8] to be nearly 7 times larger than the corresponding critical surface density of the intermediate grafting regime Σ_T^{**} (see eqn.(5.9)). It is seen that the model predictions are in a good agreement with the experimental data over a wide range of shear rates up to the critical shear rate $\dot{\gamma}_{cr}$. In Figure 5.13, the critical shear rate $\dot{\gamma}_{cr}$ is shown versus the surface density Σ_{0T} of tethered chains. The model predictions are compared with the data on slip by Durliat et al [48]. It is seen that the model is able to predict $\dot{\gamma}_{cr}$ over a wide range of surface densities, including those where interactions between neighboring tethered chains start to play an important role in the dynamics of the interfacial layer.

In this chapter, a molecular model for cohesive slip was formulated in the absence of desorption. In the next chapter, we will extend this model to incorporate possible desorption of tethered chains. As will be shown later on, the model for cohesive slip can still be applied for die walls with high surface energy for which desorption plays only a minor role in the melt dynamics.

Chapter 6

Unified slip model

In the previous chapters, we developed a molecular model for cohesive slip in which desorption was ignored. In reality, however, desorption may play an essential, if not dominant, role in the dynamics of the melt. In particular, it is probably the dominant slip mechanism in a case of a low adsorbing die wall, where even a slow flow may initiate a massive detachment of adsorbed polymer molecules from the wall. In this chapter, a slip model is developed which unites both disentanglement and desorption into a single mathematical framework.

6.1 Surface density of adsorbed molecules in the absence of flow

Despite being attached to the wall, each adsorbed polymer molecule undergoes constant Brownian oscillations within the mesh of the surrounding constraints. Strong enough oscillations may cause its sudden detachment from the wall after which it becomes unattached. This implies that adsorption is a reversible process. Hereafter, desorption due to the thermal oscillations will be referred to as thermal desorption. Note that after some time the detached polymer molecule may again be adsorbed on the wall. Therefore, at equilibrium adsorbed molecules are constantly created and destroyed on the wall. The number of the adsorbed molecules per unit area of the wall is then determined by the balance between desorption and adsorption. Let us calculate the number of unattached polymer molecules in the melt which can be adsorbed on the wall. To this end, imagine for a moment that there is no interaction between the melt and the wall. According to the freely-jointed chain model [31], in the absence of flow each molecule in the melt has a coil-like shape with the diameter R_B given by

$$R_B \approx \sqrt{N_B} b \,. \tag{6.1}$$

Here N_B and b are the number of monomers per molecule and monomeric size, respectively. The near wall-layer of thickness R_B then contains both complete and incomplete coils (see Figure 6.1). Next, if a_0 is the mean distance between entanglements, then the total number of entanglements per unit area of the wall in this layer is equal to R_B/a_0^3, where a_0^3 is the average volume "occupied" by one entanglement. Let Z_B be the mean number of constraints per polymer in the melt. If all the entanglements in the melt are pair-wise contacts between neighboring polymers, then each molecule contributes to $Z_B/2$ entanglements. The equilibrium number of compete coils per unit area of the wall in the near-wall layer is then estimated to be

$$\Sigma_{0B} = \frac{R_B}{a_0^3}\frac{2}{Z_B}\,. \tag{6.2}$$

Now we "switch on" the interaction between the melt and the wall. The attractive potential of the wall is localized on its surface, so that only those coils that nearly "touch" the wall will be adsorbed. Short fragments of molecules penetrating the near-wall layer from above are unlikely to touch the wall (see Figure 6.2). So one may think that only complete coils will interact with the wall and eventually become adsorbed. The surface density Σ_{0B} in Eq.(6.2) can therefore be associated with the maximal number of bulk molecules which can be adsorbed per unit area of the wall. In reality, due to the presence of desorption, the actual number of the adsorbed molecules will be smaller then Σ_{0B}. Let Σ_S be the actual number of the adsorbed molecules per unit area of the wall. Then, in the presence of desorption, the corresponding number of the bulk molecules in the near-wall layer that are able to interact with the wall is given by

$$\Sigma_B = \frac{R_B}{a_0^3}\frac{2}{Z_B} - \Sigma_S\,. \tag{6.3}$$

Here the second term on the RHS represents those bulk molecules that have already been adsorbed on the wall. Due to the presence of adsorption, each of these Σ_B bulk molecules can be assigned a characteristic lifetime τ_a after which it will be adsorbed by the wall. Similarly, due to the presence of thermal desorption, each of Σ_S surface molecules is assigned a certain lifetime τ_d. From the above, the equation of motion for Σ_S in the absence of flow is given by

$$\frac{\partial}{\partial t}\Sigma_S = -\frac{1}{\tau_d}\Sigma_S + \frac{1}{\tau_a}\left\{\frac{R_B}{a_0^3}\frac{2}{Z_B} - \Sigma_S\right\}\,. \tag{6.4}$$

It has the form of a balance equation with the first and the second term on the RHS pertaining to thermal desorption and adsorption, respectively. Eqn.(6.4) makes it explicit that exchanges between the adsorbed and unattached molecules are governed by the first-order kinetics with the coefficients equal to the corresponding reciprocal lifetimes. To solve eqn.(6.4), we need to specify τ_d and τ_a. As was recognized by Lau and Schowalter [12], exchanges between attached

and unattached states can be interpreted in terms of first order chemical reactions for which the activation rate theory of chemical kinetics is known to apply [55]. From the activation rate theory, the frequency with which a molecule passes over a potential energy barrier, through an activated state, can be presented as a product of a pre-exponential frequency factor and an activation term (see also Chernyak and Leonov [56])

$$k = C\,\frac{k_B T}{h}\exp\big(-\frac{E}{k_B T}\big) \tag{6.5}$$

where h, k_B, and T are the Planck and Boltzmann constants, and the absolute temperature, respectively. In eqn.(6.5), E is the height of the barrier. The pre-factor C is independent of the temperature. From eqn.(6.5), the ratio τ_a/τ_d can be written in the form

$$\tau_a/\tau_d = k_d/k_a = A\,e^{-E_{adh}/k_B T}\,, \tag{6.6}$$

where k_d and k_a are the corresponding rates of desorption and adsorption, respectively. In eqn.(6.6), A is a constant and E_{adh} is equal to a difference between the average free energies of a polymer molecule in the adsorbed and unattached state. E_{adh} represents the average work necessary to detach one adsorbed molecule from the wall in the absence of flow. Hereafter, E_{adh} will be referred to as adhesion energy. The value of the adhesion energy characterizes the strength of the polymer-wall interaction, and is specific for a particular polymer/wall pair. It depends on the material of the wall, the chemical structure of the polymer, and the roughness of the wall surface. Note that in a real experiment E_{adh} can easily be varied by choosing an appropriate wall material or using different chemical wall coatings.

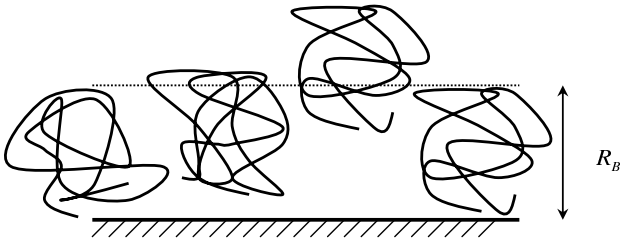

Figure 6.1: No polymer-wall interaction

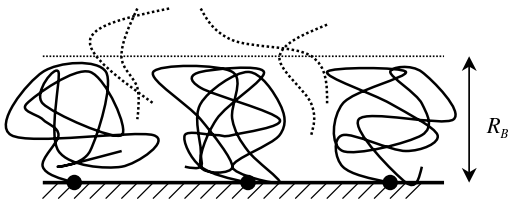

Figure 6.2: With polymer-wall interaction

Eqn.(6.6) makes it explicit that the actual number of the adsorbed polymer molecules on the wall does not only depend on the molecular parameters of the melt and material of the wall, but also is temperature dependent. In particular, as follows from eqn.(6.6) and eqn.(6.4), an increase in T leads to a decrease in Σ_S. Note that in the limit $T \to 0$ the desorption time $\tau_d \to \infty$. This implies that at low temperatures thermal desorption is suppressed so that the adsorbed molecules can be considered as grafted permanently on the wall. From eqn.(6.4) it then immediately follows that in the absence of desorption,

Σ_S is maximal and equal to

$$\Sigma_S^{(max)} = \frac{R_B}{a_0^3}\frac{2}{Z_B}\,. \tag{6.7}$$

Clearly, $\Sigma_S^{(max)}$ can be considered as the low temperature limit of the actual surface density Σ_S. In general, we therefore have $\Sigma_S \leq \Sigma_S^{(max)}$. Notice that $\Sigma_S^{(max)}$ is only a function of the molecular parameters of the melt, and does not depend on the wall material.

6.2 Desorption in the presence of flow

In the presence of flow, tails of the adsorbed molecules undergo, in parallel to the Brownian force, a certain drag force produced by the moving mesh of constraints, which rotates and stretches them. By stretching the tails, this drag force "weakens" the attractive potential of the wall, thereby facilitating their desorption. So in the presence of flow, the mean lifetime τ_d of a tethered chain on the wall is a function of the flow rate. In particular, since stronger flows detach tethered chains more easily, τ_d is expected to decrease as the flow rate is increased. On the other hand, adsorption is controlled by chemical interactions between the polymer and the wall, which implies that the adsorption time τ_a in eqn.(6.4) is hardly affected by the flow.

Following Hill [15], the effect of the flow on the desorption rate of tethered chains can be presented as a decrease in the activation energy E_{adh} by a value of $\Delta U > 0$, the mean excess elastic energy gained by a tethered chain due to flow. Note that ΔU pertains to the physical tethered chain. If τ_0 is the mean lifetime of a tethered chain on the wall at equilibrium, then from eqn.(6.6) its corresponding lifetime τ in the presence of flow can be written as

$$\tau = \tau_0 e^{-\Delta U/k_B T}\,, \tag{6.8}$$

Eqn.(6.8) shows explicitly that $\tau < \tau_0$, as expected. To calculate ΔU, let us present the tethered chain as a bead-spring system with N_T beads, where N_T is the number of monomers per single tethered chain. According to [31], the elastic energy of such a system is given by

$$U = \frac{3}{2}\frac{k_B T}{b^2}\sum_{n=1}^{N_T}\left|\mathrm{R}_n - \mathrm{R}_{n-1}\right|^2\,. \tag{6.9}$$

Here b is the equilibrium distance between adjacent beads, whilst $|\mathrm{R}_n - \mathrm{R}_{n-1}|$ gives the actual distance between beads n and $n-1$. In the case of small stretch, $|\mathrm{R}_n - \mathrm{R}_{n-1}|$ can be written as $b+\alpha_n$, where $|\alpha_n| << b$. Then, neglecting

terms of order α_n^2, from eqn.(6.9) one can find that the elastic energy U of the tethered chain can be approximated by

$$U \approx 3\frac{k_B T}{b} \sum_{n=1}^{N_T} \left| \frac{\partial \mathbf{R}(n,t)}{\partial n} \right| , \tag{6.10}$$

where the position vector $\mathbf{R}_n$ of the n-th bead is now considered as a continuous function of n. Next, summation over the beads in eqn.(6.10) can be replaced with the corresponding integral over n. After this, eqn.(6.10) can be rewritten in the following form

$$U \approx 3k_B T N_T \left\{ \frac{1}{L_n} \int_0^{L_n} dx \left| \frac{\partial \mathbf{R}(x,t)}{\partial x} \right| \right\} , \tag{6.11}$$

where $x = nb$. In eqn.(6.11), $L_n = bN_T$ is the length of the physical tethered chain. The expression in the curved brackets is equal to the value of $\partial \mathbf{R}(x,t)/\partial x$ averaged along the physical chain. Attention must be paid to the fact that eqn.(6.11) includes the fast Brownian oscillations of the physical chain. Averaging it over time yields that the expression in the curved brackets should be replaced with the corresponding average over the primitive path of the tethered chain.

$$U = 3k_B T N_T \left\{ \frac{1}{L_{0T}} \int_0^{L_{0T}} ds_0 \left| \frac{\partial \hat{\mathbf{R}}(s_0,t)}{\partial s_0} \right| \right\} , \tag{6.12}$$

where L_{0T} is the primitive path length of the tethered chain and $\hat{\mathbf{R}}(s_0,t)$ its parametrization function (see Figure 2.6). According to eqn.(2.2), the derivative $\partial \hat{\mathbf{R}}(s_0,t)/\partial s_0$ in eqn.(6.12) is equal to the bond vector $\hat{\mathbf{b}}(s_0,t)$ of the tethered chain. This implies that the expression in the curved brackets gives the local stretch $\hat{\lambda}(s_0,t)$ averaged along the chain contour. Attention must be paid to the fact that eqn.(6.12) pertains to a single tethered chain. From the above, the mean excess elastic energy of the tethered chain gained in the presence of flow is given by

$$\Delta U \approx 3k_B T N_T (\bar{\bar{\lambda}} - 1) \quad , \quad \bar{\bar{\lambda}} = \frac{1}{L_{0T}} \int_0^{L_{0T}} ds_0 \, \bar{\lambda}_T(s_0,t) \, . \tag{6.13}$$

Here $\bar{\lambda}_T(s_0,t)$ is the mean local stretch of the tethered chain at s_0 and time t. $\bar{\bar{\lambda}}$ is the mean lengthening of the tethered chain given by the ratio $\bar{L}_T/L_{0T}$, where $\bar{L}_T$ and L_{0T} are the mean actual and equilibrium length of the tethered chain, respectively. Note that ΔU is proportional to the number N_T of monomers per tethered chain. According to eqn.(6.8), this implies that in the presence

of flow the desorption rate of tethered chains becomes very sensitive to their molecular weight. In view of eqn.(6.13), eqn.(6.8) reads as

$$\tau = \tau_0 e^{-3N_T(\bar{\bar{\lambda}}-1)}, \tag{6.14}$$

Eqn.(6.14) reveals that the mean lifetime of the tethered chain in the presence of flow decreases exponentially with the number N_T of monomers per chain. As a consequence, long tethered chains have a much smaller lifetime on the wall than short ones.

In general, desorption of one of the tails of an adsorbed polymer molecule does not result in detachment of the whole molecule from the wall, but instead leads to a new configuration of the molecule with a longer tail. However, in the presence of flow the new configuration has a much smaller lifetime than the original one. Moreover, desorption is expected to play a role in the melt dynamics only for relatively low surface energy walls for which many loops configurations of adsorbed molecules are unlikely (see Figure 1.3). From the above, it follows that in the presence of flow the mean desorption time τ_d of the adsorbed molecule is nearly equal to the mean lifetime of a tethered chain. As a result, one may think that desorption of one tail of the adsorbed molecule inevitably leads to detachment of the whole molecule. From eqn.(6.14), we therefore have that in the presence of flow the mean desorption time τ_d of an adsorbed molecule (whose tails consist of N_T monomers) can be written as

$$\tau_d = \tau_d^0 \, e^{-3N_T(\bar{\bar{\lambda}}-1)} \tag{6.15}$$

where τ_d^0 is the thermal desorption time introduced earlier. Since τ_d^0 is flow independent, eqn.(6.15) explicitly shows how the flow affects the desorption rate of adsorbed molecules via induced chain stretch. According to Hooke's law, $\bar{\bar{\lambda}}$ is proportional to the mean tensile force $\bar{F}$ induced in tethered chains by the flow, so that eqn.(6.15) can be rewritten in the form similar to that found by Yarin and Graham [23]. Moreover, as follows from eqn.(2.10) and eqn.(2.18), in a steady shear flow $\bar{\bar{\lambda}} - 1$ is proportional to the wall shear stress σ_w (with the proportionality coefficient being a function of the normal stresses at the wall). This implies that eqn.(6.15) can also be written in the form proposed by Lau and Schowalter [12]

Once eqn.(6.15) is known, the equation of motion for the surface density Σ_S of adsorbed molecules at equilibrium (see eqn.(6.4)) can readily be generalized to a case with a flow. As we will see later on, desorption from a low surface energy wall mostly occurs in flow regimes for which the equilibrium random coil structure of polymers is disturbed only slightly. So eqn.(6.7) can still be used for the maximal surface density $\Sigma_S^{(max)}$ of adsorbed molecules. Therefore, the equation of motion for Σ_S in the presence of flow has the form of eqn.(6.4) with the desorption time τ_d now given by eqn.(6.15). Its steady state solution gives us the corresponding surface density Σ_T of tethered chains (since $\Sigma_T = \Sigma_S/2$),

which can be written as follows

$$\Sigma_T = \frac{\Sigma_{0T}}{X_0 + (1 - X_0)\, e^{3N_T(\bar{\bar{\lambda}}-1)}}\,, \tag{6.16}$$

where Σ_{0T} is the equilibrium surface density. The dimensionless parameter X_0 is given by

$$X_0 = \frac{\Sigma_{0T}}{\Sigma_T^{(max)}} = \frac{1}{1 + A\, e^{-E_{adh}/k_BT}}\,, \tag{6.17}$$

where $\Sigma_T^{(max)} = 2\Sigma_S^{(max)}$. According to eqn.(6.17), X_0 gives the fraction of $\Sigma_S^{(max)}$ sites on the wall occupied by polymer molecules in the absence of flow. For a given temperature T, an increase in the adhesion energy E_{adh} enables the wall to capture more polymer chains on its surface and X_0 increases. On the other hand, for a given E_{adh} an increase in the temperature enhances desorption from the wall and therefore X_0 decreases.

Since X_0 is flow independent, eqn.(6.16) quantifies the effect of the flow on the surface density Σ_T of tethered chains. Specifically, since $X_0 < 1$, from eqn.(6.16) we have that $\Sigma_T < \Sigma_{0T}$, as expected. Eqn.(6.16) shows that Σ_T decreases as the wall shear rate $\dot{\gamma}_w$ is increased (as follows from eqn.(3.31), at small shear rates $\bar{\bar{\lambda}} \propto \dot{\gamma}_w^2$). The amplitude of this change depends, however, on the strength of the polymer-wall interaction, measured by the adhesion energy E_{adh}. At low E_{adh}, X_0 is small and Σ_T is very sensitive to $\dot{\gamma}_w$. In this regime, even a rather slow flow for which $(\bar{\bar{\lambda}} - 1) > 1/3N_T$ may cause massive detachment of adsorbed molecules (after which $\Sigma_S << \Sigma_{0S}$) and ultimately adhesive slip. At high E_{adh}, X_0 is close to unity and $\Sigma_T \approx \Sigma_{0T}$ over a wide range of flow rates. In this case, adsorbed molecules are permanently grafted on the wall, and so the melt is most likely to slip cohesively.

Since $\Sigma_T^{(max)}$ is temperature independent, eqn.(6.17) shows that the no-flow density Σ_{0T} decreases as T is increased. In a flow, the temperature dependence of Σ_T is more complicated. In this case, it is not only determined by the temperature dependence of Σ_{0T}, but also by that of $\bar{\bar{\lambda}}$. This implies that in the case of intermediate E_{adh}, for which both slip mechanisms are expected to work in parallel, the temperature dependence of the stick-to-slip transition cannot normally be inferred from adhesive failure or disentanglement based theories. Clearly, an analysis of extrusion systems with intermediate E_{adh} requires a consideration of a more general model in which both slip mechanisms are combined self-consistently.

According to eqn.(3.23), the mean local stretch $\bar{\lambda}_T$ of a tethered chain in eqn.(6.13) can be expressed in terms of the bond vector correlator $S^T_{\alpha\beta}$ of tethered chains introduced earlier. As a result, the mean chain lengthening $\bar{\bar{\lambda}}$

in eqn.(6.15) can be written as

$$\bar{\bar{\lambda}} \approx \frac{1}{L_{0T}} \int_0^{L_{0T}} ds_0 \sqrt{S^T_{\alpha\alpha}}\,, \tag{6.18}$$

where summation is implied over the repeating indices. Let us recall that it is $\bar{\bar{\lambda}}$ that determines the effect of the flow on the desorption rate of adsorbed molecules from the wall (see eqn.(6.15)). On the other hand, $S^T_{\alpha\alpha}$ in eqn.(6.18) depends on the surface density Σ_T of tethered chains via the corresponding frequency ν_T of constraint release. This implies that $\bar{\bar{\lambda}}$ is in fact a function of Σ_T so that the equation of motion for the surface density Σ_S (see eqn.(6.4)) becomes nonlinear in the presence of flow. The non-linearity of eqn.(6.4) is a distinctive feature of the present model, which has not been revealed in earlier adhesive failure theories.

According to eqn.(6.15), the desorption/adsorption kinetics of polymer molecules depends on the correlator $S^T_{\alpha\beta}$ (via the mean chain lengthening $\bar{\bar{\lambda}}$). On the other hand, the dynamics of tethered chains depends on the surface density Σ_S of adsorbed molecules (via the frequency ν_T of constraint release). This implies that the two slip mechanisms are in fact coupled and therefore cannot be studied separately. The adhesive failure or disentanglement based theories for slip can therefore be interpreted at the limiting case $E_{adh} \to 0$ or $E_{adh} \to \infty$ of the more general theory developed here. Since the present theory accounts for the coupling between the two mechanisms in a self-consistent way, it is able to predict correctly the rheological behavior of extrusion systems with intermediate adhesion energies for which pure adhesive failure or disentanglement theories are not applicable.

6.3 Stick-to-slip transition in the presence of desorption

The equation of motion for tethered chains (see eqn.(3.31)) and for bulk molecules (see eqn.(4.10)) extended with eqns.(5.1, 5.2) and the equation of motion for the surface density Σ_T form a closed system of equations which governs the overall polymer flow in the parallel plate rheometer. This system lies at the heart of the model. It must be emphasized that in this system Σ_T is no longer a free parameter, as was the case in the previous chapter, but satisfies a nonlinear balance equation of the form of eqn.(6.4) with the desorption time τ_d given by eqn.(6.15).

The final system of equations was solved numerically according to the procedure described earlier in Chapter 5. The steady-state model predictions for the polymer flow near the wall are presented in Figs.(6.3 - 6.8). The independent

input parameters for this system are: the mean number Z_B of constraints per bulk chain, the mean number Z_T of constraints per tethered chain, the Rouse time T_{RB} of bulk chains, the mean entanglement spacing a_0, the step length a of the primitive path, and the dimensionless parameter X_0 (see eqn.(6.17)). Attention must be paid to the fact that Z_T, as well as X_0, is a function of the adhesion energy E_{adh}. In the case of a low adsorbing wall (i.e., small E_{adh}), adsorbed molecules make on average only one connection with the wall so that $Z_T \approx Z_B/2$. At large E_{adh}, adsorbed molecules can make several connections with the wall (see Figure 1.3). In this regime, tethered chains are expected to be shorter than in the case of small E_{adh}.

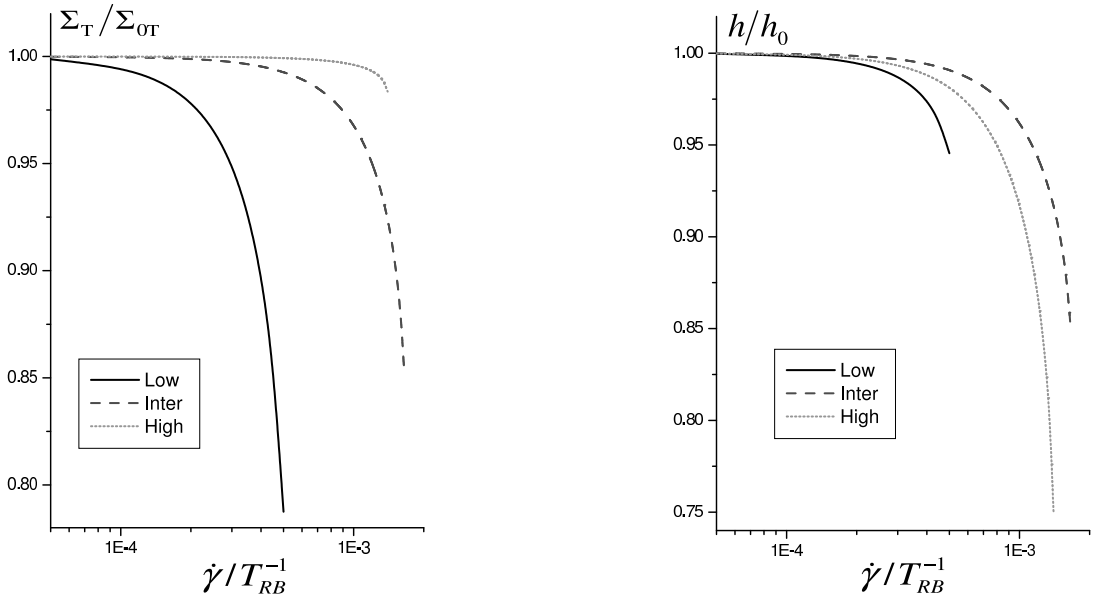

Figure 6.3: Surface density Σ_T (on the left) and layer thickness h (on the right) vs shear rate for three different adhesion energies (see the text). Σ_{0T} and h_0 are the equilibrium surface density of tethered chains and layer thickness, respectively. Results for $Z_B = 40$.

In Figure 6.3, the surface density Σ_T of tethered chains and thickness h of the interfacial layer are shown as functions of the global shear rate $\dot{\gamma} = V_p/H$ (see Figure 5.1) up to the transition point for different values of E_{adh} and a fixed temperature. According to eqn.(6.17), the parameter X_0 increases monotonically with E_{adh}, whereas Z_T is expected to decrease. The "low" energy curve in Figure 6.3 corresponds to the no-loops configuration of adsorbed molecules (each molecule makes only one connection with the wall) for which $Z_T = Z_B/2$. For certainty, we take $X_0 = 0.2$. For the "high" energy curve we take $Z_T = Z_B/4$ and $X_0 = 0.8$. And for the "intermediate" energy curve we take $Z_T = Z_B/3$ and $X_0 = 0.4$.

As is seen in Figure 6.3, at small E_{adh} the surface density Σ_T starts to drop rapidly near the critical shear rate $\dot{\gamma}_{cr}$, which indicates the onset of massive chain desorption induced by the flow. In contrast, h remains nearly equal to its no-flow value h_0 over a wide range of shear rates up to $\dot{\gamma}_{cr}$. As was discussed earlier, at small surface densities of adsorbed molecules, desorption of one

adsorbed molecule "destroys" $2\,Z_T$ bulk-tethered (B-T) entanglements in the interfacial layer, and hence decreases the resistibility of the layer to cohesive slip. A further increase in the shear rate $\dot{\gamma}$ enhances desorption and leads to a further decrease in the number of the B-T entanglements. At $\dot{\gamma}_{cr}$, the number of B-T entanglements in the layer becomes insufficient to prevent alignment of tethered chains by the flow. At this point, the "survived" tethered chains are suddenly smashed against the wall by the flow and slip occurs. Since for small E_{adh} the decrease in the number of the B-T entanglements in the layer is caused by desorption, the corresponding value of $\dot{\gamma}_{cr}$ can be associated with the onset of adhesive slip. Notice that the massive desorption is only initiated in the vicinity of $\dot{\gamma}_{cr}$, as is typical for activation processes.

At high E_{adh}, Figure 6.3 shows a sharp decrease in h near $\dot{\gamma}_{cr}$, whereas Σ_T remains nearly equal to Σ_{0T}. Apparently, this implies slip via disentanglement. This regime was discussed in detail in the previous chapter. Finally, for intermediate E_{adh} both h and Σ_T deviate substantially from their equilibrium values at $\dot{\gamma}_{cr}$, which clearly indicates that in this regime desorption and disentanglement compete with each other. In this regime, the B-T entanglements in the interfacial layer are released by desorption and disentanglement so that $\dot{\gamma}_{cr}$ can be associated with the onset of "mixed" slip. Apparently, for intermediate E_{adh} the adhesive failure of cohesive slip theories are no longer applicable and a more general mixed-slip theory is needed.

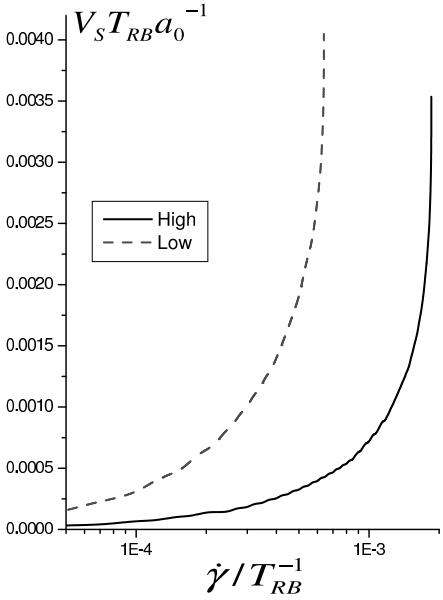

Figure 6.4: Slip velocity vs shear rate for different adhesive energies. Results for $Z_B = 40$.

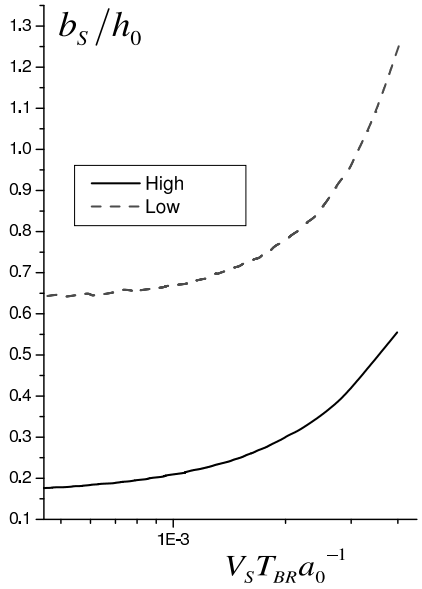

Figure 6.5: Slip length vs slip velocity for different adhesion energies. Results for $Z_B = 40$.

In Figure 6.4, the slip velocity $V_s = h\dot{\gamma}_w$ is shown as a function of the global shear rate $\dot{\gamma}$ for two different adhesion energies corresponding to adhesive and cohesive slip. The "high" adhesion energy curve pertaining to slip via disentanglement was discussed in the previous chapter. The "low" adhesion

energy curve $V_s(\dot{\gamma})$ in Figure 6.4 is associated with adhesive slip. Figure 6.4 then shows that, despite a different slip mechanism, $V_s(\dot{\gamma})$ also comprises the three slip regimes, similar to the case of cohesive slip. This behavior has not been revealed in the previous slip theories. Note that for adhesive slip the transition between the weak and the strong slip regime is not so sharp in comparison to cohesive slip. Moreover, as is seen in Figure 6.4, larger slip velocities are found in the case of adhesive slip. This agrees with the behavior predicted by Stewart [14] and experimental data of Hatzikiriakos and Dealy [57] who observed an increase in the slip velocity when lowering the surface energy of the wall by fluoropolymer coatings.

In Figure 6.5, the slip length $b_s = V_s/\dot{\gamma}_b$ is shown versus V_s for two different adhesion energies corresponding to adhesive and cohesive slip. As is seen, the curves corresponding to different slip mechanisms have a qualitatively similar behavior. At small V_s, b_s is microscopic and almost independent of V_s for both adhesive and cohesive slip. The nearly constant slip length in the weak slip regime was predicted earlier by Brochard and de Gennes [18] and Joshi et al [21, 22] for cohesive slip. In the vicinity of $\dot{\gamma}_{cr}$, b_s starts to grow rapidly with V_s. At $\dot{\gamma}_{cr}$, the system enters the strong slip regime in which b_s is independent of V_s and equal to $\beta\eta$, where η is the melt viscosity and β the friction coefficient between the melt and the wall. Since η and β have a roughly similar temperature dependence [23], this implies that in the strong slip regime b_s is nearly temperature independent for both cohesive and adhesive slip. A similar conclusion was made by Yarin and Graham [23] who recognized that the temperature independence of b_s could not only be attributed to cohesive slip, as assumed in [58]. The temperature dependence of the slip length in the weak slip regime depends on the value of E_{adh}. As is seen in Figure 6.5, in this regime b_s is nearly inversely proportional to X_0 (see eqn.(6.17)), the dimensionlized surface density Σ_{0T} of tethered chains. At high E_{adh}, X_0 is a smooth function of the temperature T so that b_s is nearly temperature independent. In contrast, at low E_{adh}, X_0 rapidly decreases if T is increased. In this regime, b_s is a monotonically increasing function of T. In conclusion, Figure 6.5 shows that for a given temperature a larger slip length is found (prior to the transition point) for lower energy walls, similar to the behavior reported by Wang and Drda [49].

6.4 Temperature dependence of the stick-to-slip transition

In Figure 6.6, the critical shear rate $\dot{\gamma}_{cr}$ and corresponding shear stress σ_{cr} are shown versus X_0 for a specific polymer melt and different wall materials. According to eqn.(6.17), in this case a decrease in X_0 is only related to an increase in the melt temperature T. So Figure 6.6 actually shows the temper-

ature dependence of σ_{cr} and $\dot{\gamma}_{cr}$ for the melt and the chosen wall materials. To establish the dominant slip mechanism at a certain temperature, the curves in Figure 6.6 are accompanied with the corresponding values of $(\Sigma_T/\Sigma_{0T},\, h/h_0)$. The data on the "high" adhesion energy curve show that Σ_T remains nearly equal to Σ_{0T} over the whole range of temperatures. Clearly, on a wall for which E_{adh} is high slip mainly occurs due to disentanglement. In contrast, on the "low" adhesion energy curve three different regions can be discerned. At small T, for which $X_0 > 0.65$, chain desorption is suppressed and cohesive slip is expected even at low E_{adh}. At a certain critical temperature T^{**}, for which $X_0 \approx 0.65$, desorption is suddenly initiated. In the vicinity of T^{**}, both slip mechanisms occur in parallel, which implies a regime of the "mixed" slip. At higher temperatures, adhesive slip becomes dominant. Note that the massive chain desorption is initiated over a rather narrow temperature interval (corresponding to $X_0 = 0.65...0.7$), as expected for an activation process.

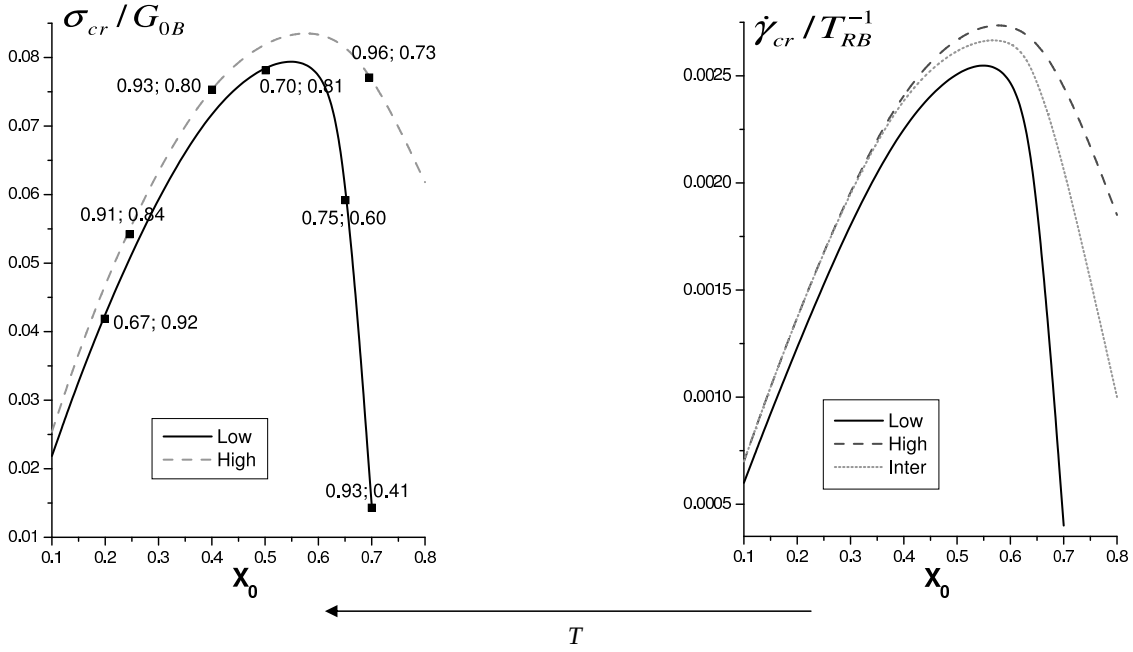

Figure 6.6: Critical shear stress (on the left) and critical shear rate (on the right) vs parameter X_0 defined in eqn.(6.17) for two values of the adhesion energies. For points the corresponding values of Σ_T/Σ_{0T} and h/h_0 are given. Results for $Z_B = 40$.

Figure 6.6 reveals that for both cohesive and adhesive slip σ_{cr} and $\dot{\gamma}_{cr}$ are nonmonotonous functions of T with a maximum at a certain temperature T^*. The amplitude of the maximum varies only slightly with E_{adh} (or, equivalently, with the wall material). Its position corresponds to $X_0 \approx 0.5$ (for $Z_B = 40$). Note that T^* is a function of E_{adh}, so the actual values of T^* are generally different for the "low" and "high" adhesion energy curves. The nonmonotonous temperature dependence of σ_{cr} and $\dot{\gamma}_{cr}$ has not been predicted earlier. Instead, the existing slip theories predict σ_{cr} to increase linearly with T (for cohesive slip) or monotonically decrease with T (for adhesive slip). Let us show now that the earlier predictions can be interpreted as the limiting case $E_{adh} \to \infty$ or $E_{adh} \to 0$ of the more general theory developed here. For temperatures

$T > T^*$ (i.e., $X_0 < 0.5$) both σ_{cr} and $\dot{\gamma}_{cr}$ increase almost linearly with X_0, and so

$$\sigma_{cr} = C_1 G_{0B} X_0 \quad , \quad \dot{\gamma}_{cr} = C_2 X_0 T_{BR}^{-1} , \tag{6.19}$$

where C_1 and C_2 are constants independent of X_0. As seen in Figure 6.6, in this regime the curves corresponding to different E_{adh} (and so to different slip mechanisms) nearly coincide which yields that C_1 and C_2 are independent of E_{adh}. So equations (6.19) are universal and do not depend on the actual slip mechanism. Brochard and de Gennes [18] found that in the case of cohesive slip at small surface densities of tethered chains, σ_{cr} is given by

$$\sigma_{cr} \propto \Sigma_T k_B T \tag{6.20}$$

This clearly agrees with eqn.(6.19) if one recalls eqn.(6.17) and eqn.(5.10). Eqns.(6.19, 6.20) show that in the absence of desorption (when X_0 is constant) the critical shear stress σ_{cr} is a linear function of the melt temperature T, similar to the behavior reported in [49, 59]. In this regime, $\dot{\gamma}_{cr}$ also increases linearly with T (since the Rouse time $T_{RB} \propto T^{-1}$). Clearly, the linear temperature dependence of σ_{cr} and $\dot{\gamma}_{cr}$ can be attributed to cohesive slip. As mentioned earlier, eqn.(6.19) also holds for adhesive slip at $T > T^*$. However, this does not imply a similar temperature dependence of σ_{cr} and $\dot{\gamma}_{cr}$. Namely, for low E_{adh} X_0 rapidly decreases as T is increased. In this regime, both σ_{cr} and $\dot{\gamma}_{cr}$ are more likely to decrease with T, as predicted by adhesive failure theories. A decrease in σ_{cr} with the temperature T was reported by Joshi et al [60] who studied a flow of polyethylene slipping on a low-adsorbing fluoropolymer surface. Note that in the case of the mixed slip (at intermediate E_{adh}) the actual temperature dependence of σ_{cr} and $\dot{\gamma}_{cr}$ in the regime $T > T^*$ strongly depends on the value of E_{adh}.

Figure 6.6 shows that for temperatures below T^*, at which both σ_{cr} and $\dot{\gamma}_{cr}$ have a maximum, σ_{cr} and $\dot{\gamma}_{cr}$ become very sensitive to the value of E_{adh}, as opposed to the regime $T > T^*$ considered above. For $T < T^*$, σ_{cr} and $\dot{\gamma}_{cr}$ are larger (at a given X_0) for higher E_{adh}. In this regime, both σ_{cr} and $\dot{\gamma}_{cr}$ increase with the temperature, irrespective the dominant slip mechanism. For example, the shear stress $\sigma_{cr} \propto T^{\alpha}$, where $\alpha > 1$ is a function of E_{adh}. The deviation from the linear dependence was reported by Wang and Drda [50] who observed an increase in σ_{cr}/G_{0B} with T for polyethylene resins below 200^0C. They called it "a low-temperature anomaly" and hypothesized that it stems from a flow-induced transition to an ordered phase. The present theory makes it clear that this anomaly can be explained in terms of disentanglement and/or desorption. The existing theories for slip do not, however, explain the low temperature anomaly. Note that an increase in σ_{cr} and $\dot{\gamma}_{cr}$ with T at low E_{adh}, which is unexpected for adhesive slip, arises from the fact that for $T < T^*$ the system is actually in the regime of the "mixed" slip.

Another consequence of the nonmonotonous temperature dependence of σ_{cr} and $\dot{\gamma}_{cr}$ predicted by the model is a sudden elimination of wall slip (and ultimately extrudate distortions) during a controlled rate extrusion over a narrow

temperature window, similar to the behavior reported by Kolnaar and Keller [61]. The absence of extrudate distortions in [61] was hypothesized to be a result of the existence of a flow-induced mesophase. The present model, however, is able to explain this phenomenon in terms of disentanglement and/or desorption.

6.5 Wall material dependence

Here the dependence of the stick-to-slip transition on the material of the wall is discussed for a polymer melt at a fixed temperature. In this case, variations in X_0 are related (via E_{adh}) to variations in the surface energy of the wall. In Figure 6.7, the critical shear stress σ_{cr} and shear rate $\dot{\gamma}_{cr}$ are shown versus X_0. According to eqn.(6.17), for a given temperature, X_0 increases with E_{adh} so that in Figure 6.7 the adhesion energy E_{adh} increases from left to right.

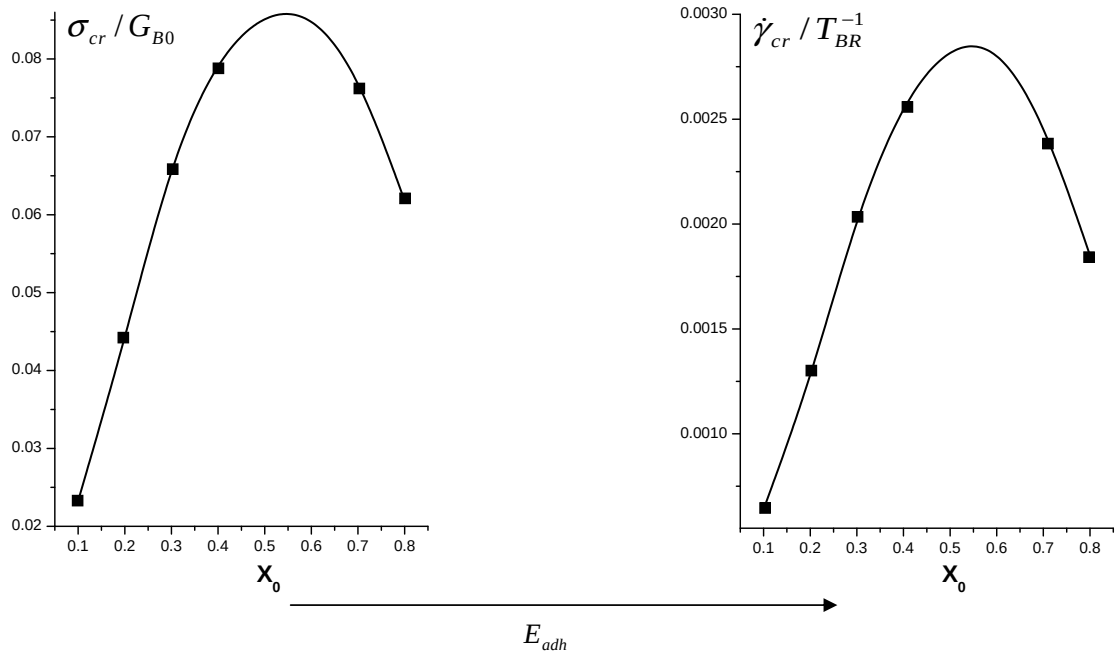

Figure 6.7: Critical shear stress (on the left) and critical shear rate (on the right) vs parameter X_0. The curve is obtained via interpolation of low, intermediate, and high adhesion energy regimes. Results for $Z_B = 40$.

Similar to the behavior depicted in Figure 6.6, both σ_{cr} and $\dot{\gamma}_{cr}$ are found to be nonmonotonous functions of E_{adh} with a maximum at a certain critical E^*_{adh} corresponding to $X_0 \approx 0.5$. At low E_{adh}, the surface density Σ_T of tethered chains is small so entanglements between nearby chains are unlikely. In this regime, the tethered chains move independently of each other, so both σ_{cr} and $\dot{\gamma}_{cr}$ are linear functions of Σ_T, in accordance with eqn.(6.19). At low E_{adh}, the absolute values of σ_{cr} and $\dot{\gamma}_{cr}$ are small, which means that even a rather slow flow may cause the stick-to-slip transition. This is due to the fact that at

low E_{adh} the polymer-wall interaction is not strong enough to capture a large number of polymers on the wall and prevent their desorption by the flow.

A further increase in E_{adh} "creates" more adsorbed molecules on the wall and "impedes" their desorption. According to eqns.(5.14, 6.19), for $E_{adh} < E^*_{adh}$ both σ_{cr} and $\dot{\gamma}_{cr}$ are proportional to the number of bulk-tethered entanglements in the interfacial layer and therefore increase with E_{adh}. At E^*_{adh}, the number of the bulk-tethered entanglements is maximal, which implies maximal σ_{cr} and $\dot{\gamma}_{cr}$. However, above E^*_{adh} it starts to decrease with E_{adh} due to the increasing role of tethered-tethered entanglements. Besides that, these entanglements suppress constraint release in the layer, thereby decreasing its resistibility to cohesive slip. As a consequence, a further increase in E_{adh} above E^*_{adh} will result in a decrease in σ_{cr} and $\dot{\gamma}_{cr}$.

The model predictions for the material dependence of the stick-to-slip transition are in agreement with the data of Anastasiadis and Hatzikiriakos [62], who reported an increase in σ_{cr} with E_{adh} at a fixed temperature. Apparently, they studied the regime $E_{adh} < E^*_{adh}$. Lèger and coworkers [8] reported a nonmonotonous dependence of $\dot{\gamma}_{cr}$ on the surface energy of tethered chains permanently attached to the wall, which also confirms the model predictions. Note that the nonmonotonous wall material dependence of the stick-to-slip transition is not revealed by other "mixed" slip theories. For example, the transient network model of Joshi et al [24] predicts σ_{cr} to be independent of E_{adh} for both low and high adhesion energies. In the intermediate regime, σ_{cr} was predicted to increase linearly with the adhesion energy E_{adh}.

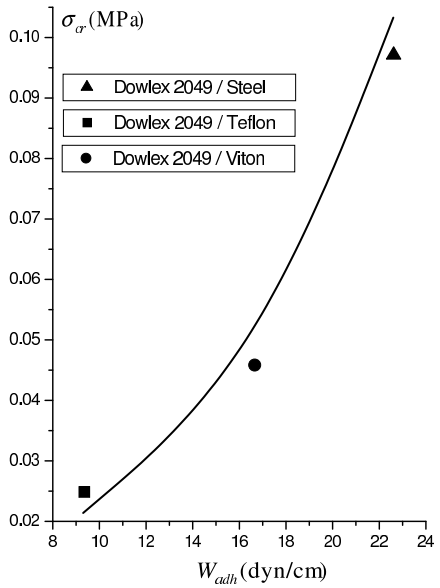

Figure 6.8: Critical shear stress vs surface density of adhesion energy. The solid line is the model prediction.

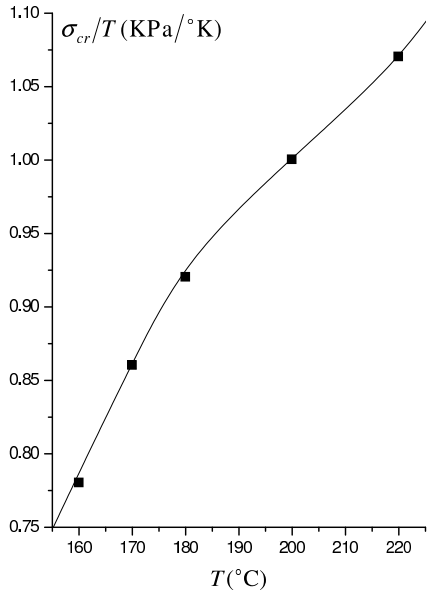

Figure 6.9: Critical shear stress vs melt temperature. The solid line is the model prediction.

In the rest of this chapter, predictions of the model will be compared with

available data on slip. Recently, Anastasiadis and Hatzikiriakos [62] measured adhesion energies of various polymer-wall pairs and found an apparent relation between σ_{cr} and E_{adh}. Let us compare their data on LLDPE of molecular weight $M = 119600$ g/mol (Dowlex 2049 from Dow Chemical) on various wall materials, including stainless steel, fluoropolymers Teflon®, and Viton®. The reported values of the adhesion energy W_{adh} per unit area of the wall for Dowlex 2049 on stainless steel, Viton®, and Teflon® are 22.6, 16.8, and 9.3 dyn/cm, respectively. Based on the molecular data of Fetters et al [54], the input model parameters for Dowlex 2049 were found in [28]. Specifically, the mean number Z_B of constraints per bulk chain, the elastic modulus G_{0B} of the bulk, the mean entanglement spacing a_0, and the maximum surface density $\Sigma_T^{(max)}$ of tethered chains were estimated to be 120, 2.6 MPa, 1.6 nm, and $2.8 \cdot 10^{17}$ chains/m^2, respectively. The adhesion energy per tethered chain E_{adh} is estimated as $W_{adh}/\Sigma_T^{(max)}$. Since the value of the parameter A (see eqn.(6.17)) and the mean number of constraints Z_T per tethered chain are not known, we will regard them as adjustable parameters. In Figure 6.8, the model predictions for σ_{cr} vs W_{adh} are compared with the data of Anastasiadis and Hatzikiriakos. A good agreement between the theory and experiment is found for $A \approx 100$ and $Z_T \approx 25$.

In Figure 6.9, model predictions for σ_{cr} versus the melt temperature T are compared with the data of Wang and Drda [50] on HDPE of molecular weight $M = 130500$ g/mol (MH07 from BP Chemicals). The values of E_{adh} and parameter A for MH07 on steel are taken the same as for Dowlex 2049. The molecular weight between entanglements $M_e \approx 1500$ g/mol, the elastic modulus $G_{0B} \approx 2.5$ MPa, and the mean number $Z_T \approx 15$ of constraint per tethered chain for MH07 were found by the best fit to the data. The found value for G_{0B} and M_e are in a good agreement with the estimates from [63]. The mean number Z_B of constraints per bulk chain and mean entanglement spacing a_0 (corresponding to these M_e and G_{0B}) are estimated to be 80 and 1.8 nm, respectively. Figure 6.9 clearly shows a nonlinearity in the temperature dependence of the critical shear stress, earlier referred to as the low temperature anomaly. Since the surface energy of a steel wall is rather high, Figure 6.9 corresponds to a regime where cohesive slip is dominant. The existing cohesive slip theories predict the ratio σ_{cr}/T to be temperature independent. In contrast, as is seen in Figure 6.9, the present model is able to provide a good quantitative description of the observed low temperature phenomenon.

So far we have studied the case of monodisperse polymer bulk flowing over a grafted polymer brush of monodisperse tethered chains. In reality, polymer melts are always polydisperse and contain various fractions of polymer molecules with different molecular weights. In the next chapter, we will incorporate polydispersity of the bulk and the tethered chains into the developed formalism and study its effect on the parameters of the stick-to-slip transition.

Chapter 7

Effect of polydispersity on wall slip

In the previous chapters, we studied a flow of a monodisperse polymer melt near a die wall. In reality, melts are always polydisperse. Here we will extend the developed theory to include polydispersity of bulk and tethered chains, and ultimately discuss the effect of polydispersity on the parameters of the stick-to-slip transition. For simplicity, we will assume that the interaction between the melt and the wall is strong enough to prevent desorption of adsorbed molecules from the wall. In this regime, slip can only occur via disentanglement.

7.1 Bond vector correlator of a polydisperse bulk

Let us first study the effect of polydispersity on the dynamics of the polymer bulk. As was shown earlier, the dynamics of an ensemble of bulk polymer chains, with equilibrium length L_{0B}, can be successfully described by the so-called bond vector correlator $S^B_{\alpha\beta}(s_0,t)$ defined as

$$S^B_{\alpha\beta}(s_0,t) =< \hat{b}_\alpha(s_0,t)\hat{b}_\beta(s_0,t) >_B \quad , \quad -L_{0B}/2 \le s_0 \le L_{0B}/2\,, \tag{7.1}$$

where $< \ldots >_B$ denote averaging over the ensemble and $\hat{b}_\alpha(s_0,t)$ is the α component of the bond vector $\hat{\mathbf{b}}(s_0,t)$ of a bulk chain. Parameter s_0, defined as the equilibrium arclength of a segment of the primitive path (see Figure 2.6), serves as a curvilinear coordinate for the chosen segment. It runs over a fixed interval from $-L_{0B}/2$ to $L_{0B}/2$, the same for all bulk chains. Once $S^B_{\alpha\beta}$ is known, one can readily calculate various properties of the ensemble. For example, according to eqn.(4.2), the local stress $\sigma^B_{\alpha\beta}$ in the melt is given by (the elastic modulus G_{0B} of the bulk is given by eqn.(5.10))

$$\sigma^B_{\alpha\beta}(t) = \frac{G_{0B}}{L_{0B}} \int\limits_{-L_{0B}/2}^{L_{0B}/2} ds_0\, S^B_{\alpha\beta}(s_0,t)\,, \tag{7.2}$$

A polydisperse melt contains various fractions of polymers with different molecular weights. Hereafter, polymers with molecular weight M_i will be referred to as i-chains. Let n_i be the concentration of the i-chains in the melt. If P is the total number of different fractions of polymers in the melt, then the numbers $\{n_i\}_{i=1}^{i=P}$ represent the melt composition. In what follows, these numbers are assumed to be macroscopic so that each fraction of polymers of the same sort can be considered as an ensemble. For example, the number of the i-chains per unit volume of the melt yields an ensemble of monodisperse polymers whose equilibrium length is equal to L_{i0B}. For this ensemble, the bond vector correlator $S^B_{i\alpha\beta}$ can be introduced defined as

$$S^B_{i\alpha\beta}(s_0,t) =< \hat{b}_\alpha(s_0,t)\hat{b}_\beta(s_0,t) >_i , \tag{7.3}$$

where the averaging is taken over the i-chains. Note that parameter s_0 in eqn.(7.3) runs from $-L_{i0B}/2$ to $L_{i0B}/2$. Certainly, the dynamics of the polydisperse melt cannot be described by a single bond vector correlator. Instead, one must specify the correlator for each sort of polymers in the melt. Once $S^B_{i\alpha\beta}$ is known for each melt component, the dynamics of the melt is completely defined, and thus its macroscopic properties can easily be calculated. For example, the local stress $\sigma^B_{\alpha\beta}$ in the polydisperse melt is given by

$$\sigma^B_{\alpha\beta}(t) = \sum_{i=1}^{P} \frac{G_{i0B}}{L_{i0B}} \int\limits_{-L_{i0B}/2}^{L_{i0B}/2} ds_0\, S^B_{i\alpha\beta}(s_0,t) , \tag{7.4}$$

where the elastic modulus G_{i0B} is defined by

$$G_{i0B} = \frac{n_i M_i k_B T}{M_e} , \tag{7.5}$$

where M_i, n_i, T and M_e are the molecular weight of the i-chains, their concentration in the melt, the melt temperature, and the mean molecular weight between entanglements, respectively. Let us show that eqn.(7.4) can be presented in a more convenient form. To this end, let us formally rewrite the correlator $S^B_{i\alpha\beta}$ of the i-chains as $S^B_{i\alpha\beta}(s_0,t) = S^B_{i\alpha\beta}(xL_{i0B},t)$, where $x = s_0/L_{i0B}$ is a dimensionless coordinate. Since for each sort of polymer chains $-L_{i0B}/2 \le s_0 \le L_{i0B}/2$, we have that x runs over the same interval from $-1/2$ to $1/2$ for all the chains present in the melt. With the help of the dimensionless coordinate x, eqn.(7.4) now can be rewritten as follows

$$\sigma^B_{\alpha\beta}(t) = \frac{\rho k_B T}{M_e} \int\limits_{-1/2}^{1/2} dx\, \Phi^B_{\alpha\beta}(x,t) , \tag{7.6}$$

where ρ is the density of the melt given by

$$\rho = \sum_{i=1}^{P} \rho_i M_i . \tag{7.7}$$

The tensor $\Phi^B_{\alpha\beta}(x,t)$ in eqn.(7.6) can be regarded as the "generalized" bond vector correlator of the polydisperse melt. Its components are given by

$$\Phi^B_{\alpha\beta}(x,t) = \sum_{i=1}^{P} \omega_i S^B_{i\alpha\beta}(xL_{i0B},t)\,, \tag{7.8}$$

where $\omega_i = \rho_i M_i/\rho$ is the weight fraction of the i-chains in the melt. Apparently, the fractions $\{w_i\}_{i=1}^{i=P}$ represent the molecular weight distribution (MWD) of the components of the melt. Note that this distribution is normalized, that is $w_1 + w_2 + ... + w_P = 1$. Eqn.(7.6) shows that calculation of the local stress in the polydisperse melt amounts to calculation of the tensor $\Phi^B_{\alpha\beta}$, which is in turn equal to the value of the "partial" bond vector correlator $S^B_{i\alpha\beta}$ averaged over the MWD of the melt. In order to find the equation of motion for $S^B_{i\alpha\beta}$, let us recall that $S^B_{i\alpha\beta}$ describes the dynamics of the ensemble of the monodisperse i-chains. In Chapter 4, we were able to derive the equation of motion for the bond vector correlator of monodisperse polymer molecules (see eqn.(4.10)) and the corresponding boundary conditions (see eqn.(4.8)). Based on these results, one can immediately write down the equation of motion for the bond vector correlator $S^B_{i\alpha\beta}$ of the i-chains (for $0 < s_0 < L_{i0B}/2$):

$$\begin{aligned}\frac{\partial S^B_{i\alpha\beta}}{\partial t} &= K^B_{\alpha\gamma} S^B_{i\beta\gamma} + K^B_{\beta\gamma} S^B_{i\alpha\gamma} + \left[D_{ic} + \nu_i a_0^2\right]\frac{\partial^2 S^B_{i\alpha\beta}}{\partial s_0^2} \\ &\quad + 2\,\bar{\xi}_{iB} S^B_{i\alpha\beta} + \left[\int_0^{s_0} dx \bar{\xi}_{iB}(x,t)\right]\frac{\partial S^B_{i\alpha\beta}}{\partial s_0} - \frac{1}{\tau_{iB}}(S^B_{i\alpha\beta} - S^{eq}_{\alpha\beta})\,.\end{aligned} \tag{7.9}$$

The first two terms on the RHS pertain to convection, where $K^B_{\alpha\beta}$ is the gradient velocity tensor in the polymer bulk. The third term corresponds to reptation and constraint release. The coefficients D_{ic} and ν_i are the diffusion coefficient of reptation and the frequency of constraint release on the i-chains, respectively. The last term pertains to contour length fluctuations (CLF) of the i-chains. The corresponding relaxation time $\tau_{iB}(s_0)$ is given by

$$\tau_{iB}(s_0) \approx \frac{1}{4} T_{iRB}\, e^{0.75\, Z_{iB}\,(1-2\,s_0/L_{i0B})^2}\,,$$

where Z_{iB} is the mean number of constraints per i-chain and T_{iRB} its Rouse time. The forth and fifth terms stem from retraction of the i-chains, with $\bar{\xi}_{iB}$ being the corresponding local retraction rate of the chain contour:

$$\bar{\xi}_{iB}(s_0,t) \approx -\frac{\bar{\lambda}_{iB}(s_0,t) - 1}{T_{iRB}} \quad , \quad T_{iRB} = \frac{\varsigma N_e L^2_{i0B}}{3\pi^2 k_B T}\,.$$

Here $\bar{\lambda}_{iB}(s_0,t)$ is the mean local stretch of the i-chains at s_0 and time t. In a regime where the i-chains are stretched only slightly, we have that $\bar{\lambda}_{iB}(s_0,t) \approx \sqrt{S^B_{i\alpha\alpha}(s_0,t)}$, where summation is implied over the repeating indices.

We have established that the correlator $S^B_{i\alpha\beta}$ of the i-chains satisfies a nonlinear integro-partial differential equation in which the coefficients also depend on the sort of polymer chains under consideration. This implies that, in general, there is no closed equation of motion for the tensor $\Phi^B_{\alpha\beta}$. To calculate $\Phi^B_{\alpha\beta}$, one must solve the equation of motion for the correlator $S^B_{i\alpha\beta}$ for each component of the melt. Attention must be paid to the fact the equation of motion for $S^B_{i\alpha\beta}$ contains, as a parameter, the corresponding frequency ν_i of constraint release of the i-chains. In a polydisperse melt, different sorts of polymers may interact with each other via entanglements. In the presence of convective constraint release (CCR), this implies that ν_i is actually a function of all the bond vector correlators $S^B_{j\alpha\beta}$ $(j = 1...P)$ present in the melt

$$\nu_i = \nu_i(S^B_{1\alpha\beta}, S^B_{2\alpha\beta}, \ldots, S^B_{P\alpha\beta})\,. \tag{7.10}$$

Therefore, calculation of the "generalized" bond vector correlator $\Phi^B_{\alpha\beta}$ of a polydisperse melt with P components amounts to solving a system of P coupled equations of motion (see eqn.(7.9)), one for each sort of molecules. Note that in the linear viscoelastic regime, where CCR gives only a minor contribution to the melt dynamics and can be neglected, these equations decouple. In this regime, constraint release in the melt is driven by reptation so that ν_i is only a function of the molecular parameters of the melt. As was shown in [29], in this regime ν_i does not only depend on the molecular parameter of the i-chains, but depends on the molecular parameters of all the sorts of polymer chains present in the melt. In the next section, we will study CR in the polydisperse melt and derive an explicit expression for ν_i.

7.2 Constraint release in a polydisperse melt

In a polydisperse polymer melt which contains P sorts of chains, each molecule has, in general, P sorts of constraints. For example, constraints of the j-th sort are imposed by j-chains. In what follows, they will simply be referred to as j-constraints. Each sort of constraints has its own characteristic lifetime. The mean lifetime τ_j of the j-constraints depends on the molecular parameters of the j-chains. Let $\phi^{(i)}_j$ be the mean fraction of the j-constraints per i-chain. Then, the frequency ν_i of constraint release of the i-chains can be written as

$$\nu_i = \sum_{j=1}^{P} \frac{1}{\tau_j}\phi^{(i)}_j\,. \tag{7.11}$$

To calculate $\phi^{(i)}_j$, let us assume that all the entanglements in the melt are pairwise contacts between neighboring polymers. Then, the entanglement network in the melt can be considered as consisting of interacting "half-entanglements". If Z_{iB} is the mean number of constraints per i-chain, then

each i-chain contributes to $Z_{iB}/2$ entanglements, or, equivalently, provides Z_{iB} half-entanglements of the i-th sort. Each half-entanglement interacts with another one present in the melt. Two half-entanglements build an entanglement of one of $P(P+1)/2$ sorts. Let W_i be the fraction of the half-entanglements of the i-th sort per unit volume of the melt. If n_i is the concentration of the i-chains in the melt, then the number of the half-entanglements of the i-th sort per unit volume of the melt is $n_i M_i/M_e$, where M_e is the mean molecular weight between entanglements. On the other hand, it is equal to $2W_i/a_0^3$, where a_0 is the mean entanglement spacing. Therefore, W_i can be written as

$$W_i = \frac{\rho a_0^3}{2M_e}\omega_i \,, \tag{7.12}$$

where ω_i is the mass fraction of the i-chains in the melt. Once the fractions W_i are known, one can readily calculate the corresponding volume fractions of entanglements of each sort in the melt. Since half-entanglements are distributed homogeneously in the melt, they are given by

$$W_{ii} = W_i W_i \quad , \quad W_{i\neq j} = 2W_i W_j \,, \tag{7.13}$$

where the prefactor 2 in the expression for W_{ij} stems from the fact that $W_{ij} = W_{ji}$. Given the volume fractions W_{ij} of entanglements, the CR matrix $\phi_j^{(i)}$ in eqn.(7.11) can be written as

$$\phi_j^{(i)} = \frac{W_{ij}}{\sum\limits_{m=1}^{P} W_{im}} \,. \tag{7.14}$$

Finally, substitution of eqs.(7.12, 7.13) into eqn.(7.14) yields

$$\phi_i^{(i)} = \frac{\omega_i}{2-\omega_i} \quad , \quad \phi_{j\neq i}^{(i)} = \frac{2\omega_j}{2-\omega_i} \,. \tag{7.15}$$

It is seen that the components of the CR matrix $\phi_j^{(i)}$ are only functions of the molecular weight distribution of the melt. The existence of the nondiagonal components $\phi_{j\neq i}^{(i)}$ reveals that the motions of different sorts of polymer chains in the polydisperse melt are coupled via constraint release. The strength of this coupling, as measured by $\phi_{j\neq i}^{(i)}$, is a function of the melt MWD.

Let us now find the mean lifetime τ_j of the j-constraints, which amounts to calculation of the mean lifetime of the half-entanglements of the j-th sort (or, for short, "j" half-entanglements) in the melt. At rest, they are released via reptation of the j-chains. Let δt_j be the average time needed for a j-chain to reptate over a distance a_0. In the absence of CLF, reptation of the j-chain during the time interval $0...\delta t_i$ will release (on average) one constraint on another chain, or, in other words, will "destroy" two half-entanglements.

These half-entanglements, however, may have different sorts. The probability to destroy one "i" and one "j" half-entanglement is equal to W_{ij} (see eqn.(7.13)), whereas two "j" half-entanglements W_{jj}. The number N_j of the "j" half-entanglements per unit volume of the melt at time $t = \delta t_j$ is then

$$N_j(t = \delta t_j) = N_j(t = 0) - n_i \Bigg[\sum_{i=1, i \neq j}^{P} W_{ij} + 2W_{jj} \Bigg] , \tag{7.16}$$

where the entanglements "creation" mechanism has been ignored. In eqn.(7.16), n_i is the concentration of the i-chains in the melt, and $N_j(t = 0) = n_j Z_j$ the number of the "j" half-entanglements per unit volume of the melt at time $t = 0$. On the other hand, if τ_j is the mean lifetime of a "j" half-entanglement, then we have that

$$N_j(t = \delta t_j) = N_j(t = 0) \cdot e^{-t/\tau_j} . \tag{7.17}$$

By comparing eqn.(7.16) with eqn.(7.17), one finally arrives at

$$\tau_j = \frac{Z_j}{2W_j} \, \delta t_j . \tag{7.18}$$

where use has been made of eqn.(7.13) and the fact that the distribution function W_i over the half-entanglements in the melt is normalized, that is $W_1 + ... + W_P = 1$. According to Doi and Edwards [31], $\delta t_j \approx a_0^2 / 2D_{jc}$ so that finally we have that

$$\tau_j = \frac{Z_j}{2W_j} \frac{a_0^2}{2D_{jc}^f} \quad , \quad D_{jc}^f = \frac{D_{jc}}{\Big[1 - \dfrac{1.5}{\sqrt{Z_j}} \Big]^2} , \tag{7.19}$$

where we have also included an effect of CLF on the mean lifetime of the j-constraints (see the discussion after eqn.(4.21)). Substitution of eqns.(7.11, 7.15, 7.19) into eqn.(7.9) yields that in the polydisperse melt, thermal constraint release on the i-chains is mostly driven by reptation of the low molecular weight components of the melt. Clearly, in contrast to a monodisperse melt, thermal constraint release may play an important role in the dynamics of the polydisperse melt and therefore must be taken into account into any realistic description of the melt behavior.

In the presence of flow, the j-constraints can also be released, in parallel to reptation, via retraction of the j-chains. In order to calculate the mean lifetime of a j-constraint due to CCR, let us recall eqn.(7.18). In the case of retraction, δt_j can be associated with the average time needed for an end of a j-chain to retract (along the tube) a distance equal to the mean entanglement spacing a_0. According to eqn.(4.19), δt_j is given by

$$\delta t_j = a_0 \Bigg[\int_0^{L_{j0B}/2} ds_0 \, \bar{\xi}_{jB}(s_0, t) \Bigg]^{-1} , \tag{7.20}$$

where $\bar{\xi}_{jB}$ is the mean local retraction rate of the chain contour so that the integral in eqn.(7.20) gives the average velocity between the chain end and the melt. Taking into account that both ends of the j-chain contribute to CCR and the fact that thermal and convective constraint release work independently of each other, from eqn.(7.18) and eqn.(7.20) we finally have that in the presence of flow the mean lifetime τ_j of the j-constraint is given by

$$\tau_j^{-1} = \frac{2W_i}{Z_j}\left[\frac{2D_{jc}^f}{a_0^2} + 2\frac{1}{a_0}\int_0^{L_{j0B}/2} ds_0\,\bar{\xi}_{jB}(s_0,t)\right] \tag{7.21}$$

Eqn.(7.21) represents a combined action of thermal and convective constraint release. In a case of a monodisperse melt ($P = 1$), it boils down to eqn.(4.19) derived earlier in Chapter 4. Since the fractions W_j in eqn.(7.21) are functions of the melt MWD, eqn.(7.21) reveals that the mean lifetime of the j-constraint is not only a function of the molecular parameters of the j-chains, as assumed in many molecular theories for polydisperse systems (see, for example, Rubinstein and Colby [64]), but also depends on the melt MWD. Therefore, as follows from eqn.(7.15) and eqn.(7.21), constraint release in the polydisperse melt shows a complex nonlinear dependence on its molecular weight distribution. In what follows, the reciprocal mean lifetime τ_j of the j-constraints will be referred to as the mobility of the j-constraints.

Once the mobility of each sort of constraints in the melt and the matrix $\phi_j^{(i)}$ are known, constraint release in the melt is completely defined. The components of $\phi_j^{(i)}$ represent the mobility distribution of the constraints for every sort of polymers in the melt. For example, according to eqn.(7.11), the frequency ν_i of constraint release of the i-chains is equal to the mobility of the j-constraints averaged over the corresponding distribution $\phi_j^{(i)}$ ($j = 1...P$). Most of the existing constitutive theories for polydisperse systems do not normally acknowledge the constraints mobility distribution, thus assigning all the constraints on a polymer chain a single characteristic lifetime. So the present model offers a more accurate treatment of CR in the melt in comparison to other theories. Since constraint release plays an essential role in the dynamics of polydisperse systems, the thorough treatment of CR enables the present model to provide a more accurate description of the melt dynamics.

The system of equations of motion for each correlator $S_{j\alpha\beta}^B$ ($j = 1...P$) extended with eqns.(7.11, 7.15, 7.21) forms a closed system of coupled equations which determines the behavior of the polydisperse polymer melt in a flow. This system is valid in both the linear and nonlinear viscoelastic regime, and therefore is applicable over a wider range of flow rates than most of the existing constitutive theories for polydisperse melts. The present approach is different from the conventional mixing rule models based on the Tsenoglou / des Cloizeaux concept of "double reptation" [65, 66, 67, 68], in which the dynam-

ics of the polydisperse melt is analyzed in terms of the rheological behavior of monodisperse melts. In fact, the presence of the nondiagonal components of the CR matrix $\phi^{(i)}_{j\neq i}$ in eqn.(7.15) makes it explicit that even in the linear viscoelastic regime motions of different sorts of polymer molecules in the melt are coupled and cannot be considered independently. This implies that the dynamics of the polydisperse melt cannot, in general, be described in terms of the dynamics of its monodisperse components. In the next section, the developed formalism will further be used to study an affect of polydispersity of bulk molecules on the onset of cohesive slip.

7.3 Polydispersity of the bulk: effect on wall slip

In this section, we will study how polydispersity of the bulk may affect the onset of cohesive slip. For simplicity, we assume that the interfacial layer is monodisperse, that is all the tethered chains have the same equilibrium length L_{0T}. As was established earlier, in order to quantify the stick-to-slip transition, both the constitutive equation for the bulk and for the layer must be solved simultaneously. In a case of a polydisperse bulk, the "bulk" constitutive equation is presented by a system of P coupled equations (see eqn.(7.9)), each for one component of the melt. The constitutive equation for monodisperse tethered chains was derived in Chapter 3 (see eqn.(3.31)). As a parameter, it contains the frequency ν_T of constraint release on tethered chains which in turn is inversely proportional to the mean lifetime of constraints in the polymer bulk (see eqn.(5.4)). A polydisperse bulk with P sorts of polymer chains contains P sorts of constraints whose mean lifetimes are given by eqn.(7.21). This implies that the monodisperse tethered chains entangled with polydisperse bulk molecules have, in general, P sorts of bulk constraints. If τ_i is the mean lifetime of the i-constraints in the polymer bulk and ϕ_{iZ} is the mean fraction of bulk constraints of the i-th sort per tethered chain, then the average frequency ν_T of constraint release of the tethered chains has the form

$$\nu_T = \sum_{i=1}^{P} \frac{1}{\tau_i}\,\phi_{iZ}\,. \tag{7.22}$$

According to eqn.(5.8), ϕ_{iZ} is given by

$$\phi_{iZ} = \frac{2W_{iB}}{W_T + 2W_B}\,, \tag{7.23}$$

where W_T and W_{iB} are the fractions of tethered (see the discussion after Figure 5.3) and bulk half-entanglements of the i-th sort per unit volume in the interfacial layer, respectively. The total volume fraction W_B of the bulk

half-entanglements in the interfacial layer is given by

$$W_B = \sum_{i=1}^{P} W_{iB} \,. \tag{7.24}$$

Note that $W_T + W_B = 1$. In order to calculate W_{iB}, let us again consider the entanglement network in the polydisperse bulk. In the previous section, we were able to calculate the fraction W_i of half-entanglements of the i-th sort per unit volume (see eqn.(7.12)). Since fractions of half-entanglemens of the i-th sort in the bulk and in the layer are equal, we have that

$$W_{iB} = W_i W_B \,, \tag{7.25}$$

where W_i is defined in eqn.(7.12). Since the distribution W_i is normalized, W_{iB} given by eqn.(7.25) satisfies eqn.(7.24). Therefore, from eqns.(7.22, 7.23, 7.25) one may find that the average frequency ν_T of constraint release of tethered chains can be written as

$$\nu_T = \sum_{i=1}^{P} W_i \tau_i^{-1} \phi_Z \quad , \quad \phi_Z = \frac{2(1-W_T)}{W_T + 2(1-W_T)} \,, \tag{7.26}$$

where the volume fraction W_T of "tethered" half-entanglements in the interfacial layer was calculated earlier in Chapter 5 (see eqn.(5.6)). According to eqn.(5.6), it is a function of the molecular weight and the surface density of tethered chains. The mean lifetime τ_i of the bulk constraints of the i-th sort is given by eqn.(7.21).

Finally, to calculate the stick-to-slip law for the polydisperse bulk, we must also specify explicitly the MWD of bulk chains, or in other words, the fractions $\{\omega_i\}_{i=1}^{i=P}$ (see eqn.(7.8)). As an example, we will take the continuous log-normal molecular weight distribution $\omega(M)$, found to be a good approximation for the actual MWD of many industrial polymers (see, for example, van Ruymbeke et al [69]). The log-normal MWD $\omega(M)$ has the form

$$\omega(M) = \frac{1}{\sqrt{2\pi} M \sigma} \; e^{-\frac{1}{2}\left[\frac{\ln(M) - \ln(M_0)}{\sigma}\right]^2} \quad , \quad 0 < M < \infty \,, \tag{7.27}$$

where M_0 and σ are the parameters of the distribution. Note that $\omega(M)$ is normalized, that is

$$\int_0^\infty dM \, \omega(M) = 1 \,. \tag{7.28}$$

The typical behavior of $\omega(M)$ as a function of the molecular weight M is depicted in Figure 7.1. The value of M_0 determines the position of the maximum of the distribution. In contrast, the value of σ controls the "width"

of the distribution. Apparently, a small σ corresponds to a narrow MWD, inherent to monodisperse melts. Large values of σ pertain to highly polydisperse systems which contain various fractions of long and short polymer chains. Note that an increase in σ "shifts" the maximum of the distribution to lower molecular weights (for a fixed value of M_0). Other properties of the log-normal distribution are described in detail in [70].

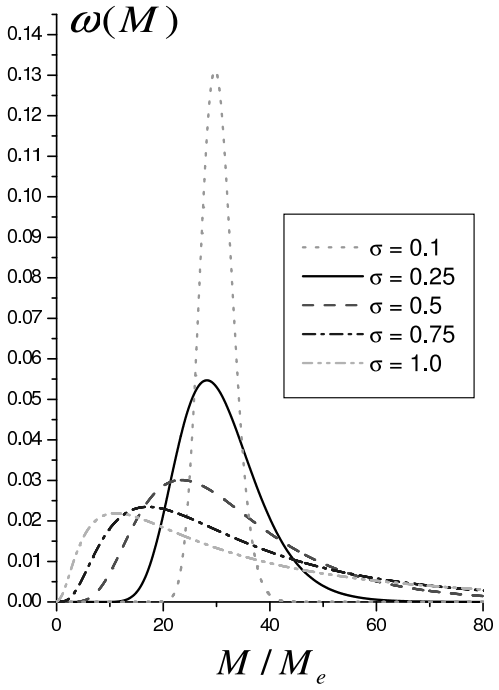

Figure 7.1: Log-normal distribution for $M_0/M_e = 30$ and different values of the parameter σ. M_e is the mean molecular weight between entanglements.

The system of constitutive equations for the polydisperse bulk (see eqn.(7.9)) together with the constitutive equation for the interfacial layer (see eqn.(3.31)) and eqns.(5.1, 5.2) was solved numerically for the case $M_0 = 30M_e$ and different values of the parameter σ. The molecular weight of tethered chains M_T is assumed to be equal to $10M_e$. The geometry of the system is the same as in Figure 5.1. The numerical procedure was described in detail in Chapter 5 (see Section 5). Note that in the case of the polydisperse bulk, instead of solving a single "bulk" constitutive equation, one has to solve a system of P coupled equations. Here P is the number of steps used to "discretize" the log-normal distribution. The dependence of the critical shear rate $\dot{\gamma}_{cr}$ for the onset of macroscopic slip (and ultimately spurt oscillations) on the parameter σ of the MWD is shown in Figure 7.2. It is seen that $\dot{\gamma}_{cr}$ increases monotonically with σ. This dependence becomes especially strong at larger values of σ, where even a small increase in σ leads to a sharp increase in $\dot{\gamma}_{cr}$. Clearly, a polydisperse melt has a larger value of $\dot{\gamma}_{cr}$, or equivalently, is more resistant to cohesive slip than that with a narrow MWD.

The observed increase in the "resistibility" of the melt to slip with increasing σ can be explained as follows. As mentioned earlier, the onset of slip via

disentanglement is determined by the strength of constraint release on tethered chains, measured by the frequency ν_T. According to eqn.(5.4), the value of ν_T is in turn determined by the dynamics of bulk molecules. In particular, thermal constraint release on the tethered chains stems from reptation of the bulk molecules, and therefore is a function of the corresponding reptation time T_{DB} (see eqn.(4.9)). In fact, as follows from Figure 5.9, $\dot{\gamma}_{cr}$ is inversely proportional to T_{DB} and thus scales with the molecular weight M of bulk chains as $M^{-3.4}$. The presence of shorter polymer chains in the bulk with smaller T_{DB} enhances the strength of CR on the tethered chains and therefore postpones the onset of slip to larger shear rates. As mentioned earlier, an increase in the parameter σ of the log-normal distribution moves its maximum to lower molecular weights. In other words, the increase in σ adds to the system more shorter ($M < M_0$) chains than those with molecular weight larger than M_0. This eventually leads to the increase in $\dot{\gamma}_{cr}$.

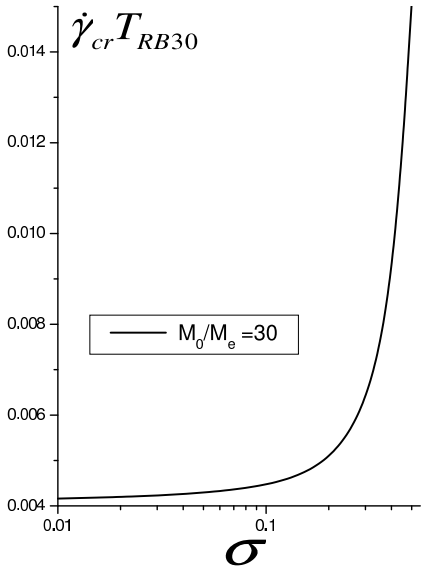

Figure 7.2: Critical shear rate for the onset of macroscopic wall slip versus width of the log-normal distribution for $M_0 = 30M_e$. The molecular weight M_T of tethered chains is equal to $10M_e$. T_{RB30} is the Rouse time of bulk chains (see eqn.(4.12)) with $Z_B = 30$.

The parameters of the log-normal distribution (M_0 and σ) for a given polydisperse melt can be determined from molecular measurements. Namely, for each polydisperse melt the mean number molecular weight $\bar{M}_n$ and mean weight molecular weight $\bar{M}_w$ can be measured, which are defined as follows

$$\bar{M}_n = \frac{\sum_{i=1}^{P} n_i M_i}{\sum_{i=1}^{P} n_i} \quad , \quad \bar{M}_w = \frac{\sum_{i=1}^{P} n_i M_i^2}{\sum_{i=1}^{P} n_i M_i} , \tag{7.29}$$

where n_i and M_i are the concentration of polymer chains of the i-th sort in the melt and their molecular weight, respectively. Note that for a monodisperse

melt ($P = 1$) we have that $\bar{M}_n = \bar{M}_w$. For polydisperse melts, $\bar{M}_w$ is normally larger than $\bar{M}_n$. Therefore, the ratio

$$I = \frac{\bar{M}_w}{\bar{M}_n} \geq 1 \tag{7.30}$$

can be used as a measure of the degree of polydispersity of a melt. The parameter I is commonly referred to as the index of polydispersity. The values of $\bar{M}_n$ and $\bar{M}_w$ calculated with the help of the log-normal MWD in eqn.(7.27) are given by [70]

$$\bar{M}_n = M_0 e^{-\sigma^2/2} \quad , \quad \bar{M}_w = M_0 e^{+\sigma^2/2} \, . \tag{7.31}$$

Therefore, in this case the polydispersity index I has the form

$$I = \frac{\bar{M}_w}{\bar{M}_n} = e^{+\sigma^2} \, . \tag{7.32}$$

The value of I is only determined by the parameter σ and thus is a measure of the width of the MWD, as expected. Moreover, I rapidly increases with σ. As we saw in Figure 7.2, an increase in σ (or equivalently in I) postpones the onset of cohesive slip to larger shear rates in comparison to the case of the monodisperse polymer bulk.

7.4 Polydispersity in the layer: effect on wall slip

In the previous section, we studied the flow of a polydisperse melt over a layer of monodisperse tethered chains. Here we will try to account for polydispersity of the tethered chains and its effect on the onset of wall slip. For simplicity, we now assume that the polymer bulk is monodisperse. As was found in Chapter 5, in the case of the monodisperse tethered chains entangled with the monodisperse polymer bulk, the wall shear stress can be written as

$$\sigma_{xy}^{I} = G_{0B} \Psi_{BT}^{0} \frac{1}{L_{0T}} \int_{0}^{L_{0T}} ds_0 S_{xy}^{T}(x,t) \, , \tag{7.33}$$

where L_{0T} is the equilibrium length of the tethered chains. The bond vector correlator $S_{\alpha\beta}^{T}$ describes the dynamics of the ensemble of tethered chains present in the interfacial layer. It satisfies a nonlinear equation of motion (see eqn.(3.31)) with the boundary conditions given by eqn.(3.32). In eqn.(7.33), G_{0B} is the elastic modulus of the bulk and Ψ_{BT}^{0} is the equilibrium fraction of bulk-tethered entanglements per unit volume of the interfacial layer (see the discussion before Figure 5.5). According to eqn.(5.14), Ψ_{BT}^{0} is given by

$$\Psi_{BT}^{0} = 2 W_T W_B \, , \tag{7.34}$$

where W_T and W_B are the fractions of tethered and bulk half-entanglements per unit volume of the interfacial layer, respectively. The explicit form of W_T and W_B is given by eqn.(5.6). A polydisperse interfacial layer contains various fractions of tethered chains with different molecular weights. Let L_{i0T} be the equilibrium length of tethered chains of the i-th sort. In what follows, tethered chains of the i-th sort will simply be referred to as i-chains. The number of the i-chains per unit area of the wall will be denoted by Σ_{iT}. The total number of sorts of the tethered chains in the layer is P. In a case of the polydisperse layer, eqn.(7.33) generalizes to

$$\sigma_{xy}^I = G_{0B} \sum_{i=0}^{P} \Psi_{iBT}^0 \int_0^1 dx\, S_{ixy}^T(xL_{i0T}, t)\,, \tag{7.35}$$

where $x = s_0/L_{i0T}$ is a dimensionless coordinate. Ψ_{iBT}^0 is the fraction of entanglements per unit volume of the layer which tethered chains of the i-th sort make with bulk chains present in the layer. According to eqn.(7.34), for the monodisperse bulk, Ψ_{iBT}^0 can be written as

$$\Psi_{iBT}^0 = 2W_{iT}^0 W_B^0\,, \tag{7.36}$$

where W_{iT}^0 is the equilibrium volume fraction of tethered half-entanglements of the i-th sort in the layer. According to eqn.(5.6), W_{iT}^0 can be expressed via the surface density Σ_{iT} of the i-chains as follows

$$W_{iT}^0 = \frac{Z_{iT}\Sigma_{iT}}{2h_0} a_0^3\,. \tag{7.37}$$

Here h_0 is the equilibrium thickness of the interfacial layer, Z_{iT} the number of constraints per i-chain, and a_0 the mean distance between entanglements. Once W_{iT}^0 are given, the total volume fraction W_T^0 of the tethered half-entanglements in the interfacial layer is given by

$$W_T^0 = \sum_{i=1}^{P} W_{iT}^0\,. \tag{7.38}$$

Note that $W_T^0 + W_B^0 = 1$, so eqn.(7.36) can be rewritten in terms of W_{iT}^0 as

$$\Psi_{iBT}^0 = 2W_{iT}^0(1 - W_T^0)\,. \tag{7.39}$$

Let us introduce the fractions Ω_i $(i = 1...P)$ of tethered chains defined by

$$\Omega_i = \frac{Z_{iT}\Sigma_{iT}}{\Omega}\,, \tag{7.40}$$

where

$$\Omega = \sum_{i=1}^{P} Z_{iT}\Sigma_{iT}\,. \tag{7.41}$$

The values $\{\Omega_i\}_{i=1}^{i=P}$ represents the molecular weight distribution of the tethered chains. Note that this distribution is normalized, that is $\Omega_1+\ldots+\Omega_P = 1$. In terms of Ω_i, the equilibrium fraction W_{iT}^0 of tethered half-entanglements of the i-th sort in the layer can be written as

$$W_{iT}^0 = \frac{a_0^3\Omega}{2h_0}\Omega_i\,. \tag{7.42}$$

According to eqn.(7.41), Ω is proportional to the average molecular weight of the tethered chains. To show this explicitly, let us introduce the overall surface density Σ_T of the tethered chains, i.e., the total number of the tethered chains per unit area of the wall, defined as

$$\Sigma_T = \sum_{i=1}^{P} \Sigma_{iT}\,. \tag{7.43}$$

From eqn.(7.41) and eqn.(7.43) one may find that Ω can be rewritten as

$$\Omega = \bar{Z}_T\Sigma_T \quad , \quad \bar{Z}_T = \frac{1}{\Sigma_T}\sum_{i=1}^{P} \Sigma_{iT}Z_{iT}\,. \tag{7.44}$$

Clearly, $\bar{Z}_T$ represents the mean number of constraints per tethered chain. If M_e is the mean molecular weight between entanglements, then we have that $\bar{Z}_T = M_T/M_e$, where M_T is the average molecular weight of tethered chains. Eqn.(7.44) shows that Ω is equal to the product of the mean number $\bar{Z}_T$ of constraints per tethered chain and the overall surface density Σ_T. Let us show that with the help of $\bar{Z}_T$, eqn.(7.39) can be rewritten in a more convenient form. To this end, we introduce the surface density Σ_{0T}^* defined as

$$\Sigma_{0T}^* = \frac{2h_0}{a_0^3\bar{Z}_T}\,. \tag{7.45}$$

In view of eqn.(7.45), the fraction W_{iT}^0 in eqn.(7.42) can be rewritten as

$$W_{iT}^0 = \frac{\Sigma_T}{\Sigma_{0T}^*}\Omega_i\,. \tag{7.46}$$

Therefore, eqn.(7.39) finally reads as

$$\Psi_{iBT}^0 = 2\,\frac{\Sigma_T}{\Sigma_{0T}^*}\left[1 - \frac{\Sigma_T}{\Sigma_{0T}^*}\right]\Omega_i\,. \tag{7.47}$$

It is seen that $\Psi_{iBT}^0 = 0$ if $\Sigma_T = \Sigma_{0T}^*$, which implies the absence of entanglements between bulk and tethered chains at Σ_{0T}^*. Apparently, Σ_{0T}^* represents the surface density of the dry-brush regime (see discussion after eqn.(5.7)) for the case of the polydisperse interfacial layer.

According to eqn.(5.4), the frequency of constraint release on the monodisperse tethered chains is proportional to the average fraction ϕ_Z of the bulk constraints per tethered chain. The fraction ϕ_Z, given by eqn.(5.8), was found to be a function of the molecular weight of the tethered chains. This implies that in the case of a polydisperse interfacial layer and a monodisperse bulk the frequency ν_{iT} of constraint release of the i-chains can be written as

$$\nu_{iT} = \nu_B \phi_{iZ} \,, \tag{7.48}$$

where ν_B is the frequency of constraint release in the polymer bulk. The explicit form of ν_B as a function of the molecular and flow parameters of the bulk was calculated earlier in Chapter 4 (see eqn.(4.21)). The fraction ϕ_{iZ} of bulk constraints per i-chain can be written as (see eqn.(5.8))

$$\phi_{iZ} = \frac{2W_B}{W_{iT} + 2W_B} \,, \tag{7.49}$$

where W_B and W_{iT} are the fractions of bulk and tethered half-entanglements of the i-th sort, respectively. In view of eqn.(7.46), they are given by

$$W_{iT} = \frac{\Sigma_T}{\Sigma_T^*}\Omega_i \quad , \quad W_B = 1 - \frac{\Sigma_T}{\Sigma_T^*} \,. \tag{7.50}$$

Here use was made of the fact that $W_B = 1 - W_T$, where W_T is the total fraction of tethered half-entanglements in the layer. In eqn.(7.50), Σ_T^* is given by eqn.(7.42) in which the equilibrium thickness h_0 of the interfacial layer is replaced with its actual thickness h. Eqn.(7.49) and eqn.(7.50) show that in the dry brush regime, for which $\Sigma_T = \Sigma_T^*$, the fraction $\phi_{iZ} = 0$ so that the tethered chains have only tethered constraints, as expected.

The constitutive equation for the monodisperse bulk (see eqn.(4.10)) together with the constitutive equation for the interfacial layer and eqns.(5.1, 5.2) was solved numerically for a case in which the interfacial layer contains only two sorts of tethered chains: short (with molecular weight M_T is $8M_e$) and long (with molecular weight M_T is $16M_e$). The molecular weight of bulk chains M_B is assumed to be equal to $45M_e$. The geometry of the system is the same as in Figure 5.1. The numerical procedure was described in detail in Chapter 5 (see Section 5). Note that in the case of a polydisperse interfacial layer containing two sorts of tethered chains, the "layer" constitutive equation is represented by a system of two equations of motion (similar to eqn.(3.31)), each for one sort of the tethered chains. These two equations can be solved independently as long as the characteristic lifetimes of the tethered constraints are larger than those imposed by bulk molecules (see the discussion after Figure 5.2).

Figure 7.3 shows the dependence of the critical shear rate $\dot{\gamma}_{cr}$ for the onset of cohesive slip on the mass fraction Ω_S of the short tethered chains in the layer. The mass fraction of the long tethered chains is then given by $\Omega_L = 1 - \Omega_S$. As is seen, $\dot{\gamma}_{cr}$ has a nonmonotonous behavior as a function of Ω_S. The

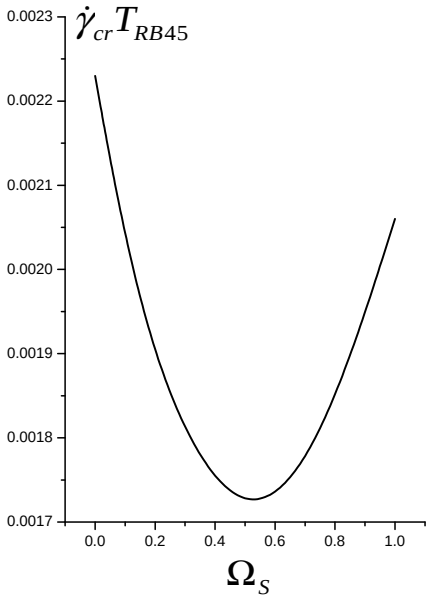

Figure 7.3: Critical shear rate vs fraction of short tethered chains in the layer. The interfacial layer is assumed to contain two sorts of tethered chains: short ($M_T = 8M_e$) and long ($M_T = 16M_e$). The molecular weight of bulk chains is equal to $M_B = 45M_e$. T_{RB45} is the corresponding Rouse time of bulk chains (see eqn.(4.12)).

minimum of the curve approximately corresponds to $\Omega_S = 0.5$. The values $\Omega_S = 0$ and $\Omega_S = 1.0$ correspond to purely monodisperse tethered chains with $M_T = 8M_e$ and $M_T = 16M_e$, respectively. Notice that the difference between the maximum and the minimum of the curve in Figure 7.3 is rather small. This implies that the polydispersity of the interfacial layer has only a subtle effect on the onset of wall slip, especially when compared to the corresponding effect of the "bulk" polydispersity studied in the previous section.

7.5 Conclusions

We studied effect of polydispersity on the onset of cohesive slip described by the critical shear rate $\dot{\gamma}_{cr}$. Two scenarios were analyzed: polydispersity in the bulk and polydispersity in the interfacial layer. As found, the "bulk" polydispersity has a strong effect on the onset of slip. In particular, in the case of the log-normal MWD, a sharp increase in $\dot{\gamma}_{cr}$ with the polydispersity index I was found. So a polydisperse melt starts to slip at larger shear rates than that with a narrow MWD. Such a strong dependence of the parameters of the stick-to-slip transition on the melt composition can be used in practice to postpone the onset of spurt. In contrast, the parameters of the stick-to-slip transition show a rather weak dependence on the polydispersity of tethered chains. So the single molecular weight approximation used in the previous chapters, in which all the tethered chains are assumed to have the same molecular weight equal to their actual average one, is reliable for practical calculations.

Chapter 8

Summary

What was studied?

The focus of this work is the study of the interaction between a flowing polymer melt and a die wall. It is known that under certain conditions the flow becomes unstable which manifests itself via various distortions of the extrudate, commonly referred to as extrusion instabilities. Some of these instabilities are shown to be interfacial in nature, or in other words, originate from the violation of the no-slip boundary condition at the polymer/die wall interface. This is the reason why special attention in this work is paid to the predictions of the stick-slip law in terms of the molecular and flow parameters, as well as the extruder geometry.

We remind you that for ordinary (Newtonian) liquids the no-slip boundary condition is usually satisfied. However, as shown by Greenberg and Demay [71], Georgiou and Crochet [72] and Dubbeldam and Molenaar [73], when the no-slip boundary condition is modified to include a possible stick-to-slip transition above a certain critical stress, even a Newtonian flow starts to show large pressure oscillations at the die outlet, qualitatively similar to those observed for polymer melts. This clearly indicates the importance and the effect of the boundary conditions on the polymer flow in the die.

A possibility for a polymer melt to slip was predicted by de Gennes [9] already a long time ago in the 1970's. He pointed out that due to its high viscosity the melt will always show a significant amount of slippage when flowing past an ideal non-adsorbing surface, whatever the flow rate may be. In a real extruder, the melt flows over a "brush" of polymer molecules adsorbed on the wall. In this case, the onset of wall slip may be associated with a sudden disentanglement between the bulk and surface molecules, after which the polymer melt slips freely over the wall, covered by a thin "lubrication" layer of smashed surface chains. In the picture used by de Gennes and then adopted in other models on slip, the boundary conditions for a polymer melt at the melt/wall interface are governed by the dynamics of surface polymer molecules which

occupy a narrow boundary layer between the melt and the wall. This layer is of a molecular size and therefore must be studied microscopically. Therefore, in order to calculate the stick-slip law, we first focused on the description of the dynamics of polymer molecules attached to the die wall.

What has been done?

First, starting from a microscopic consideration of the interfacial layer, we derived an equation of motion for a single tethered chain in a flow. It was further used to find the corresponding equation of motion for an ensemble of tethered chains attached to the wall surface. This equation actually describes the behavior of the ensemble-averaged configuration of a tethered chain in flow and takes into account all the major physical mechanisms for tethered chains, such as convection, retraction, constraint release, and contour length fluctuations.

Since the dynamics of the tethered chains is coupled to that of the polymer molecules in the bulk, the derived equation is not closed. In order to complete it, an equation of motion for bulk chains has been derived based on a microscopic consideration of the melt. Since bulk chains undergo the same physical mechanisms as tethered ones and can also reptate, this derivation amounts to incorporation of reptation into the existing equation of motion for tethered chains. Moreover, using a simple geometrical analysis, we calculated the frequency of constraint release on bulk chains as a function of the molecular parameters of the melt. The equation of motion for the interfacial layer and for the bulk together with the continuity of stress and velocity, and the balance equation for the surface density of tethered chains form a closed system of equations which lies at the heart of the model. We emphasize that the developed model consistently unites desorption and disentanglement into a single mathematical formalism. In Chapter 7, the proposed model was extended to include polydispersity of bulk and tethered chains.

What was found?

We found that the polymer melt always shows a certain amount of slippage when flowing past a die wall, whatever the flow rate may be. At small flow rates, however, the slip velocity is microscopic and therefore cannot be inferred from experimental stress-strain curves. The presence of a polymer "brush" of surface molecules entangled with the bulk drastically reduces the slip velocity, compared to the case of a polymer melt flowing over an ideal non-adsorbing wall. A decrease in the number of entanglements between bulk and surface molecules due to flow-induced desorption or disentanglement results in an increase of the slip velocity. At the critical shear rate, a massive chain desorption or disentanglement occurs after which the interaction between the melt and the wall is only determined by monomer-monomer friction. This regime is characterized by macroscopically large values of the slip velocity. These results are in a good agreement with the earlier predictions of Brochard and

de Gennes [18].

We found that the dominant slip mechanism is determined by both the value of the adhesion energy E_{adh} and melt temperature T. For large E_{adh}, the melt slips cohesively (i.e., via disentanglement) over the whole range of temperatures. In this regime, desorption gives only a small contribution to the dynamics of the tethered chains so that the actual surface density of tethered chains is nearly equal to its no-flow value for all flow rates up to the critical point. For small E_{adh}, the melt may slip via desorption, desorption plus disentanglement, or even disentanglement alone, depending on the melt temperature. Note that in industrial practice steel dies are often used. Since steel is known to have a large surface energy, one would expect in this case slip via disentanglement as the dominant slip mechanism. In the case of a fluoropolymer-coated die wall, which has a much lower surface energy than a steel one, the regime of mixed slip is expected.

The analysis of the stick-slip law for various polymer-wall pairs has revealed its complex non-linear and non-monotonous dependence on the melt temperature T. The parameters of the stick-slip transition become especially sensitive to T in the case of slip via desorption, as expected for an activation process. Therefore, the temperature dependence of the stick-slip law can conveniently be used to figure out the dominant slip mechanism for a particular polymer-wall pair. Similar to the temperature dependence, the stick-slip law shows a non-monotonous dependence on the wall material, in agreement with available experimental observations. The maximum in the critical shear stress and shear rate correspond to a grafting regime for which the number of entanglements between surface and bulk molecules is maximal. This grafting regime pertains to intermediate surface densities of tethered chains, that is where the interfacial layer contains a lot of tethered chains but the interactions between them are not yet strong enough to allow their orientation by the flow. At very low or very high surface densities of tethered chains, an early onset of slip is predicted, that is to say at lower values of the critical shear stress and shear rate. This is due to the lack of bulk-tethered entanglements or suppressed constraint release on tethered chains, respectively.

Finally, the effect of polydispersity of bulk and tethered chains on the parameters of the stick-to-slip transition was studied. It was found that polydispersity of bulk chains "postpones" the onset of the macroscopic slip regime to larger shear rates. Such a dependence of the stick-slip law on the composition of the melt can indeed be used in practice to suppress spurt oscillations and thus increase the production rate of polymers. On the contrary, the stick-slip law shows a rather weak dependence on polydispersity of tethered chains.

From wall slip to spurt?

As was mentioned in the Introduction, in order to explain the origin of extrusion instabilities, several mechanisms were proposed including constitutive

instabilities, oscillating boundary layers, and wall slip. Experimentally, it has been observed that there is a significant influence of the material of the die on both the onset and development of surface distortions (see, for example, Ramamurthy [74]). Moreover, apparent slip at the die wall has been found in polymer melts prior to the onset of spurt oscillations (see, for example, Münstedt et al [75]). Therefore, the recent experimental data corroborates the hypothesis that spurt, that is large pressure oscillations of the extrudate, originates from slip of the polymer melt over the die wall.

Attempts to explain the occurrence of spurt oscillations via the onset of wall slip have also been made on the phenomenological level. The relaxation oscillation (RO) model of Molenaar and Koopmans [51] and its refined version by den Doelder et al [52, 53] model spurt on the basis of conservation of mass over the system together with conservation of momentum in the die extended with appropriate stick-slip boundary conditions. The boundary conditions are presented as a switch curve in which a transition from the "no-slip" to "slip" regime occurs at a certain critical wall stress. Is is shown that the non-monotonous form of the switch curve and incompressibility of the melt in the die are the ingredients necessary to obtain pressure oscillations. In Figure 8.1, we present a simple flow curve, qualitatively similar to those measured during extrusion for polymers that exhibit spurt.

The flow curve represents the relation between the imposed flow rate Q through the die and the measured pressure drop P over the die during extrusion. The flow rate Q is defined as an integral of the melt velocity over the cross-section of the die. The geometry of the die is the reason that the melt compressibility in the die can be ignored (contrary to the situation in the barrel). This yields that Q is uniform over the die. Then, the mass flux which leaves the die per unit of time can be written as ρQ where ρ is the (constant) polymer density. The pressure drop over the die P is defined as the difference $P_{in} - P_{out}$, where P_{in} and P_{out} are the pressure in the die entry and die exit region, respectively. Clearly, the flow curve is a global relation which is characteristic for the given extrusion system and is determined by the molecular properties of the polymer, the properties of the die wall, and the die geometry.

In Figure 8.1, it is seen that for polymer melts that exhibit spurt oscillations the flow curve is discontinuous and has two branches. As seen in Figure 1.1, movement of the plunger pumps the melt into the die and therefore creates a non-zero mass flux at the die outlet. At small extrusion speed (or equivalently small plunger velocities) the pressure difference P and the flow rate Q are small, so the state of the extrusion system is represented by a point on the first (lower) branch. An increase in the extrusion speed leads to an increase in Q. The flow rate Q is proportional to the melt velocity in the die which in turn is proportional to the corresponding bulk shear rate $\dot{\gamma}_b$ (see Figure 5.1). Moreover, the increase in the plunger velocity results in an increase in the die inlet pressure P_{in} so that the pressure difference P also increases. So the

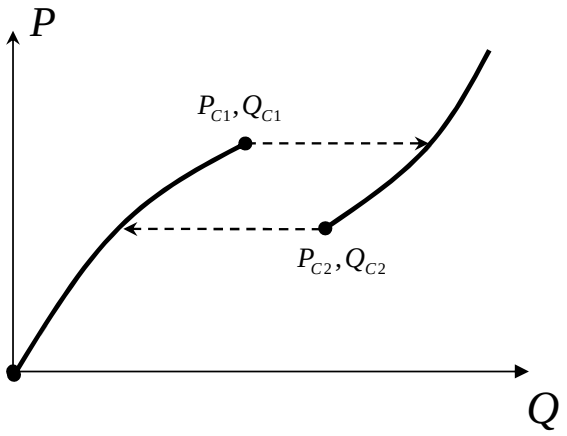

Figure 8.1: Qualitative sketch of the flow curve.

system "slides" up along the first branch of the flow curve.

When the plunger velocity approaches a certain critical value, a sudden transition from microscopic to macroscopic slip occurs along the whole die. After this, the polymer melt slips freely over a bare metallic wall (in the case of pure desorption) or over a thin lubrication layer of smashed surface molecules (in the case of disentanglement). The occurrence of slip implies that a larger amount of material can be transferred through the die so that the flow rate in the die Q jumps to a higher value. This means that the system "jumps" onto the second branch characterized by macroscopic slip. For a constant plunger speed, the incompressibility of the melt in the die implies that the amount of the material per unit of time which enters the die is also constant. Therefore, in the presence of wall slip, after a while, the flow rate in the die will drop to a certain value at which new entanglements between bulk and surface molecules can again be restored via readsorption of bulk molecules or thermal motion of smashed surface chains. The creation of the entanglements between bulk and surface molecules reduces the flow rate in the die so the system "jumps back" onto the first branch. After this the cycle repeats itself.

So the occurrence of spurt oscillations can be explained by the hysteresis in the two-branched flow curve. The analysis of the flow curve shows that the upmost point of the first branch is associated with the critical point of the stick-to-slip transition. As discussed earlier, the slip velocity remains small compared to the plunger velocity up to this point. Therefore, the first branch of the flow curve can be associated with microscopic slip. In contrast, the second branch in Figure 8.1 corresponds to a regime of macroscopic slip.

The fact that the slip velocity remains microscopic up to the transition point after which it jumps to macroscopic values implies that in practice the boundary condition at the die wall can be approximated by a simple switch function, similar to the behavior assumed in [52, 53]. The present model is able to calculate the parameters of the switch function in terms of the molecular properties of polymer melt, the properties of the die wall, and the extruder geometry.

The predictions of the relaxation oscillation model [51, 52, 53] for the amplitude and period of spurt oscillations are shown to be in a good quantitative agreement with available experimental data, provided that the parameters of the stick-slip transition are chosen properly. Therefore, using the results obtained in this work, the RO model, which takes the stick-slip law as an input, can be made fully quantitative. The conclusion is that the present model is not only capable of predicting the onset of wall slip, and hence spurt. It may also be used to predict the period and amplitude of the spurt oscillations from readily accessible rheological data and processing conditions.

Why is this model important?

As was mentioned in the Introduction, extrusion instabilities cause a serious problem for the processing industry, limiting the production rate and quality of resins. Despite the fact that extrusion instabilities are known for more than 50 years, for many of these instabilities a reliable mathematical model, which is able to describe quantitatively their onset and evolution, is still lacking. The reason for this is the complexity of polymeric systems and their intermolecular interactions. The ability to model and ultimately manipulate the onset of extrusion instabilities therefore poses a very serious challenge. The focus of the presented work is wall slip and related spurt phenomena. Spurt is one of the major issues that confront the polymer processing industry. A successful theory for spurt should at least be able to answer the following three questions:

- why does spurt occur?
- when does spurt occur?
- what should we do to postpone the onset of spurt?

In order to answer all these questions, the theory must be able to model the flow of a polymer melt near the die wall over a wide range of flow rates and wall materials. Moreover, for practical purposes it is important that the theory can predict spurt from readily accessible material data and processing conditions. The present model satisfies these conditions and makes a step ahead in the modelling of flow of polymer melts. It can predict the onset of wall slip (and thus spurt) by desorption or disentanglement of surface molecules. Since desorption and disentanglement are taken into account self-consistently, the model can be applied over a wide range of adhesion energies, including those where both slip mechanisms occur in parallel. The model contains no adjustable parameters and allows to formulate the stick-slip law in terms of the extruder geometry, molecular and surface parameters. Finally, the predictions of the model can further be used in practice to postpone or even eliminate spurt, e.g. by varying the material properties of the die wall or choosing an appropriate temperature regime of processing.

Bibliography

[1] H. K. Nason, A high temperature, high pressure rheometer for plastics, J. Appl. Phys. 16, 338 (1945).

[2] C. J. S. Petrie, M. M. Denn, Instabilities in polymer processing, AIChE. J. 22, 209 (1976).

[3] R. G. Larson, Instabilities in viscoelastic flows, Rheol. Acta 31, 213 (1992).

[4] A. I. Leonov, A. N. Prokunin, Non-linear phenomena in flows of viscoelastic polymer fluids, Chapmann&Hall: London, 1994.

[5] K. B. Migler, H. Hervet, L. Lèger, Slip transition of a polymer melt under shear stress, Phys. Rev. Lett. 70, 287 (1993).

[6] M. M. Denn, Extrusion instabilities and wall slip, Ann. Rev. Fluid Mech. 33, 265 (2001).

[7] S. Q. Wang, Molecular Transitions and Dynamics at Polymer/Wall Interfaces: Origins of Flow Instabilities and Wall Slip, Adv. Polym. Sci. 138, 229 (1999).

[8] L. Lèger, E. Raphael, H. Hervet, Surface-anchored polymer chains: their role in adhesion and friction, Adv. Polym. Sci. 138, 185 (1999).

[9] P. G. de Gennes, Mechanics of liquids, C. R. Acad. Sci. 288, (219) 1979.

[10] F. Brochard-Wyart, P. G. de Gennes and P. Pincus, C. R. Acad. Sci. 314, 873 (1992).

[11] N. Bergem, Visualization studies of polymer melt flow anomalies in extrusion, Proc. Int. Congr. Rheol., 7th, Gothenburg, Sweden: Swed. Soc. Rheol, 50 (1976).

[12] H. C. Lau, W. R. Schowalter, A model for adhesive failure of viscoelastic fluids during flow, J. Rheol. 30, 193 (1986).

[13] D. A. Hill, T. Hasegawa, and M. M. Denn, J. Rheol. 34, 891 (1990).

[14] C. W. Stewart, Wall slip in extrusion of linear polyolefins, J. Rheol. 37, 499 (1993).

[15] D. A. Hill, Wall slip in polymer melts: a pseudo-chemical model, J. Rheol. 42, 581 (1998).

[16] S. G. Hatzikiriakos, A slip model for linear polymers based on adhesive failure, Int. Polym. Process. 8, 135 (1993).

[17] W. B. Black, M. D. Graham, Wall-slip and polymer melt flow instability, Phys. Rev. Lett. 77, 956 (1996).

[18] F. Brochard-Wyart, P. G. de Gennes, Shear-dependent slippage at a polymer/solid interface, Langmuir 8, 3033 (1992).

[19] A. Ajdari, F. Brochard-Wyart, P. G. de Gennes. L. Leibler, J. L. Viovy, M. Rubinstein, Slippage of an entangled polymer melt on a grafted surface, Physica A. 204, 17 (1994).

[20] V. Mhetar, L. A. Archer, Slip in entangled polymer solutions, Macromol. 31, 6639 (1998).

[21] Y. M. Joshi, A. K. Lele, R. A. Mashelkar, Molecular model for wall slip: Role of convective constraint release, Macromol. 34, 3412 (2001).

[22] Y. M. Joshi, A. K. Lele, Dynamics of end-tethered chains at high surface coverage, J. Rheol. 46, 427 (2002).

[23] A. Yarin, M. Graham, A model for slip at polymer/solid interfaces, J. Rheol. 42, 1491 (1998).

[24] Y. M. Joshi, A. K. Lele, R. A. Mashelkar, A unified wall slip model, J. Non-Newt. Fluid Mech. 94, 135 (2000).

[25] M. A. Tchesnokov, J. Molenaar, J. J. M. Slot, Dynamics of molecules adsorbed on a die wall during polymer melt extrusion, J. Non-Newt. Fluid Mech., 126, 71-82 (2005).

[26] M. A. Tchesnokov, J. Molenaar, J. J. M. Slot, R. Stepanyan, A constitutive model with moderate chain stretch for linear polymer melts, J. Non-Newt. Fluid Mech., 123, 185-199 (2004).

[27] M. A. Tchesnokov, J. Molenaar, J. J. M. Slot, R. Stepanyan, A molecular model for cohesive slip at polymer melt/solid interfaces, J. Chem. Phys. 122, 1 (2005).

[28] M. A. Tchesnokov, J. Molenaar, J. J. M. Slot, R. Stepanyan, A molecular model for slip at polymer melt/solid interfaces, submitted to Phys. Rev. E.

[29] M. A. Tchesnokov, J. Molenaar, J. J. M. Slot, R. Stepanyan, A constitutive model for linear polydisperse polymer melts, to be submitted to J. Rheol.

[30] S. F. Edwards, Statistical mechanics with topological constraints : I, Proc. Phys. Soc. 92, 9 (1967).

[31] M. Doi, S. F. Edwards, The theory of polymer dynamics, Oxford Press: New York, 1986.

[32] P. E. Rouse, A theory of the linear viscoelastic properties of dilute solutions of coiling polymers, J. Chem. Phys. 21, 1272 (1953).

[33] P. H. Verdier, W.H. Stockmayer, Monte Carlo calculations on the dynamics of polymers in dilute solution, J. Chem. Phys. 36, 227 (1962).

[34] J. L. Viovy, M. Rubinstein, R. H. Colby, Constraint release in polymer melts - tube reorganisation versus tube dilation, Macromol. 24, 3587 (1991).

[35] S. T. Milner, T. C. B. McLeish, A. E. Likhtman, Microscopic theory of convective constraint release, J. Rheol. 45, 539 (2001).

[36] S. T. Milner, T. C. B. McLeish, Parameter-Free theory for stress relaxation in star polymer melts, Macromol. 30, 2159 (1997).

[37] J. L. A. Dubbeldam, J. Molenaar, Self-consistent dynamics of wall slip, Phys. Rev. E 67, 011803 (2003).

[38] P. G. de Gennes, Concept of reptation for one polymer chain, J. Chem. Phys. 55, 572 (1971).

[39] S. T. Milner, T. C. B. McLeish, Reptation and Contour-Length fluctuations in melts of linear polymers, Phys. Rev. Lett. 81, 725 (1998).

[40] G. Marrucci, Dynamics of entanglements: A nonlinear model consistent with the Cox-Merz rule, J. Non-Newt. Fluid. Mech. 62, 279 (1996).

[41] A.E.Likhtman, T.C.B. McLeish, Quantitative theory for linear dynamics of linear entangled polymers, Macromol. 35, 6332 (2002).

[42] M. Bercea, C. Peiti, B. Simonescu, P. Navard, Shear Rheology of semidilute poly(methylmethacrylate) solutions, Macromol. 26, 7095 (1993).

[43] J. J. Magda, C. S. Lee, S. J. Muller, R. G. Larson, Rheology, Flow instabilities, and shear induced diffusion in polystyrene solutions, Macromol. 26, 1696 (1993).

[44] G. Marrucci, N. Grizzuti, Fast flows of concentrated polymers: Predictions of the tube model on chain stretching, Gaz. Chim. Ital. 118, 179 (1988).

[45] E. V. Menezes, W. W. Graessley, Nonlinear rheological behavior of polymer systems for several shear-flow histories, J. Polym. Sci., Polym. Phys. Ed. 18, 295 (1982).

[46] A. Ajdari, F. Brochard-Wyart, P. G. de Gennes, L. Leibler, J. L. Viovy, M. Rubinstein, Slippage of an entangled polymer melt on a grafted surface, Physica A. 204, 17 (1994).

[47] P. G. de Gennes, Scaling concepts in polymer physics, Cornell University Press: Ithaca, 1979.

[48] E. Durliat, H. Hervert, L. Lèger, Influence of grafting density on wall slip of a polymer melt on a polymer brush, Europhys. Lett. 38, 383 (1997).

[49] S. Q. Wang, P. A. Drda, Superfluid-like stick-slip transition in capillary flow of linear polyethylene melts. 1. General features., Macromol. 29, 2627 (1996).

[50] S. Q. Wang, P. A. Drda, Stick-slip transition in capillary flow of polythylene. 2. Molecular weight dependence and low temperature anomaly, Macromol. 29, 4115 (1996).

[51] J. Molenaar, R. J. Koopmans, Modeling polymer melt-flow instabilities, J. Rheol. 38, 99 (1994).

[52] C. F. J. den Doelder, R. J. Koopmans, J. Molenaar, A. A. F. van de Ven, Comparing the wall slip and the constitutive approach for modelling spurt instabilities in polymer melt flows, J. Non-Newt. Fluid. Mech. 75, 25 (1998).

[53] C. F. J. den Doelder, R. J. Koopmans, J. Molenaar, Quantitative modelling of HDPE spurt experiments using wall slip and generalised Newtonian flow, J. Non-Newt. Fluid Mech. 79, 503 (1998).

[54] L. Fetters, D. J. Lohse, D. Richter, T. A. Witten, and A. Zirkel, Connection between polymer molecular weight, density, chain dimensions, and melt viscoelastic properties, Macromol. 27, 4639 (1994).

[55] S. Glasstone, K. Leidler, H. Eyring, The theory of rate processes, McGraw-Hill, New York (1941).

[56] Y. B. Chernyak, A. I. Leonov, On the theory of the adhesive friction of elastomers, Wear 108,, 105 (1986).

[57] S. G. Hatsikiriakos, J. M. Dealy, Wall slip of molten high density polyethylenes II. Capillary rheometer studies, J. Rheol. 36, 703 (1992).

[58] Drda P.A., S.Q.Wang, Stick-slip transition of polymer melt/solid interfaces, Phys. Rev. Lett. 75, 2698 (1995)

[59] X. Yang, S. Q. Wang, A. Halasa, H. Ishida, Fast flow behaviour of highly entagled monodisperse polymers. 1. Interfacial stick-slip transition of polybutadiene melts, Rheol. Acta. 37, 415 (1998).

[60] Y. M. Joshi, P. S. Tapadia, A. K. Lele, R. A. Mashelkar, Temperature dependence of critical stress for wall slip by debonding, J. Non-Newt. Fluid. Mech. 94, 151 (2000).

[61] J. W. H. Kolnaar, A. Keller, A temperature window of reduced flow resistance in polyethylene with implications for melt rheology: 1. The basis effect and principal parameters, Polymer 35, 3863 (1994).

[62] S. H. Anastasiadis, S. G. Hatzikiriakos, The work of adhesion of polymer/wall interfaces and its association with the onset of wall slip, J. Rheol. 42, 795 (1998).

[63] E. van Ruymbeke, R. Keunings, A. Hagenaars, and C. Bailly, Evaluation of Reptation Models for Predicting the Linear Viscoelastic Properties of Entangled Linear Polymers, Macromol. 35, 2689 (2002).

[64] M. Rubinstein, R. H. Colby, Self-consistent theory of polydisperse entangled polymers: Linear viscoelasticity of binary blends, J. Chem. Phys. 89, 5291 (1988).

[65] C. Tsenoglou, Molecular weight polydispersity effects on the viscoelasticity of entangled linear polymers, Macromol. 24, 1762 (1991).

[66] J. des Cloizeaux, Double reptation versus simple reptation in polymer melts, Europhys. Lett. 5, 47 (1988).

[67] W. H. Tuminello, Molecular weight and molecular weight disribution from dynamic measurements of polymer melts, Polym. Eng. Sci. 26, 1339 (1986).

[68] S. H. Wasserman, W. W. Graessley, Effects of polydispersity on linear viscoelasticity in entangled polymer melts, J. Rheol. 36, 543 (1992).

[69] E. van Ruymbeke, R. Keunings, and C. Bailly, Determination of the molecular weight distribution of entangled linear polymers from linear viscoelasticity data, J. Non-Newt. Fluid Mech. 105, 153 (2002).

[70] D. Nichetti, I. Manas-Zloczower, Viscosity model for polydisperse polymer melts, J. Rheol. 42, 951 (1998).

[71] J. M. Greenberg, Y. Demay, A simple model of the melt fracture instability, Eur. J. Appl. Math. 5, 337 (1994).

[72] G. C. Georgiou, M. J. Crochet, Time-dependent compressible extrudate-swell problem with slip at the wall, J. Rheol. 38, 1745 (1994).

[73] J. L. A. Dubbeldam, J. Molenaar, Dynamics of the spurt instability in polymer extrusion, J. Non-Newt. Fluid Mech. 112, 217 (2003).

[74] A. V. Ramamurthy, Wall slip in viscous fluids and influence of materials of construction, J. Rheol. 30, 337 (1986).

[75] H. Münstedt, M. Schmidt, and E. Wassner, Stick and slip phenomena during extrusion of polyethylene melts as investigated by laser-Doppler velocimetry, J. Rheol. 44, 413 (2000).

List of publications

Journals

Yu. A. Vdovin, M. A. Tchesnokov, Phenomenon of electro-induced transparency in a four-level system, Collected scientific papers of Moscow State Physical Engineering Institute Volume 5 (2000) 192.

Yu. A. Vdovin, M. A. Tchesnokov, Absorption of probe radiation in a four-level system with a three-photon resonance, Laser Physics 5 (2000) 1047.

A. N. Starostin, M. A. Tchesnokov, The effect of spatial dispersion and boundaries of a medium on resonance radiation transfer, JETP 94 (2002) 46.

A. N. Starostin, M. A. Tchesnokov, On oscillations of thermionic current in composite systems, JETP 97 (2003) 1219.

M. A. Tchesnokov, J. Molenaar, J. J. M. Slot, Dynamics of molecules adsorbed on a die wall during polymer melt extrusion, J. Non-Newt. Fluid Mech., 126, 71-82 (2005).

M.A. Tchesnokov, J. Molenaar, J. J. M. Slot, R. Stepanyan, A constitutive model with moderate chain stretch for linear polymer melts, J. Non-Newt. Fluid Mech. 123, 185-199 (2004).

M.A. Tchesnokov, J. Molenaar, J. J. M. Slot, R. Stepanyan, A molecular model for cohesive slip at polymer melt/solid interfaces, J. Chem. Phys. 122, 1 (2005).

M.A. Tchesnokov, J. Molenaar, J. J. M. Slot, R. Stepanyan, A molecular model for slip at polymer melt/solid interfaces, submitted to Phys. Rev. E.

M. A. Tchesnokov, J. Molenaar, J. J. M. Slot, R. Stepanyan, A constitutive model for linear polydisperse polymer melts, to be submitted to J. Rheol.

M. A. Tchesnokov, J. Molenaar, J. J. M. Slot, R. Stepanyan, Relaxation spectrum of binary blends: extension of the Doi-Edwards theory, submitted to Phys. Rev. Lett.

Memoranda

M. A. Tchesnokov, J. Molenaar, J. J. M. Slot, Dynamics of chains grafted on solid wall during polymer melt extrusion, Memorandum 1673 of the Faculty of EEMCS, University of Twente, 2003.

M. A. Tchesnokov, J. Molenaar, J. J. M. Slot, A universal constitutive model for the interfacial layer between a polymer melt and a solid wall, Memorandum 1677 of the Faculty of EEMCS, University of Twente, 2003.

M. A. Tchesnokov, J. Molenaar, J. J. M. Slot, Bond vector probability distribution function of "bulk" molecules, Memorandum 1679 of the Faculty of EEMCS, University of Twente, 2003.

M. A. Tchesnokov, J. Molenaar, J. J. M. Slot, A rigorous model for constraint release in the bulk and near-wall region, Memorandum 1693 of the Faculty of EEMCS, University of Twente, 2003.

Curriculum vitae

Mikhail Tchesnokov was born in Uglich, Russia, on March 9, 1976. After completing his primary school education in 1991, he continued his study at the department of Mathematics and Engeneering, the Technical College, Uglich, Russia. In 1994, he continued his education at the faculty of Theoretical and Experimental Physics, Moscow State Physical Engineering Institute (Technical University), Moscow, Russia. Under supervision of Prof. Dr. Yu. A. Vdovin, Mikhail Tchesnokov completed his master's project on non-linear resonance radiation transfer and received a master's degree in Theoretical Physics in 2000. In the period 2000-2002, he worked as a junior research fellow in the group of Prof. Dr. A. N. Starostin at the Center of Theoretical Physics and Numerical Mathematics, State Research Center of Russian Federation, Troitsk Institute for Innovation and Fusion Research, Troitsk, Moscow Region, Russia. During this time, he participated in two interdisciplinary projects in the area of non-linear optics, statistical mechanics and solid matter, in which a study of propagation and adsorption of high-intensity laser beams through hot non-equilibrium media as well as an influence of the incident radiation on the thermoemission from the media was carried out. In 2002, Mikhail Tchesnokov joined a new research project in the area of industrial polymer physics and modelling of polymer dynamics at the department of Mathematical Physics and Computational Mechanics, Faculty of Electrical Engineering, Mathematics and Computer Science, University of Twente, The Netherlands. The results of this research project, supervised by Prof. Dr. Jaap Molenaar and Prof. Dr. Han Slot, are presented in this thesis.